THE INS AND OUTS OF THE CHROMATOID BODY

Tiina Lehtiniemi

THE INS AND OUTS OF THE CHROMATOID BODY

Tiina Lehtiniemi

University of Turku

Faculty of Medicine
Institute of Biomedicine
Physiology
Turku Doctoral Programme of Molecular Medicine (TuDMM)

Supervised by

Professor Noora Kotaja
Integrative Physiology and Pharmacology
Institute of Biomedicine
University of Turku
Turku, Finland

Reviewed by

PhD Mikko Frilander
Institute of Biotechnology
University of Helsinki
Helsinki, Finland

Assistant Professor Renata Prunskaite-Hyyryläinen
Faculty of Biochemistry and Molecular Medicine, University of Oulu
Oulu, Finland

Opponent

Professor Wei Yan
The Lundquist Institute at Harbor-UCLA Medical Center
David Geffen School of Medicine at UCLA
California, USA

To my boys

UNIVERSITY OF TURKU
Faculty of Medicine
Institute of Biomedicine
Physiology
TIINA LEHTINIEMI: The Ins and Outs of the Chromatoid Body
Doctoral Dissertation, 208 pp.
Turku Doctoral Programme of Molecular Medicine (TuDMM)
September 2023

ABSTRACT

Spermatogenesis is a complex differentiation process that produces millions of genetically unique sperm cells every day. During spermatogenesis the developing germ cells undergo metamorphic changes as they transform from primitive spermatogonial stem cells to large meiotic spermatocytes, divide into smaller round spermatids and finally become streamlined, compact sperm. Each cell type has a unique transcriptional profile. Early cells of spermatogenesis, especially meiotic spermatocytes express massive amounts of transcripts while transcription is completely halted later due to the nuclear condensation of spermatids. To cope with these transcriptomic challenges, large cytoplasmic ribonucleoprotein granules called germ granules appear and provide dynamic platforms for the transcripts and their regulators to come together.

Here, two proteins of the largest germ granule, the Chromatoid Body (CB), were selected for investigation: the autophagosome transporting FYCO1 and the RNA degrading endonuclease SMG6. Two mouse lines were created to reveal the roles of these germ granule components in spermatogenesis. The results show that FYCO1 is needed for the integrity of germ granules. CB morphology was disrupted in the absence of FYCO1, a phenotype that worsened under stress conditions. Nonetheless FYCO1 depleted mice were fertile. Conversely, the deletion of the second component, endonuclease SMG6, lead to infertility. The results showed that SMG6 is required for the transcriptional balance of developing germ cells which it regulates together with the piRNA pathway. Both studies highlight the importance of germ granules in spermatogenesis.

Overall, this thesis comprises three studies. First, a simple BSA-gradient method to isolate round spermatids and spermatocytes from mice using standard laboratory equipment was developed to facilitate the two main studies of this thesis work. In the first of these studies FYCO1 was identified as a link between autophagy and the CB while the second revealed the role of the endonuclease SMG6 in spermatogenesis and male germ cells transcriptional integrity. Together these two studies contribute to revealing the functions of the enigmatic germ granules and the pivotal roles they play for the maintenance of male fertility.

KEYWORDS: spermatogenesis, germ granule, chromatoid body, autophagy, nonsense-mediated RNA decay

TIIVISTELMÄ

Tahaton lapsettomuus on maailmanlaajuisessa kasvussa ja erityisesti miesten hedelmällisyyden häiriöistä tiedetään edelleen vähän. Spermatogeneesi on ainutlaatuinen, monimutkainen ja tarkoin säädelty kehitysprosessi. Ensin kantasolut jakautuvat mitoottisesti kasvattaakseen määräänsä. Meioosissa ne sekoittavat geneettisen materiaalinsa luoden uusia yhdistelmiä, mahdollistaen evoluution. Lopulta ne käyvät läpi morfologisen muodonmuutoksen pyöreästä solusta siittiölle tyypilliseen virtaviivaiseen ulkomuotoonsa. Sukusolut ilmentävät genomiaan aktiivisesti ja niiden RNA profiili onkin poikkeuksellisen monimuotoinen verrattuna muihin erilaistuneisiin soluihin. RNA-säätely on erittäin tärkeässä asemassa, ja onnistuneeseen kehitykseen tarvitaan laaja kirjo erilaisia mekanismeja. Tärkeässä osassa ovat niin sanotut sukusolujyvät, joihin RNA molekyylit ja RNA:ta sitovat proteiinit kerääntyvät.

Olen väitöskirjatyössäni keskittynyt hedelmällisyyden kannalta tärkeän sukusolujyvän, kromatoidikappaleen (Chromatoid body, CB), toimintaan ja luonut kaksi poistogeenistä hiirimallia niin, että yksi CB komponentti, joko FYCO1 tai SMG6, on poistettu uroshiiriltä. Yllättäen puutteita siittiönmuodostuksesta ei löytynyt FYCO1-poistogeenisiltä uroksilta, vaikka CB:n ulkomuoto ja toiminta olikin häiriintynyt. Yhteys CB:n ja autofagian, joka on solujen oma kierrätys ja laadunvalvonta mekanismi, välillä kuitenkin paljastui. Tutkimus osoitti myös, että FYCO1 proteiinilla on tärkeä rooli sukusolujyvästen rakenteen ylläpidossa. Toisessa työssä keskityttiin tutkimaan RNA:ta hajottavan SMG6 proteiinin roolia sukusoluissa. Smg6-poistogeenisten uroshiirien siittiönmuodostus oli vakavasti häiriintynyt ja urokset olivat hedelmättömiä. Erityisesti kehittyvien siittiöiden normaalin RNA profiilin ylläpidossa oli ongelmia Smg6-poistogeenisilla uroshiirillä, mikä kertoo SMG6 proteiinin mahdollisista tehtävistä sukusoluissa. Näiden töiden lisäksi väitöskirjaani sisältyy kolmas työ, jossa kehitettiin uusi menetelmä, jolla eri sukusolujen eristäminen kiveksestä on mahdollista myös hyvin pienellä alkumateriaalilla, jolla toivomme voivamme vaikuttaa koe-eläinten käyttömäärän vähentämiseen. Tämä menetelmä myös mahdollistaa solueritellyn sukusolututkimuksen laajemmalle tutkijayhteisölle. Kokonaisuutena väitöskirjani valaisee sukusolujyvästen tärkeää tehtävää siittiönmuodostuksessa, sekä paljastaa molekyylitason mekanismeja tässä elintärkeässä prosessissa.

AVAINSANAT: spermatogeneesi, siittiönmuodostus, hedelmällisyys, RNA-säätely

Table of Contents

Abbreviations

A_{al}	type A-aligned spermatogonia
A_{pr}	type A-paired spermatogonia
A_s	type A-single spermatogonia
A_{undiff}	undifferentiated spermatogonia
ANOVA	analysis of variance
AP	alternative polyadenylation
AR	Androgen receptor
ART	assisted reproductive technologies
AS	alternative splicing
ATG5	Autophagy related 5
ATG9	Autophagy related 9
ATG12	Autophagy related 12
ATG14	Autophagy related 14
ATG16L1	Autophagy related 16 like 1
B	type B spermatogonia
BSA	bovine serum albumin
BTB	blood-testis-barrier
CB	Chromatoid Body
CCR-NOT	Carbon catabolite repression-negative on TATA
cKO	conditional knockout
CO_2	carbon dioxide
CREM	cAMP responsive element moderator
CRY2	Cryptochrome circadian regulator 2
CUL4A	Cullin 4A
CUL7	Cullin 7
CUL9	Cullin 9
DAP	3,3′-diaminobenzidine
DAPI	4′, 6-diamidino-2-phenylindole
DAZ	Deleted in azoospermia
DDX4	DEAD [Asp-Glu-Ala-Asp] box helicase 4
DDX25	DEAD [Asp-Glu-Ala-Asp] box healicase 25

DE	differential expression
dEJ	downstream exon–exon junction
devAS	developmentally dynamic alternative splicing
DMEM	Dulbecco´s modified eagle medium
DNA	deoxyribonucleic acid
DNase	deoxyribonuclease
dpp	days post partum
DPY19L2	dpy-19 Like 2
DTT	dithiothreitol
ECL	electrochemiluminescence
EDTA	ethylenediaminetetraacetic acid
EIF4G3	Eukaryotic translation initiation factor 4γ3
EM	electron microscopy
eRF1	eukaryotic release factor 1
eRF3	eukaryotic release factor 3
ER	endoplasmic reticulum
ES/ESC	embryonic stem cell
Est1	Even shorter telomere 1
EtOH	ethanol
EU	ethynyl uridine
FACS	fluorescence-activated cell sorting
FAM209A	family with sequence similarity 209 member A
FAM71F2/GARI	Golgi-associated RAB2B interactor
FBS	fetal bovine serum
FRAP	fluorescence recovery after photobleaching
FPKM	fragments per kilobase per million mapped fragments
FSH	follicle-stimulating hormone
FYCO1	FYVE and coiled-coil domain containing 1
FXR1	Fragile X mental retardation syndrome related 1
GATA4	GATA binding protein 4
GBA2	Glucosylceramidase beta 2
GIM	genoinformative markers
GO	gene ontology
GOPC	Golgi associated PDZ coiled-coil motif containing
HCD	higher-energy C-trap dissociation
HENMT1	S-adenosylmethionine-dependent methyltransferase
HEPES	4-(2-hydroxyethyl)-1-piperazineethanesulfonic acid
HPLC	high performance liquid chromatography
HRP	horse radish peroxidase
ICSI	intracytoplasmic sperm injection

IF	immunofluorescence
IFT	intraflagellar transport system
IHC	immunohistochemistry
IMC	inter mitochondrial cement
IMPC	international mouse phenotyping consortium
KIF5C	Kinesin family member 5C
KIFC2	Kinesin family member C2
KIFC3	Kinesin family member C3
KIF3A	Kinesin family member 3A
KIF3B	Kinesin family member 3B
KO	knock out
LAMP1	Lysosomal-associated membrane protein 1
LAMP2A	Lysosomal-associated membrane protein 2A
LC3/MAP1LC3	(microtubule-associated protein 1) light chain 3
LC/ESI-MS/MS	liquid chromatography electrospray ionization tandem mass spectrometric
LH	luteinizing hormone
LLPS	liquid-liquid phase separation
LIR	LC3-Interacting Region
MDR	Modified Density gradient for Round spermatids
MVB	multivesicular bodies
NIF	NMD inducing feature
NMD	nonsense mediated RNA decay
miRNA	microRNA
mRNA	messenger RNA
mTOR	mammalian target of rapamycin
P-bodies	Processing bodies
p62/SQSTM1	Sequestosome 1
PABPC1	Poly(A) binding protein C1
PAS	periodic acid-Schiff
PBS	phosphate buffered saline
PBST	phosphate buffered saline tween20
PCR	polymerase chain reaction
PDCL2	Phosducin like 2
PFA	paraformaldehyde
PGC	primordial germ cell
PGL-1	Phenolic glycolipid 1
PI3K	Phosphatidylinositol 3-kinase
PI3P	Phosphatidylinositol 3-phosphate
PICK1	Protein interacting with PRKCA 1

piRNA	Piwi-interacting RNA
PIWI	P-element-induced *wimpy* testis
PIWIL1/MIWI	Piwi-like RNA-mediated gene silencing 1
PIWIL2/MILI	Piwi-like RNA-mediated gene silencing 2
PIWIL4	Piwi-like RNA-mediated gene silencing 4
PLD6	Phospholipase D family member 6
PLVAP	Plasmalemma vesicle-associated protein
PLZF	Promyelocytic leukemia zinc finger protein
PMSF	Phenylmethylsulfonyl fluoride
PNA	Rhodamine-conjugated peanut agglutinin
Pol I/II/III	Polymerase I/II/III
PNLDC1	PARN like RNAse domain containing exonuclease 1
PRM1	Protamine 1
PRM2	Protamine 2
pSPC	pachytene spermatocyte
PTC	premature termination codon
PTM	peritubular myoid cell
PVDF	polyvinylidene fluoride
RBP	RNA-binding protein
RIPA	radioimmunoprecipitation assay (lysis buffer)
RNA	ribonucleic acid
RNAse	ribonuclease
RNF17	Ring finger protein 17
RNP	ribonucleoprotein
rRNA	ribosomal RNA
ROSI	round spermatid injection
RPL39	Ribosomal protein L39
RPL39L	Ribosomal protein L39 like
RS	round spermatid
RSEM	RNA-Seq by expectation-maximization
rsRNA	rRNA-derived small RNAs
RT	room temperature
RT-PCR	reverse transcription PCR
RT-qPCR	quantitative RT-PCR
SC	Sertoli cell
SDS	sodium dodecyl sulfate
SDS-PAGE	SDS- polyacrylamide gel electroforesis
SEPA-1	Suppressor of ectopic P granule in autophagy 1
SIDT2	SID1 transmembrane family member 2
SMG6/EST1A	Telomerase-binding protein EST1A

SPC	spermatocyte
shRNA	short hairpin RNA
SOX3	SRY box transcription factor 3
SOX9	SRY box transcription factor 9
SPACA1	sperm acrosome associated 1
SPC	spermatocyte
SRY	sex determining region of chromosome Y
SSCs	spermatogonial stem cells
SSMEM1	Serine rich single-pass membrane protein 1
STK31	Serine/threonine kinase 31
SUMO	small ubiquitin-related modifier
TAM	transcription-associated mutagenesis
TBS	tris-buffered saline
TCDM	Turku Center for Disease Modeling
TCR	transcription-coupled repair
TDRD1	Tudor domain containing 1
TDRD3	Tudor domain containing 3
TDRD5	Tudor domain containing 5
TDRD6	Tudor domain containing 6
TDRD7	Tudor domain containing 7
TE	transposable element
TMM	trimmed mean of M-values
TNP1	Transition protein 1
TNP2	Transition protein 2
tRNA	transfer RNA
TSKS	Testis specific serine kinase substrate
TSSK1	Testis Specific Serine Kinase 1
TSSK2	Testis Specific Serine Kinase 2
tsRNA	transfer RNA-derived small RNAs
TUNEL	terminal deoxynucleotidyl transferase dUTP nick-end labeling
uORF	upstream open reading frame
ULK1	Unc-51-like autophagy-activating kinase
UPF1	Up-frameshift 1
UPF2	Up-frameshift 2
UPF3A	Up-frameshift 3A
UPF3B	Up-frameshift 3B
UTR	untranslated region
WHO	World Health Organization
ZPBP1	Zona pellucida binding protein 1

List of Original Publications

This dissertation is based on the following original publications, which are referred to in the text by their Roman numerals:

I   **Lehtiniemi T***, Da Ros M*, Olotu O, Meikar O and Kotaja N. Enrichment of Pachytene Spermatocytes and Spermatids from Mouse Testes Using Standard Laboratory Equipment. The Journal of Visualized Experiments. 2019 10.3791/60271.
(*equal contribution).

II   **Lehtiniemi T***, Da Ros M*****, Olotu O, Fischer D, Vihinen H, Jokitalo E, Sironen A, Toppari J and Kotaja N. FYCO1 and autophagy control the integrity of the haploid male germ cell-specific RNP granules. *Autophagy*. 2017, 132: 302–321
(*equal contribution).

III   **Lehtiniemi T**, Bourgery M, Ma L, Ahmedani A, Mäkelä M, Asteljoki J, Olotu O, Laasanen S, Zhang F, Tan K, Chousal J, Burrow D, Koskinen S, Laiho A, Elo L, Chalmel F, Wilkinson M and Kotaja N. SMG6 localizes to the chromatoid body and shapes the male germ cell transcriptome to drive spermatogenesis. *Nucleic Acid Research.* 2022, Oct 19;gkac900.

The original publications have been reproduced with the permission of the copyright holders.

1   Introduction

In a healthy male individuals' testis, a process known as spermatogenesis (*i.e.* the production of spermatozoa) produces hundreds of millions of spermatozoa each day. Disturbances at any given point of spermatogenesis may lead to a reduced ability to conceive offspring. Infertility causes significant psychological and social distress and poses individuals and the society alike under considerable economic pressure. A recent report by the World Health Organization (WHO) estimates around 17.5% of the adult population – roughly 1 in 6 worldwide – experience fertility issues[1]. WHO characterizes infertility as the failure to conceive after at least 12 months of regular, unprotected sexual intercourse. An estimation of 8-12% of reproductive-aged couples struggle to conceive in this time with the male factor contributing to roughly half of the cases, being solely responsible in 20-30%[1–3]. The prevalence of infertility was also found to be on the rise in both men and women in a large Global Burden of Disease survey covering 195 countries and territories from 1990 to 2017[4].

Male-factor infertility and subfertility arise from multifactorial pathological conditions that can be related to a combination of congenital, acquired, or idiopathic factors. Compromised fertility can display via phenotypes ranging from a reduced number of spermatozoa or reduced mobility to an increased number of morphological abnormalities to the most dramatic scenario, a complete absence of spermatozoa in semen – a condition known as azoospermia – that can arise from an obstruction or from a serious spermatogenetic defect[3]. Importantly, as health conditions can affect fertility, for some males, treatment could significantly improve, or even reverse fertility problems as long as proper diagnosis was reached. To that effect, advanced diagnostic tests to investigate sperm quality and function have been developed in recent years to improve diagnosis and management[5].

The use of assisted reproductive technologies (ART) has substantially improved the chances of having a biological child in case of fertility issues. For example, in cases of mild to moderate sperm abnormalities, intrauterine insemination is a valuable option that involves the direct placement of carefully prepared sperm into the uterus during the woman's ovulation period. When sperm release is impaired in obstructive azoospermia, testicular sperm extraction and testicular sperm aspiration, have enabled the retrieval of sperm directly from the testes. In more

challenging situations, intracytoplasmic sperm injection (ICSI) has emerged as a powerful tool. ICSI, a procedure where a single sperm is injected directly into the egg, is becoming the most widely used insemination method worldwide and is currently used in ~66% of fertility centers[6]. Despite its success in overcoming all forms of male factor infertility, the accumulating information over the past ~30 years regarding the health of ICSI offspring is raising some concerns[7]. Abnormal sperm with poor-quality chromatin can have a long-standing impact on both genetic and epigenetic levels potentially compromising the health of the offspring[6,8]. However, the evolution of ART is moving towards even more radical approaches and away from proper male evaluation and treatment. Round spermatid injection (ROSI) has emerged in recent years. In theory, ROSI provides an option for the rare cases of infertility where no sperm is found within the scrotum but the earlier cell types, round spermatids, are present. Successful pregnancies and deliveries have been reported using ROSI, but its clinical outcomes are low[9]. While the technology of reproductive medicine is moving fast, deep molecular knowledge on spermatogenesis needs to be acquired to ensure that the novel technologies are not only effective but also safe for the new individual and their germline. Furthermore, reproductive health is not only about reproduction but instead mirrors the health status of an individual in multiple ways.

A higher risk of illness and mortality among men with male factor infertility has been identified by several studies. A greater incidence of cancers among men with severe infertility has been found[10]. A large study on Danish men, on the other hand, found an elevated higher risk of death among men with azoospermia[11]. Impaired male reproductive health has also been linked to a higher Charlson Comorbidity Index, a proxy of decreased general health status[12,13]. Metabolic conditions, pre-diabetes and diabetes have been also associated to decreased semen status[14–16]. Most importantly, there is also accumulating evidence that paternal health at the time of conception can affect the offspring's metabolic health and reproductive potential, through a myriad of potential mechanisms of transgenerational epigenetic inheritance[17]. Therefore, the need to understand spermatogenesis thoroughly extends beyond reproduction and the desire for progeny of couples. It is important to look beyond a simple semen analysis and instead view male infertility as a condition connected to overall health and metabolism and, with that in mind, investigate the origin of the condition.

The underlying genetic causes of male infertility currently remain unknown in 40% of patients[18]. When the etiology of infertility is unknown, prediction of choice of treatment or ART outcome becomes exceedingly difficult. And even when genetic screening is performed satisfactory results can only be obtained when a gene has already been linked to spermatogenesis. Wide consortium-based whole-exome and whole-genome studies are being conducted to discover the remaining idiopathic

causes[5]. However, demonstrating causation beyond an association and their mechanism of action is prerequisite for understanding the patient phenotype and key to guiding clinical decision-making and providing appropriate genetic counseling.

Genetically modified mouse models have greatly contributed to our knowledge of male fertility by providing a tool to manipulate and study each gene in the context of mammalian spermatogenesis. Information regarding the molecular events taking place during spermatogenesis is increasing fast as new models are created and genes pivotal for spermatogenesis identified[19]. As described below, this thesis work contributes to this pool of genetically modified mouse models by presenting two new models. Furthermore, while a significant obstacle in the spermatogenesis field is the fact that most cell culture methods are not applicable for germ cells, especially at the post-meiotic phase, efficient cell enrichment methods and the evolution of tissue culture models are enabling new avenues of research[20]. Each spermatogenetic cell type has a distinct biochemical and molecular profile. Many different strategies to separate and/or enrich specific cell types from testis exist. The most successful methods to date are centrifugal elutriation based on counterflow centrifugation[21], FACS sorting[22,23] which is based on DNA content or specific markers and the STA-PUT velocity sedimentation by unit gravity[24]. In this thesis work another enrichment method, a simple and fast BSA-gradient based protocol to isolate round spermatids and spermatocytes from mouse testis using standard laboratory equipment was developed. The optimization of this method was done in parallel to the other two studies.

Two new genetically modified mouse lines were designed and created to study two proteins that are highly expressed by male germ cells. During spermatogenesis, at different points of germ cell development, specific ribonucleoprotein (RNP) granules arise and take part in organizing and maintaining the transcriptomic profiles of developing germ cells. The importance of these germ granules, largest of them the Chromatoid Body (CB), is undeniable in spermatogenesis as demonstrated by numerous germ granule protein targeted knockout (KO) mouse models[25]. For this body of work, two germ granule proteins were selected. Both of these proteins were discovered in the CB proteome analysis in a previous study done in our lab[26] but otherwise share no obvious resemblances and appear to function in different pathways. FYCO1 (FYVE and coiled-coil domain containing 1) is a phosphatidylinositol 3-phosphate-binding protein involved in the transport of autophagosomes[27] while SMG6 is the sole endonuclease in the nonsense-mediated RNA decay (NMD) pathway[28]. To reveal the role of FYCO1 and SMG6 in germ granules and spermatogenesis each was deleted from postnatal male germ cells and the arising phenotypes studied. The data obtained shows that FYCO1 plays a critical role in the maintenance of the CBs physical integrity while SMG6 is crucial for the maintenance of its transcriptomic profile. In the absence of FYCO1 the morphology

of the CB is fragmented, a phenotype which worsened under stress conditions. Nonetheless FYCO1 depleted mice are fertile. SMG6 depleted mice on the other hand had morphologically intact CBs but their transcriptomic profile and the transcriptome of the cell itself was clearly altered. Furthermore, male mice lacking SMG6 do not produce sperm and are thus sterile proving yet again the importance of germ granule components for male fertility. Both studies provide important clues to the enigmatic functions of germ granules and the role they play in the maintenance of male fertility.

2 Review of the Literature

Throughout a male reproductive age, a process known as spermatogenesis (*i.e.*, the production of spermatozoa) produces hundreds of millions of spermatozoa each day. In the testes, the developing germ cells undergo complex changes as they transform from the primitive spermatogonial stem cells to large meiotic spermatocytes, split to smaller haploid round spermatids and finally compress themselves to form sleek and compact spermatozoa. Before the sperm are transferred from the testis to the epididymis for further maturation and to wait for ejaculation via vas deferens, a complex series of processes make sure that each sperm cell contains all the necessary genetic and epigenetic information needed for the offspring[29,30].

During maturation, at different points of germ cell development, specific RNP granules, germ granules, arise and take part in organizing and maintaining the RNA landscape of each developing cell. These granules are unique to developing germ cells and though their existence has been known for more than 100 years[31], their specific molecular functions are still unclear.

The following contains a concise description of the main structures and cell types involved in spermatogenesis and a synapsis of RNA biology basics. Unless otherwise specified, the focus is on mammalian biology, particularly on mice. Spermatogenesis is described in more detail regarding postmeiotic germ cells, their development, unique features, and the peculiarities of their RNA biology.

Large RNP granules of germ cells, particularly the CB, are introduced. The connection of RNPs to autophagy and maintaining cellular homeostasis as well as maintaining transcriptomic balance and nonsense mediated RNA decay is discussed to the extent that is currently known before presenting the results of this thesis work and how they contribute to the state-of-the-art. The review part of this thesis can also be viewed as an overall background and an introduction to the research environment to which we the method part of this thesis was designed, the development of a germ cell isolation protocol.

2.1 Testes – an overview

The testes have two important tasks for male reproduction: 1) the production of sperm – spermatogenesis and 2) the biosynthesis of steroid hormones – steroidogenesis. These functions can be compartmentalized within the testis to the seminiferous epithelium – where developing germ cells are maintained – and the interstitial space that contains blood and lymphatic vessels, immune cells, and the steroidogenic Leydig cells. Between is a layer of basement membrane and layers of modified myofibroblastic cells known as peritubular myoid cells. The seminiferous tubules together with the interstitial space are all encased by a connective tissue capsule, the tunica albuginea (Figure 1)[32].
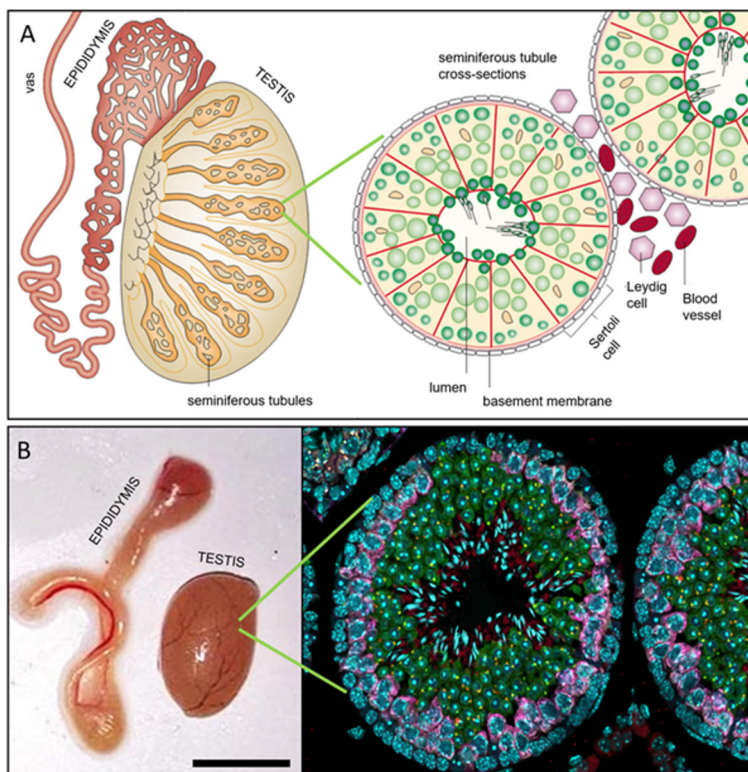
Figure 1. Epididymis, testis and seminiferous tubules. Spermatogenesis takes place in the seminiferous tubules of the testis, and sperm maturation continues in the epididymis from which the mature sperm is transported via vas deferens (vas). **A)** A schematic illustration of the epididymis, testis and seminiferous tubule cross-sections with the interstitial space between them. Germ cells (in different shades of green) are enclosed by Sertoli cells (cells outlined in red with orange nuclei). Mature sperm cells are found inside the lumen of the seminiferous tubules. Testosterone producing Leydig cells (in purple) reside in the interstitial space with blood vessels both separated from the germ cells by the peritubular myoid cells (in white) (*Modified from SpermatogenesisOnline*[33]). **B)** A photograph of a dissected mouse epididymis and testis and an immunofluorescence image of seminiferous tubule cross-sections stained by diverse markers to visualize cell layers (right). (*Modified from Lehtiniemi et al.*[34]). Scale bar= 5 mm.

2.1.1   The three phases of spermatogenesis

Spermatogenesis – the key process in male fertility – produces haploid spermatozoa that fertilize eggs and eventually produce progeny. In the seminiferous tubules, germ cells develop, differentiate, and metamorphose into spermatozoa (Figure 1, Figure 2). As the male germline differentiation begins in the embryo, the initial steps towards spermatogenesis begin with the determination of the primordial germ cells (PGC). The postnatal spermatogenesis, beginning a few days after birth in rodents, can be subdivided into three crucial phases: 1) proliferation phase 2) meiotic divisions phase and 3) haploid differentiation; the post-meiotic phase that is also known as spermiogenesis[32]. The first wave of spermatogenesis, takes 35 days in mice and full fertility is reached by 6–7 weeks of age[35].

The mitotic proliferation of spermatogonia takes place near the basal lamina where, after birth, the maintenance of spermatogenesis depends on the biological competence of the extremely scarce spermatogonial stem cells (SSCs) estimated to represent less than 0.05% of total testis cells[36,37]. They have three possible fates: self-renewal to produce new stem cells, differentiation into more mature spermatogonia, or apoptosis. SSCs are known as A single (A_s) and they are the only spermatogonia without intercellular bridges[38]. Beside single cells, the undifferentiated spermatogonia exist linked by intracellular bridges either as paired cells, (A paired = A_{pr}) or chains of 4, 8 and 16 cells, named (A aligned =A_{al}). In mice, A_{al} give rise to A_1 spermatogonia, first of the following mitotic cells, differentiating spermatogonia, which undergo six successive divisions, resulting in A_2, A_3, A_4, In (=intermediate) and B types (Figure 2). Eventually a subset of spermatogonia differentiate into spermatocytes which enter meiosis[39].

The meiotic phase consists of two consecutive cell divisions, meiosis I and meiosis II. Meiosis I begins with DNA synthesis resulting in a tetraploid cell. The long meiosis I prophase licenses the induction of DNA repair, homologous recombination, and chromosome synapsis which allow genetic information between paired chromosomes to mix, creating genetic diversity between the arising gametes. During the several days long prophase developing spermatocytes go through phases of leptotene (L), zygotene (Z), pachytene (P) and diplotene (D) spermatocytes. At the end of the prophase of meiosis I, the homologous chromosomes separate and move toward opposite poles of the cell. This is followed by a rapid reductive division, known as meiosis I, which separates the two sets of chromosomes into two haploid daughter cells called secondary spermatocytes. The secondary spermatocytes then undergo the second stage of meiosis, meiosis II. During meiosis II, the sister chromatids within the secondary spermatocytes separate and move towards opposite poles of the cell resulting in four haploid round spermatids[40].
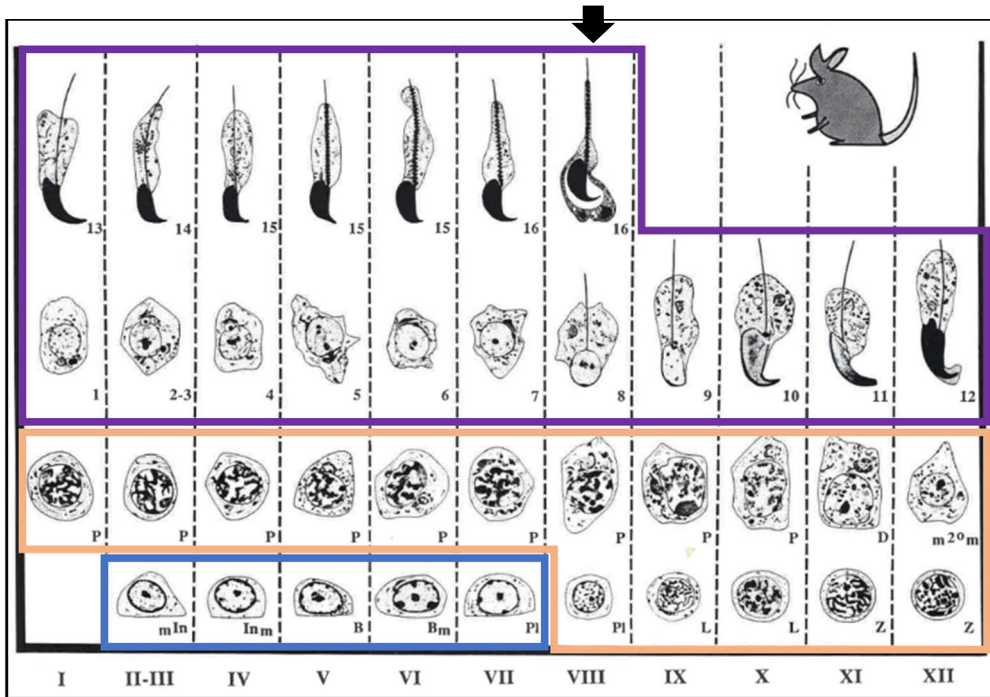
Figure 2. **A schematic illustration of developing germ cells in mice.** Spermatogenesis can be subdivided into three crucial phases: 1) mitotic proliferation phase (blue) 2) meiotic divisions phase (orange) and 3) haploid differentiation aka the post-meiotic spermiogenesis (violet) which consists of 16 steps. The acrosome and the flagellum start forming already in round spermatids (steps 1-8) while elongation (steps 9-16) and nuclear condensation (steps 11-16) take place later. In the schematic, the progression of spermatogenesis occurs from left to right and bottom to top, with each column representing a specific stage (marked by roman numerals I-XII) and encompassing all the cell types at a particular developmental phase. These twelve stages can be visually distinguished from each other by transillumination-assisted microscopy where stages differ from each other by their light absorption characteristics[41]. This is due to the fact that each stage from I to XII contains a different set of cells as the reader can tell by comparing the contents of each column. For instance, at stage VIII (black arrow), the seminiferous epithelium contains preleptotene (Pl) spermatocytes, pachytene (P) spermatocytes, lightly elongated round spermatids (8), and mature sperm, which are frequently released from the epithelium. In mice, spermiogenesis spans approximately 14 days during which developing cells "take" the 16 steps represented by Arabic numbers 1-16. During steps 1-8, the developing spermatids are referred to as round spermatids (corresponding to stages I-VIII), while steps 9-16 encompass elongating spermatids (associated with stages IX-XII). The abbreviations used are as follows: In = intermediate spermatogonia; B = type B spermatogonia; Pl = preleptotene spermatocyte; L = leptotene spermatocytes; Z = zygotene spermatocytes; P = pachytene spermatocytes; D = diplotene spermatocytes; m2°m = meiotic divisions *(Modified from Russell et al.[42])*

Spermiogenesis, *i.e.*, spermatid differentiation, covers the post-meiotic phase of spermatogenesis from round spermatids to spermatozoa. Spermiogenesis is further divided into 16 developmental steps (Figure 2), including 8 steps of round spermatid (steps 1-8) and 8 steps of elongating spermatid (steps 9-16) differentiation. During spermiogenesis dramatic morphological changes take place as round spermatids evolve towards mature spermatozoa equipped with specialized structures enabling their independent movement and fertilization upon encountering an egg. The major morphological transformations that take place are: polarization of round spermatids which encompasses the development of the acrosome (the head) on one side and a flagellum (the tail) on the other side followed by chromatin compaction and head shaping[32].

The acrosome is a membrane-bound vesicle that contains hydrolytic enzymes, such as hyaluronidase, acid phosphatase, glycohydrolases and proteases (acrosin), that when secreted help the sperm penetrate and fertilize an egg. In addition to its role in fertilization, the acrosome also contains other proteins involved in sperm motility and signaling pathways that help guide the sperm cell towards the egg[43]. Acrosomes vary in size and morphology, from the sickle shape in mice to cap-like structure in humans, but their basic structure and function are well-conserved[44,45]. Acrosome formation (Figure 3) begins early, in step 1 round spermatids, where the Golgi provides vesicles for it. Proacrosomal vesicles are detected in step 2 spermatids and a single round acrosomal vesicle emerges by step 3. This early formation is often referred to as the Golgi phase (step 1-3 in mouse). The following Cap phase (steps 4–7) is initiated as vesicles accumulate to expand the proacrosomal vesicle gradually over the anterior nucleus and finally, by step 8, the acrosome makes contact with the cellular membrane. By the time the Acrosome phase (steps 8-12) ends, a fully developed acrosome spreads over the entire anterior half of the developing sperms head[46]. Proper acrosome biogenesis requires coordination between different organelles including the endoplasmic reticulum (ER), the trans-Golgi network, the acroplaxome, the manchette and the nucleus[47,48]. Abnormalities in acrosome biogenesis can lead to morphologically compromised sperm and fertility problems. Owing to a plethora of KO mouse model studies, several proteins essential for proper acrosome development have been identified, including DPY19L2[49,50], FAM209[51], FAM71F1[52], GBA2[53,54], GOPC[55], PDCL2[56], PICK1[57], SPACA1[58], SSMEM1[59], ZPBP1[60,61] and AU040320[62]. In humans, defective acrosome biogenesis can lead to a rare but severe teratozoospermia known as globozoospermia i.e. round-headed sperm[63]. Mutations in two genes have been clearly demonstrated to cause this form of infertility: DPY19L2[49,64,65], and SPATA16[64,66,67] and putative mutation reported for other two: PICK1[61] and ZPBP1[61].
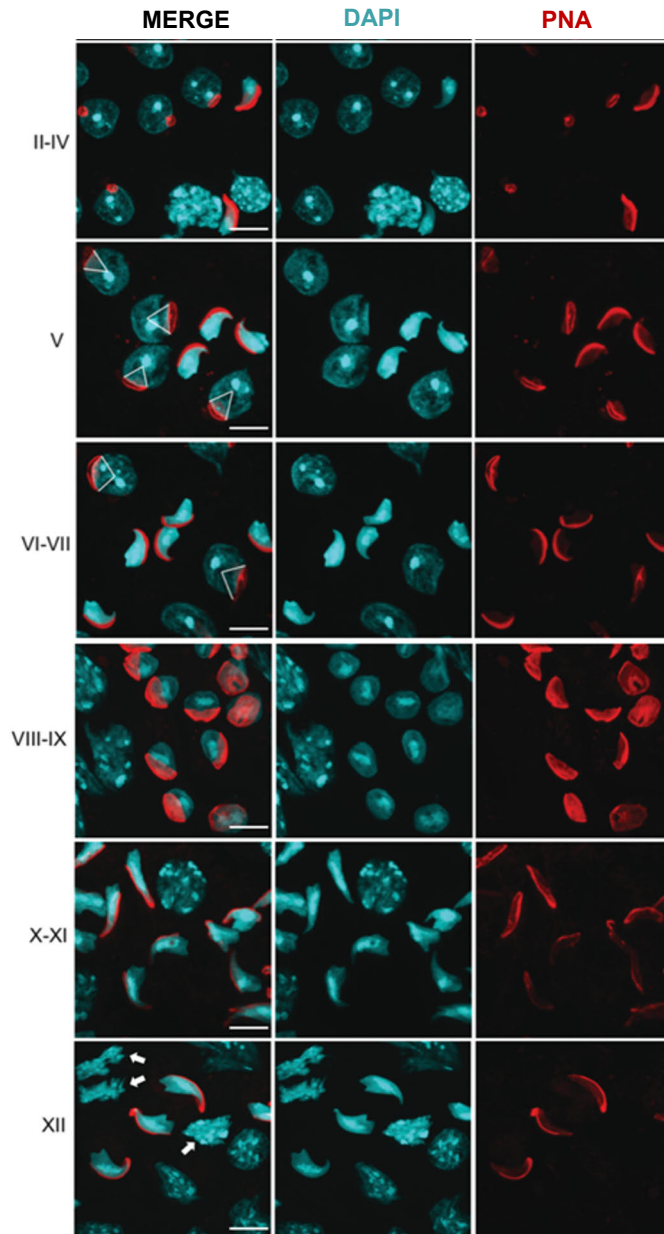
Figure 3. Acrosome development in mice. Formation of the acrosome is visualized by Rhodamine-conjugated peanut agglutin (PNA) in acetone-fixed squash preparations of mouse testis. Nuclei (cyan blue) are stained by DAPI. MERGE shows the overlay of nuclei and acrosome-stained channels. From top to bottom (from stage II-IV to XII): A single round acrosomal structure (red) on the nucleus (cyan blue) appears and subsequently flattens by step 4 spermatids (II-IV). The acrosome then extends from 40° to 95° (V) and further extends from 95° to 120° (VI-VII) finishing the Golgi and Cap phases of the acrosomal development. The Acrosome phase begins in step 8 round spermatids where the acrosome is fully extended (VIII-IX). By the time the acrosome phase ends the fully developed acrosome spreads over the entire anterior half of the developing sperms head. Scale bars: 10μm. (*Modified from Mäkelä et al.*[41])

Flagellum construction takes place on the opposite side of the nucleus to the acrosome. The flagellum can be divided into three parts: mid-piece, principal piece, and end piece. The flagellum first appears at step 2–3 round spermatids and it rapidly elongates after that (Figure 2). The building of the tail begins with the formation of an axoneme to which accessory structures such as outer dense fibers, fibrous sheath and mitochondrial sheath are later added. The axoneme is the major flagellar component and comprises nine doublet microtubules and the central microtubule pair (9 + 2 structure) which are surrounded by other protein complexes. During the axoneme formation, motor proteins are needed to actively transport proteins and lipids bidirectionally along the intraflagellar transport system (IFT) as no ribosomes exist in the flagellum[46,68,69].

The manchette is another microtubular-based structure that appears during spermiogenesis. The manchette is a transient structure that surrounds the caudal region of the sperm head. The manchette can be detected from step 8 when it is assembled until its disassembly at step 14. The manchette takes part in spermatid head shaping and nuclear remodeling. If its formation or function is disturbed abnormally shaped sperm heads and abnormally formed or flimsy tail structures can arise. The manchette also serves as a microtubular transport platform for intra-manchette transport. The origin of the microtubules of the manchette is not known but a region of the centriole has been suggested[69].

Nuclear condensation reduces the nuclear size gradually as chromatin within is packed tighter and tighter. This is accomplished by a genome wide near complete replacement of histones first by the nuclear transition proteins 1 and 2 (TNP1, TNP2) and then by the protamine 1 and 2 (PRM1, and PRM2). For roughly 1-10% of the genome histones are retained though the significance of this phenomenon is still unclear[70,71]. Finally, the nucleus obtains its typical ovoid shape with an acrosomal cap and fully developed tail attached to it via the mitochondria rich midpiece. At spermiation, sperm is released into the lumen, extra cytoplasm is shed, and sperm is transported to the epididymis for further maturation.

2.1.2   Stages of the seminiferous epithelial cycle

As depicted by Figure 2, the differentiating germ cells form concentric layers with predictable and recognizable compositions during spermatogenesis. The developmental trajectory of germ cells originates from the basement membrane and continues toward the lumen of the seminiferous tubules. At any given moment within any tubule segment, Sertoli cells together with 4-5 generations of germ cells are always present and at each point a certain type of haploid cell will only be found associating with specific types of spermatocytes and spermatogonia. Based on these

association patterns, in mice, the seminiferous epithelium can be divided into 12 stages (I-XII) that follow each other in a logical order[72,73].

Importantly, the stages do not present fixed states but continually change and develop as the differentiation of germ cell groups differentiate in synchrony. A full set of sequential stages corresponds to one cycle of the seminiferous epithelium. The completion of one round of spermatogenesis takes four cycles, and the layers of differentiating germ cells at any given time at any cross-section are temporally one seminiferous cycle apart from each other. In the mouse, the completion of one cycle takes 8.6 days, and the overall differentiation from a spermatogonia to a mature spermatozoon takes around 35 days[42].

While the concept of the cycle of the seminiferous epithelium was originally based on studies using periodic acid-Schiff (PAS) reaction to distinguish acrosomal development phase and thus specific steps of spermatid differentiation, the shear transillumination pattern of the seminiferous tubule at a specific stage is enough to facilitate the dissection of separate stages[74]. When observing intact seminiferous tubules, each stage absorbs and scatters light in a manner relative to the chromatin condensation of late post-meiotic spermatids present at any given stage. For example, at stage IX-XI, step 9-11 elongating spermatids have a low level of chromatin condensation which results in a visibly lower amount of light absorption. At stage IV-VIII, the step 15-16 elongating spermatids have maximal light absorption due to their fully condensed chromatin. The location of elongating spermatids within the epithelium (basal vs. apical) and bundling of elongating spermatids also facilitate the recognition of stages through the light microscope. Though not included in this thesis, we recently produced a protocol to use transillumination-assisted dissection of specific stages for downstream immunostaining analyses enabling a precise focus to be put on biological events taking place at specific phases of spermatogenesis[41]. Given the lack of scalable *in vitro* models for spermatogenesis, this method has a unique advantage of enabling short-term developmental and toxicological studies to be performed on stage-specific tubule segments *ex vivo*. Indeed, as will later be described, this method was used in one of the studies (II) included in this thesis.

2.1.3   The somatic cells of spermatogenesis

Production of testosterone and spermatogenesis are inherently interconnected, both regulated by endocrine hormones produced by the hypothalamus and pituitary and both are important for male fertility. Upon reaching sexual maturity, the successful initiation of testicular function is dependent on the hypothalamic gonadotropin-releasing hormone (GnRH) to stimulate the production of luteinizing hormone (LH) and follicle stimulating hormone (FSH) from the anterior pituitary. LH is transported

to the testes by the bloodstream. There **Leydig cells** respond to the LH stimulus by producing testosterone, a hormone needed for the development and maintenance of many physiological functions and the production of sperm. As testosterone diffuses locally in the seminiferous tubules a negative feedback loop for GnRH is activated. The hypothalamic-pituitary-testicular axis is therefore monitored and regulated to obtain a balance. In addition, FSH is needed for the optimal testicular development and maximal sperm production. Both testosterone and FSH act on receptors found on the Sertoli cells[75–77].

Sertoli cells are tall, columnar cells extending from the basal lamina to the lumen on the seminiferous tubules (Figure 1). Sertoli cells nurse immature germ cells to divide, undergo meiosis and differentiate into highly specialized haploid spermatozoa. Sertoli cells provide support to each of the 30-50 germ cells they are supporting [73,78,79]. In addition to providing physical support for the developing cells, Sertoli cells regulate their energy metabolism. Germ cells metabolic profile changes throughout their development. Spermatogonia can use glucose as their energy source, but more specialized germ cells, like meiotic spermatocytes and spermatids cannot and instead depend on lactate which is converted from glucose by Sertoli cells[80]. Fully functional Sertoli cells are required for spermatogenesis[81].

The blood-testis-barrier (BTB) is formed by specialized junctions between adjacent Sertoli cells near the basement membrane. The BTB divides the seminiferous epithelium into basal and apical (adluminal) compartments. A fully functional BTB is a dynamic physical and immunological wall that regulates the passage of molecules and cells from the basal compartment, exposed to environmental changes, into the protected luminal compartment and *vice versa*. Intact BTB is a requirement for fertility as it allows for the microenvironment behind the barrier to remain undisturbed and keeps the developing haploid germ cells protected from any attack by the immune system. The BTB mainly consists of actin-based tight junctions, basal ectoplasmic specialization, and gap junctions, along with intermediate filament-based desmosomes. The source material for spermatogenesis, SSCs, divide mitotically at the basal compartment on the basal membrane. When specific signals trigger their differentiation, the cells pass to the apical side through BTB in a coordinated event assisted by Sertoli cells and are thereafter maintained in a secluded microenvironment for meiotic and post-meiotic cells to develop further[82].

The apical ectoplasmic specialization between spermatids and Sertoli cells at the apical compartment of seminiferous tubules allows for proper orientation of spermatids as they develop. In contrast to the basal ectoplasmic specialization, the apical ectoplasmic specialization does not coexist with other junctions but is the only junction that holds spermatids to Sertoli cells. The apical ectoplasmic specialization is a highly dynamic structure undergoing rapid rounds of assembly and disassembly. It is first assembled when spermatids at step 8 begin elongation and become

polarized *ie*. transforming from round to elongating spermatids. Sertoli cells then stay attached to spermatids until spermiation. At this point the apical ectoplasmic specialization is disassembled and simultaneously the BTB is transiently "opened" or reorganized. The fully developed elongated spermatids (aka spermatozoa) are released and transported to the epididymis[83].

The epididymis is a convoluted, crescent-shaped tubular organ that connects the testis to the vas deferens (Figure 1) and is comprised of four anatomical segments: the initial segment, caput, corpus, and cauda in mice[84]. It can also be further segmented to 10 smaller areas separated by septa though these areas are yet to be fully characterized[85]. A recent study provided evidence of a subpopulation of epididymal vesicles that originate from a single segment[86]. The epididymal transit takes 10-15 days in most mammalian species but only 2-4 days in human[87]. During this time spermatozoa interact with the unique luminal environment of each epididymal region and segment created by at least six main cell types. Principal cells comprise the major group of epididymal cells in the adult mouse. They are responsible for absorption and secretion of molecules into the lumen and they produce and release epididymosomes which are exosomes with important roles in sperm competency and that have also been suggested to play a part in the epigenetic inheritance of paternal traits[88–91]. Together the narrow cells of initial segment and the clear cells of caput, corpus and cauda are thought to be the cells responsible for the acidic luminal environment that ensures that sperm remain quiescent until mating[92]. Apical cells of the initial segment have endocytic activity. Basal cells are attached to the basement membrane forming the structure of the tubule. Halo cells are immune cells that are found throughout the epididymal epithelium[93]. As sperm travels through the epididymis its concentration is greatly increased, and it gains ability to move and fertilize. In addition, sperm undergoes changes in nuclear compaction, plasma membrane composition, cytoskeletal structure, protein and non-coding RNA payload[94,95].

2.2   RNA – an overview

The programs that direct cellular development and maintenance are encoded in an organism's genome. Although every cell of an individual contains an identical genome, regulation of gene expression defines which RNAs are produced, and the level to which they are produced in each cell. Therefore, in all cells of an organism genome-wide transcription regulation defines the cellular phenotype and the cells' fate from differentiation to specific functions[96].

2.2.1   From DNA to RNA

Chromatin can be divided into different categories based on its structure at a given space and time. The majority of chromatin is present as heterochromatin, a condensed form of chromatin that is transcriptionally less active and mainly present at pericentric regions, telomeres, and other transcriptionally repressed regions. The second type, known as euchromatin is more open and transcriptionally active. The third specialized chromatin is only present at centromeres.

The nucleosome is the fundamental unit of chromatin. One nucleosome consists of approximately 146 base pairs (bp) of double strand DNA wrapped in 1.67 left-handed superhelical turns around an octamer of histone proteins: two copies of each of the four core histones H2A, H2B, H3, and H4. Each core histone has a globular domain at their C-terminus and an N-terminal tail that protrudes out of the nucleosome. Nucleosomes are connected by stretches of up to ~80 bp long linker DNA which is bound by linker histones such as H1 and its isoforms[97].

Epigenetic modifications targeting the nucleosome influence the chromatin structure and therefore gene function in a way that depends on the site and type of the modification[96]. Epigenetic modifications can either target the DNA strand or the histone proteins. DNA strand can be modified via methylation, a process where a methyl group is added often to the fifth carbon atom of a cytosine ring usually leading to reversible but stable gene inactivation. Epigenetic modifications of histones, which primarily target the N-terminal tails, but also the globular domains, are much more versatile. There is an ever-growing list of these modifications and their impact on cellular pathways, the complexity of which is only just beginning to be understood[98]. Each histone can be modified on multiple sites and by different modification types including methylation but also acetylation, phosphorylation, ubiquitylation and SUMOylation[99,100]. For example, though not included in this thesis, we recently showed that SUMOylation of the androgen receptor – a crucial transcription factor for the regulation of the male phenotype and fertility – is essential to normal male fertility as the lack of it leads to epididymal dysfunction and disruption of post-testicular sperm maturation[101]. The androgen receptor was among the first transcription factors shown to be SUMOylated[102].

Transcription from DNA to RNA starts when a gene is activated in the nucleus. For this to happen, the chromatin needs to be at euchromatin state, open and accessible to transcription factors which the cell controls by the addition of small chemical groups to the nucleosomes - epigenetic modifications - as described in the chapter above[97]. Transcription is the process by which RNA polymerases synthesize RNA molecules from the DNA template. The RNA polymerases do not have the ability to recognize the proper sites of transcription initiation. Instead, the core promoter sequence which contains specific sequence motifs is recognized by

transcription factor proteins that then recruit the polymerase. In eukaryotes, RNA polymerase I (Pol I) synthesizes the large ribosomal RNA precursor and Pol III produces transfer RNAs, the small ribosomal RNA and other short RNAs, whereas Pol II produces mRNAs, long non-coding RNAs and primaries of microRNAs and piRNAs. Pol II-dependent transcription is initiated when transcription factors, able to recognize a specific sequence of DNA, recruit the polymerase complex. Pol II complex then transcribes the whole gene to a pre-messenger RNA molecule, pre-mRNA[96].

Pre-mRNA contains both introns and exons but during active transcription, specific spliceosome complexes recognize the borders between exons and introns, remove the introns, and link exons together in a process known as splicing. During this event different parts of the pre-mRNA may be included or excluded to produce different isoforms. Alternative splicing (AS) machineries can generate mRNAs that differ in their coding or non-coding sequence through different mechanisms including exon skipping, choosing between mutually exclusive exons, intron retention or the usage of alternative splice sites blurring the boundary between introns and exons and creating an even larger variety of mRNA isoforms. Through these mechanisms, AS impacts mRNA stability, localization, translation efficiency and potentially even the reading frame, resulting in the generation of different protein isoforms with diverse functions and/or localizations. This property of eukaryotic genes allows an increase in the complexity of the genome, without considerably increasing its size[103].

The mRNA molecule requires processed 5' and 3' ends to transform from its pre-mRNA state to mature[96]. The processed ends, among other things, protect the mRNA's integrity and help its export from the nucleus to the cytosol. A cap of a modified guanine is added to the beginning also known as the 5' end[104]. At the 3' end factors of the cleavage and polyadenylation machinery travel with RNA pol II along the mRNA. Upon encountering a polyadenylation signal, an endonucleolytic cleavage is followed by the synthesis of a poly(A) tail – the addition of 200–250 adenosine residues – on the 3' terminus[96,105]. This polyadenylation process is closely linked to transcription termination.

Ribonucleoprotein complexes which contain the newly synthesized mRNA and RBPs represent the final form of RNA before it leaves the nucleus, and the primary way mRNA is found in eukaryotic cells. RBPs are proteins that bind RNA through one or multiple globular RNA-binding domains and affect RNA function and/or metabolism. RBPs do so by binding the RNA via well-characterized RNA-binding domains like the RNA recognition motif (also known as RNA-binding domain) or the DEAD box helicase domain[106] or otherwise by non-canonical means[107] and by recruiting other proteins able to regulate RNA. RNPs coordinate mRNAs, including

their transport from the nucleus to the cytoplasm, their intracellular localization, translation efficiency of the mRNA in the cytoplasm, and the stability of mRNAs. And on the other hand, RNAs can impact the function of RBPs as well and, in fact, the interaction between RNAs and proteins in these complexes can widely be considered as crosstalk more than anything else[108,109]. In addition to RNA-protein interactions, RNP complexes can further associate with other RNP complexes potentially involved in related functions or addressed to the same subcellular location thus forming larger RNP granules. These membrane-less RNP granules have been characterized in different cell types both in the nucleus (e.g. paraspeckles[110]) and the cytoplasm (e.g. P-bodies, stress granules[111]). A subclass of RNP granules particularly relevant to this thesis – germ granules – will be discussed separately.

2.2.2   Translation

During translation, the genetic information in mRNA is decoded to create a sequence of amino acids. Each group of three bases constitutes a codon, and each codon specifies a particular amino acid. The mRNA sequence is thus used as a template to construct a chain of amino acids that folds up into its unique three-dimensional protein conformation. The translation machinery is found within a specialized organelle with peptidyl transferase activity called the ribosome[112]. Recently, a growing number of studies have shown that rather than being a one-size-fits-all machines responsible for mRNA translation, ribosomes are heterogeneous and exhibit tissue-specific functioning in the regulation of protein synthesis[113]. Tissue-specificity of ribosomal components and phenotypic analysis of ribosomal gene mutations indicate that certain subtypes may be particularly important for development processes like embryogenesis, spermatogenesis and oogenesis[114]. For example, in male germ cells a special ribosome with a specialized nascent polypeptide exit tunnel is assembled by a testis-specific paralog of ribosomal large subunit protein RPL39, RPL39L. Ribosome[ST] regulates the folding of a subset of male germ-cell-specific proteins and importantly is not replaceable by other ribosomes. Deletion of Ribosome[ST] or RPL39L leads to defective spermatogenesis in mice[115,116].

2.2.3   Untranslated regions

Importantly, not all regions of an mRNA molecule correspond to amino acids. Both ends of an mRNA molecule contain sequences flanking the coding region that are not translated and are thus called untranslated regions (UTR). UTRs partake in regulating the stability, function, and localization of the mRNA but do not directly contribute to the protein sequence and are thus non-coding.

5'UTR resides downstream the 5' end of the mRNA, located between the first nucleotide that is transcribed and the start codon (AUG) of the coding region. The 5'UTR is critical for ribosome recruitment and start codon choice[117]. In mammals, roughly half of all 5'UTRs also contain a segment known as an upstream open reading frame (uORF) with important regulatory functions and whose mutations have been connected to different diseases[118]. uORF is defined as an open reading frame situated upstream of the main open reading frame or one that overlaps with it if the uORF is out of frame with the main-ORF. uORFs can engage ribosomes and can function both by titrating them away from the main ORF through ribosome stalling or, under certain conditions, activate main ORF translation. Furthermore, recent findings of additional cis- and trans-acting mechanisms challenge the very definition of the 5'UTR as untranslated, as bioactive microproteins/micropeptides encoded by uORFs themselves have been discovered[119,120].

3'UTR resides at the 3' end of the mRNA. The 3'UTR functional structure is based on cis-regulatory elements that are short sequences, often present as clusters, recognized and bound by trans-regulatory factors, such as RBPs or other RNAs, either on sequence basis or through secondary structure motif interactions[121]. Other RNAs here mainly refers to microRNAs (miRNAs), which are 18–24 nt non-coding RNAs that function by both degrading and inhibiting translation of mRNAs[122] while RBPs represent an extremely heterogenous group of proteins that often serve as adaptors to other effector proteins. Together the miRNAs and RBPs play important roles in the post-transcriptional control of their cognate mRNA by altering degradation rates, coordinating subcellular localization, and regulating translation efficiency[123].

3'UTR length evidently determines the number of possible cis-regulatory elements within the sequence including binding the sites of RBPs and miRNAs[124]. Importantly, for many genes no set 3'UTR length or sequence exists but instead different 3'UTRs are produced depending on the tissue/cell type and cellular status[125]. 3'-end sequencing methods have been developed to try and measure the length of 3'UTRs and to quantify alternative 3' UTR variants in different cell-types and tissues opening venues for understanding the biological relevance of 3'UTR variants[126,127]. While tissue-restricted genes tend to have unique 3' UTRs, most ubiquitous genes generate multiple variants. During transformation and differentiation, fixed-UTR-genes tend to modify the mRNA abundance levels, while genes with 3'UTR length variants mostly change the variant ratios maintaining mRNA abundance[128]. Therefore, depending on prevailing conditions, the 3'UTR length of a given mRNA can change dynamically altering the availability of its cis-regulatory elements. As effector proteins cannot usually directly bind to the cis-regulatory elements, the cell regulates their access by fine-tuning the production of RBP adaptors. For example, more than 10 RBPs are known to bind to AU-rich

elements, some of them leading to the recruitment of the exosome complex and thus degradation of the mRNA and others, such as HuR that is unable to recruit the exosome, leading to stabilization of the mRNA[121]. The cell simultaneously regulates the 3'UTR length and the production of RBPs whose competition and cooperativity ultimately determines the functional outcome for the mRNA[121,129]. To understand the biological relevance of 3'UTRs one must, thus, consider the 3'UTR composition, the RBPs expressed at a given time as well as the larger context. For example, in somatic cells, shorter 3′ UTRs have been shown to generally stabilize mRNAs, at least in part due to a smaller number of possible miRNA binding sites[130]. Whereas, in mouse oocytes longer 3′ UTRs are associated with increased rather than decreased stability of their cognate mRNAs[131]. Therefore, interpreting how the length of the UTR corresponds to the stability of the cognate mRNAs is far from straightforward and general rules are hard to set.

Alternative polyadenylation (AP) usually defines the length of the 3'UTR, though alternative splicing can also impact the length if the 3'UTR contains an internal intron[132]. There is an on-going debate on whether the phenomenon of alternative polyadenylation is a beneficial regulatory process[133–136] or a non-adaptive molecular error[137,138]. In any case, more than half of human and mouse genes generate alternative mRNA isoforms that encode proteins with identical amino acid sequences that differ in their 3'UTRs[121,139]. Male germ cells are known to utilize special polyadenylation patterns that are uncommon in somatic cells. Several studies have demonstrated that the use of unique polyadenylation sites in mammalian testis usually results in mRNAs with shorter rather than longer 3′ UTRs[140,141]. However, long 3'UTR containing transcripts are also expressed in the testis where these transcripts accumulate to germ granules. Linked to RNA regulatory pathways such as the nonsense mediated RNA decay these germ granules may provide the long 3'UTR containing transcripts a safe haven, storage facility, quality control checkpoint or a platform for other regulation[142,143]. A recent study in *drosophila* male germ line demonstrated that developmentally regulated alternative 3′ end cleavage alters the translation state of many mRNAs. The study found that more than 500 genes in developing germ cells produce mRNAs with long 3'UTRs in the early stages, in proliferating spermatogonia, but shorter 3'UTRs in later stages, in spermatocytes. This change in 3'UTR length was accompanied by an effect on mRNAs translation activity. For 50 mRNAs the isoform with long 3'UTRs was not translated at all but a truncated 3'UTR expressed from the same gene lead to translation in later stages. The study also found that some mRNA molecules with short 3'UTRs that were not translated in early stages can be translated in later stages as for 200 genes, transcript isoforms with a long 3′ UTR expressed in spermatogonia were translated, while their partner short 3′ UTR mRNA isoforms produced from the same gene in young spermatocytes were not. This stage-specific on → off → on

comigration of mRNA isoforms to ribosomes suggests the AP mechanism facilitates a dynamic regulation of protein production in germ cell development by inducing 3′ UTR shortening in early spermatocytes, causing a clear reduction in protein production while transcription continues and provides mRNAs that can be translated at later stages, f.e. in round spermatids[144].

2.2.4   Nonsense mediated RNA decay

Translation termination is indicated when one of the three potential termination codons reaches the ribosome. Proper termination requires the presence of an in-frame termination codon and the engagement of eukaryotic release factor 1 (eRF1) and eukaryotic release factor 3 (eRF3). Canonical translation termination consists of: (1) recognition of the termination signal, (2) hydrolysis of the terminal peptidyl-tRNA bond and release of the peptide, and (3) dissociation of the ribosome into its 60S and 40S subunits[97]. In addition to protein synthesis, translation acts as a quality-control mechanism for template mRNAs, newly synthesized proteins, and the translation machinery itself. Under pristine conditions, the presence of a termination codon in the A site of the ribosome is recognized by eRF1 and eRF3 leading to hydrolysis of the terminal peptidyl-transfer RNA (tRNA) bond and release of the new peptide. However, when translation termination occurs under unfavourable conditions, a translation-coupled RNA degradation pathway may be activated[145].

The **nonsense-mediated RNA decay (NMD)** pathway is arguably the best-studied eukaryotic mRNA surveillance pathway. NMD is a translation-dependent RNA turnover mechanism[146] that degrades defective mRNAs harbouring premature termination codons (PTCs) that encode truncated proteins but also normal mRNAs encoding full-length proteins that are defined by a stop codon in specific contexts[147]. Thus, NMD is implicated in a wide range of biological processes affecting cellular homeostasis.

Target selection criteria *i.e.,* the translation termination conditions that result in NMD and how they differ from proper termination conditions are not yet fully understood. Known features to trigger NMD – NMD inducing features (NIFs) – include: an exon–exon junction located nucleotides downstream of the start codon defining the main open reading frame ("dEJ"), long 3′ UTRs lacking exon–exon junctions, an open reading frame upstream of the main open reading frame (uORF)[148,149].

NMD activation relies on the formation of dynamic protein complexes on the mRNA once it has been recognized as an NMD target. Briefly, interactions between (up-frameshift) proteins UPF1[150,151], UPF2[152,153], and UPF3B[154] trigger UPF1 phosphorylation by the suppressor with morphogenetic effects on genitalia (SMG) kinase SMG1 whose kinase activity is controlled by SMG8 and SMG9.

Phosphorylated UPF1 further recruits SMG6 and/or SMG5 and SMG7, which are involved in executing the actual mRNA degradation step[155].

   The final execution of decay has been described for two distinct branches involving either the SMG5-SMG7 heterodimer or the endonuclease SMG6. The former relies on the interaction of phosphorylated UPF1 with the SMG5-SMG7, which recruits the CCR4-NOT deadenylation complex[156,157]. Target mRNA is thereafter deadenylated, followed by decapping and exonucleolytic degradation[148,158]. The latter branch involves SMG6 whose interaction with UPF1 results in a single-stranded endonucleolytic cleavage of the target-transcript in the vicinity of the NMD-triggering stop codon. The resulting two decay intermediates are thereafter rapidly removed by exonucleases that are not NMD specific[148,159]. How division of labor between the degradation pathways is arranged is not known. They have long been regarded as independent pathways as the downregulation of individual factors SMG5, SMG6, or SMG7 in cell culture conditions only partially inhibits NMD. Incidentally not, however, to equal amount as the depletion of SMG6 resulted in much more severe impairment of NMD than that of SMG7, which has led to the presumption that endonucleolytic cleavage may be the primary decay pathway, while deadenylation acts as a backup system and/or supportive process, at least in HeLa cells[160]. A recent study on nonsense-codon-containing mRNAs in cystic fibrosis patients showed at all studied mRNAs harboring nonsense codons were degraded by the SMG6-mediated endonucleolytic pathway and not the SMG5-SMG7 pathway[161]. Furthermore, transcriptome-wide analysis has demonstrated the redundancy of these two pathways, as both largely target the same transcripts[160]. Recent findings, however, indicate the pathways may not act fully independently but instead there may be a mechanistic overlap. The new model suggests that when SMG5 and SMG7 – together or individually – are recruited to phosphorylated UPF1 this acts as an additional licensing step needed for endonucleolysis which is performed by SMG6. Therefore a level of double authentication seems to be active for at least certain conditions in cell culture though no animal model/tissue data currently exist to validate this model *in vivo*[162].

2.2.5   Diverse roles of NMD components

Telomere maintenance has also been linked to several NMD factors, including SMG1, SMG5, SMG6, SMG7, UPF1 and UPF2[163,164]. This overlapping involvement of NMD factors in regulating telomeres – stabilizing repetitive DNA sequences at the end of chromosomes – adds complexity to the interpretation of any phenotypic effects resulting from mutations that impair NMD factor functions in KO animal models. Originally discovered as a telomerase associated factor in yeast, mammalian *Smg5*, *Smg6*, and *Smg7* are homologs of the Ever shorter telomere 1 (*Est1*) where

mutants lacking *Est1* exhibit a gradual telomere shortening and limited cell viability[165]. Est1 acts as a bridge connecting telomerase, the RNA-dependent DNA polymerase that synthesizes telomeric DNA sequences, and Cdc13 (mammalian Pot1) while directly binding to telomerase RNA, playing a crucial role in telomerase activation and telomere maintenance[165–168]. One of *Est1* human homologs, *Smg6*, has been investigated in relation to telomerase and telomeres. Similar to its yeast counterpart, *Smg6* has been reported to participate in the regulation of telomere maintenance and the viability of human cancer cells. Intriguingly, both overexpression and knockdown of SMG6 in human cells lead to telomere shortening or loss and cell cycle arrest[163,169,170]. In human pathologies the impact of SMG6 has been linked to its role in regulating telomerase activity rather than its role in NMD[171]. On the other hand, in mice, *Smg6* has been shown to be essential for embryonic development, and somewhat surprisingly, not because of its telomere function as one might assume, but due to its role in the NMD pathway[172]. These findings underscore the significant role of SMG6 in diverse cellular processes.

2.3 RNA centric peculiarities of germ cells

The testis has long been acknowledged as the fastest-evolving organ with some recognized phenotypical and molecular peculiarities[173–176]. During spermatogenesis active transcription takes place from early spermatogonia onwards with transcript diversity peaking at meiotic spermatocytes and round spermatids, whose transcriptomes are uniquely complex. However as the following specialization replaces most of the histones with protamines the arising cells, elongating spermatids (and spermatozoa), are rendered transcriptionally inactive[177–180]. Thus, the program of spermiogenesis – the final steps of spermatogenesis - relies on gene products that are transcribed earlier and stored in RNP complexes until later need. This uncoupling between transcription and translation, is a curious feature of gene regulation in spermiogenesis. Consequently, within testicular tissue, both extremes of transcriptionally active and transcriptionally suppressed cells, can be found. Comparisons of the testis with other tissues have further uncovered unusual features. Apart from the previously mentioned, unusual polyadenylation patterns, these features include the accumulation of certain RNAs and RNA features, overall higher complexity transcriptomes and the birth of new genes. The following is a synopsis of these peculiarities.

2.3.1 Complex transcriptomes

Transcriptome complexity can be measured by how many genes are expressed in a cell or cells *i.e.* the full set of RNA molecules in a sample *i.e.* the full set of reads

corresponding to genomic loci in RNA-seq data (or equivalent analysis). When comparing sequencing results from different analysis, the different strategies and technologies used must be considered. Each RNA-seq analysis is limited by the chosen sequencing depth (library size) and can be biased depending on the sequencing approach (*e.g.,* full-length RNA-seq or 3'-biased). The results also depend on the sample type so in the case of spermatogenesis, whether the sample be full testes, isolated/enriched group of cells or single cells.

RNA-seq analyses on full testis have shown that the testes have one of the most complex transcriptomes of any organ in the body across multiple species[173,180,181]. One analysis of testis and five other organs (brain, cerebellum, heart, kidney, and liver) in human, rhesus macaque, mouse, opossum, and chicken with same sequencing parameters, revealed more autosomal protein-coding transcripts in the testis than other organs, in all five species. In a bulk tissue RNA-seq analysis, most tissues were shown to express 60-70% of the protein-coding genes while testis was shown to express 84%[182]. Furthermore more long non-coding RNAs and intergenic elements including pseudogenes, transposable elements, and unannotated intergenic sequences were detected as well demonstrating that the complexity is not limited to protein coding genes in the testis[173]. In these analyses the transcriptomic complexity could evidently originate either from the combination of different cells in a bulk tissue sample or it could be an innate property of certain somatic cells or certain germ cells within that sample. Studies on isolated germ cell populations from mouse and human later demonstrated that at a given read depth more genes are detected in certain germ cells populations compared to other tissues, and that, as spermatogenesis progresses from spermatogonia to spermatids, complexity increases[183,184]. Conversely, some recent single cell RNA-seq (scRNA-seq) studies indicate that the amount of genes expressed by later-stage cells, such as elongated spermatids, is actually less than in earlier stages[185–187]. At the same read depth, the number of genes detected in a cell progressively decreases from spermatogonia to spermatocytes to round and elongated spermatids[185]. By comparing gene expression patterns in different cell types using a Gini index, the inequality in gene expression within each cell can be measured. The Gini index reflects how evenly genes are expressed, with cells expressing many genes at very low levels being considered more uneven. After accounting for sequencing depth, systematic differences among the germ cells were detected. Specifically, as cells progressed from spermatogonia to elongating spermatids, an increasing Gini index was seen, indicating that germ cells in later stages had greater inequality in gene expression, as if the later stage cells would concentrate their expression efforts on fewer genes to serve a narrower range of biological functions[185].

In summary, while according to bulk tissue and enriched cell populations analyses the testis has more complexity, single-cell data contradicts this finding by

showing the later-stage cells are progressively less and less complex. However, as each cell undergoes fast transformative events and has a distinct transcriptomic profile, the RNA-seq data always reflects the emergent content of different ensembles, where the cells may, in fact, collectively express more genes when measured as a mixture. And as each cell follows the same trajectory eventually reaching all steps and corresponding transcriptomic profiles, cell group analysis might – in fact – reveal the full story of a cells transcriptomic profile more so than a snapshot taken from a single cell analysis. In any case, there is no denying the complexity this tissue's transcriptome exhibits[173,185–187].

2.3.2   Behind the complexity

Several research groups have sought to understand the significance and meaning behind such unique transcriptional regulation taking place during spermatogenesis. Firstly, providing the simplest answer to high complexity is the fact that as spermatogenesis relies on a wide range of proteins expressed in a timely manner at each distinct developmental a simple functional need for a wide range of proteins may be required[188,189]. However, as mentioned the transcriptome of germ cells consists of more than protein-coding RNAs and there is a notable discordance between the transcriptome and the proteome in the testis[190,191]. Therefore, widespread transcription does not simply lead to widespread protein production, as the central dogma of molecular biology would suggest. Instead, other justifications for the complexity need to be considered.

Leaky transcription as the result of massive chromatin reorganization has been proposed[192,193]. The most striking change in accessible chromatin occurs in intergenic and intronic regions and takes place early in spermatogenesis during the mitosis-to-meiosis transition. While the vast majority of accessible chromatin in spermatogonia is being closed, new areas of intergenic and intronic chromatin are becoming accessible in pachytene spermatocytes[194]. This leads to a genome-wide switch between spermatogonia and pachytene spermatocytes. Thousands of somatic/progenitor genes are suppressed, and simultaneously thousands of late spermatogenesis genes activated. Mitosis-to-meiosis transition therefore involves significant chromatin reorganisation and is marked by new areas of the chromatin to effector proteins. However, the following meiosis-to-postmeiosis transition is marked by a different program leading to chromatin closure that effectively renders most of the chromatin inaccessible. These events exposing chromatin in timely waves could create openings for the transcription machinery. And therefore, transcripts arising due to momentary and randomly occurring access of the transcriptome machinery to promoters could contribute to the wide variety of transcripts in germ cells.

Transcriptional scanning is one model currently being explored. A recent study found that spermatogenesis-expressed genes have lower germline mutation rates in the population than genes not expressed during spermatogenesis and the reduction is more evident on the transcribed strand[187]. The study suggests that the pervasive transcription taking place during spermatogenesis is beneficial for the maintenance of the germ line as it maintains DNA sequence integrity by correcting DNA damage through a mechanism they named 'transcriptional scanning'. This transcription-coupled repair (TCR) process could potentially mitigate some of the effects of transcription-associated mutagenesis (TAM)[195], which a process known to increase damage such as oxidative lesions in the coding, non-transcribed strand, and thus mutagenesis, in the germline. The study suggests that transcriptional scanning modulates mutation rates in germ cells in a gene-specific manner. For the majority of genes, DNA sequence integrity is maintained but it seems that some flexibility to allow faster evolution rates is given for specific subsets such as genes in the sensory and immune defence line[187]. Importantly, the study suggests that transcripts that arise during spermatogenesis would not only be required for filling the needs of each developing germ cell but also contribute to the modulation of evolution rates.

"Genoinformative markers" (GIMs) were recently brought up by another study supporting the TCR model. According to the study a large class of mammalian genes exhibit allelic bias linked to the haploid genotype of the cell. While haploid round spermatids are known to maintain their diploid needs by sharing gene products through cytoplasmic bridges thus decreasing phenotypic differences, single cell analysis uncovered that a substantial group of mammalian genes, "genoinformative markers" (GIMs), are not in fact fully shared. These GIMs comprise 31-52% of spermatid expressed genes in several mammalian species, and they tend to be conserved between individuals and between homologs of different species. GIMs encoding proteins that are not shared between round spermatids across cytoplasmic bridges may have an impact on sperm competition as these non-shared proteins can affect its eventual function and ability of the cell to fertilize an egg. Therefore GIMs can affect natural selection via uneven spreading of alleles through generations[196]. On average heightened selective forces are put on spermatogenesis genes, but a subset of GIMs experience further increases, loss-of-function intolerance, and transmission ratio distortion. This is consistent with a hypothesis that a group of GIMs act as selfish genetic elements spreading alleles unevenly. The study suggested that for GIMs that have functions in somatic and germ cells, an evolutionary conflict could arise when an optimal function in sperm turns out to be detrimental for somatic cells. As GIMs are significantly enriched for testis-specific gene expression, paralogs, and isoforms, a level of evolutionary pressure exists to avoid this conflict. Spermatocytes and spermatids have been shown to contain an extremely wide range of alternatively spliced protein-coding transcripts[197–200] and an unusually diverse set

of intergenic unannotated transcripts[173,201,202]. In addition, while novel isoform expression is distributed equally across spermatogenesis, new genes arise primarily in meiotic and post-meiotic cells. While most of the novel isoforms retain their protein coding potential the novel genes usually do not[203]. The GIM phenomenon may explain why the testis gene expression patterns are an outlier compared to any other tissues.

Alternative Splicing affects most multi-exonic genes[204]. AS results from the combinatorial action of multiple sequence-specific RNA binding proteins (RBPs) that recognize motifs in the pre-mRNA, and subsequently promote or repress the splicing of alternative exons[205]. Tissue-specificity of splicing is, in fact, partially controlled by the tissue-specific expression of RBPs though other factors including previously mentioned epigenetic modification of the chromatin, transcription-coupled processes and cellular pathways that modify the activity of RBPs are also involved. Combined, highly complex tissue specific splicing patterns arise. Though AS is ubiquitous for all eukaryotic cells, brain and testes express a wider repertoire of mRNA isoforms that differ by inclusion or exclusion of an exon[206,207] and have the highest variation in splicing factor expression[208]. Compared to other organs, the brain and the testis also experience more significant changes in inclusion frequencies through time (called 'developmentally dynamic AS' or devAS). While the brain's surplus of devAS events remains when restricting the analysis to pre-sexual maturity stages and therefore AS may be particularly important for this organ's development, for testis the excess of devAS disappears when considering pre-sexual maturation. Therefore in testis the high devAS number probably reflects testicular cell composition rather than a developmental AS program switch[209].

New genes that encode new proteins are a major source of evolutionary innovation. Throughout evolution, three primary mechanisms are responsible for bringing new genes about: gene duplication, retrotransposition, and the conversion of noncoding DNA to coding genes[210,211]. *De novo* genes are typically identified by comparing the genomes and transcriptomes of closely related species. By definition '*de novo* gene' refers to a gene that is found to be present in a recent species or lineage but absent in the older ones. The previously mentioned accessibility of chromatin and pervasive transcription in postmeiotic cells can create the perfect opportunity for new genes to emerge which could explain why, in mammals, testis accumulates de novo genes which tend to be highly or uniquely expressed by testis[212–214]. If a gene is beneficial for reproduction, it is likely to quickly become prevalent within a population, while those genes that are harmful to reproductive success are more likely to be eliminated from the population. This results in a rapid selection of advantageous genes and the elimination of disadvantageous ones within the population. The importance of de novo genes to fertility is still unclear. While one study, in mice, found that 17 out of the 19 studied testis-specific genes were

required for normal male fertility[215], another study demonstrated no fertility effect arose from a depletion of a single gene deletion from a group of 54 evolutionarily conserved and testis-enriched genes[216]. The discrepancy may be due to differences in the selected genes for targeting as there was no overlap between the two sets of selected genes. Similarly, in recent years, several studies targeting a single testis-enriched gene have emerged with equally contradictory results, most having no clear impact of spermatogenesis[217–219] with few exceptions where testis-enriched genes were found indispensable, either for spermatogenesis itself[220] or sperm-oocyte-fusion[221]. Furthermore, another set of 12 testis-enriched genes in male fertility were recently tested using knockout mouse models generated by clustered regularly interspaced short palindromic repeats/CRISPR-associated protein 9 (CRISPR/Cas9) technology revealing that none of them have an essential role for spermatogenesis[222]. Altogether, despite a biased testis expression, most studied testis-enriched genes to date appear to be dispensable for spermatogenesis highlighting the fact that, by itself, the high expression level of a gene is not a perfect indicator of its importance. Of note, for some of the studied genes, a very basic level of fertility investigation (*e.g.* only mating trials, sperm count, etc.) were conducted leaving thus the possibility for more subtle changes in fertility could have been missed. Overall, the functional role of testis-enriched *de novo* genes remains obscure.

2.4   Germ granules

A fundamental problem in cell biology is how cellular space is organized to enable complex biochemical reactions at optimal kinetics. One way to achieve spatiotemporal control is to regulate the localization of components by creating compartments limited by membranes. These classic organelles, such as mitochondria[223] or lysosomes[224], are surrounded by a lipid bilayer, a physical barrier impermeable to most biological molecules and what is allowed inside is regulated by protein complexes at the membrane. However, many cellular compartments that bring together proteins and nucleic acids are not bound by membranes.

Large membraneless RNP granules, germ granules, are present in the germline of most if not all sexually reproducing metazoans[25,225–227]. 'Germinal granules' of *Xenopus laevis*, 'Polar granules' or 'nuage' of *Drosophila melanogaster* and 'P granules' of *Caenorhabditis elegans* represent maternal germ granules where maternal mRNAs required for germ cell specification are stored in the early embryo to time their translation during the establishment of the germline[228]. In mammals, similar granules appear long after the germ lineage has already been established, and they instead function in germ cell differentiation. In female mice, Balbiani bodies, large cytoplasmic granules found in oocytes, contain various RNA molecules and proteins involved in early oocyte development and maturation[229]. In male mice,

during male germ cell differentiation, at a time point when a remarkably large percentage of the genome is transcribed, two particularly prominent cytoplasmic germ granules appear: the intermitochondrial cement (IMC) and the chromatoid body (CB)[25] (Figure 4). While germ granules represent a heterogenous group of structures appearing at different times and in different cells, they all contain RNA species and RNA binding proteins are thought, therefore, to partake in genome control and RNA regulation at different levels.

Germ cell condensates is another way to describe the heterogenous group of germ granules. Biomolecular condensates[230], by definition, lack surrounding membranes but concentrate proteins and nucleic acids forming distinct structures. Biomolecular condensates form through phase separation which occurs when molecules locally reach a concentration threshold at which they demix from the surrounding milieu. Some of such biomolecular condensates exist in a solid-like state with little component exchange[231] while others behave as liquid-like droplets with components dynamically diffusing in and out of the granule[232]. Biomolecular condensates are often non-uniform and distinct sub-domains or compartments within a condensate can be detected[233]. Germ granules were recently proven to behave like liquid droplets[234]. A lot of the initial pioneering work was done with P granules that were shown to exhibit multiple liquid-like behaviors including fusion, dripping, and wetting, and fluorescence recovery after photobleaching (FRAP)[235]. Similar liquid-like characteristics have since been observed in other germ granules and liquid-liquid phase separation (LLPS) is currently a flourishing topic in the germ cell field[233].
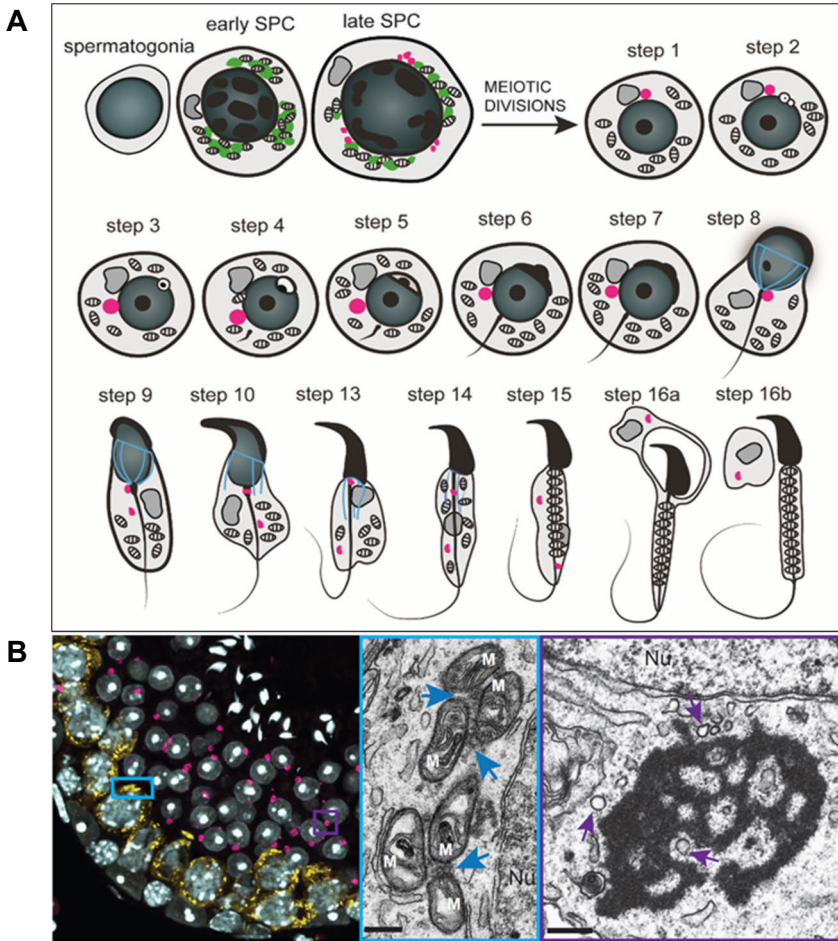
Figure 4. Male germ granules: the IMC and the CB. **A)** The IMC (green) is prominent in mid and late pachytene spermatocytes appearing as granular material intermingled with mitochondria. The CB precursors (pink) co-exist with the IMC in late spermatocytes. A single large perinuclear CB (pink) first appears in early round spermatids. In step 8 round spermatids, the CB is found at the basis of the flagellum. In elongating spermatids, the late CB splits into two separate structures. One fragment stays in the cytoplasm and the other forms a ring around the basis of the flagellum and migrates distally along the flagellum during the mitochondrial sheath formation. In step 16 elongating spermatids, the CB can no longer be detected. The steps of spermatid differentiation are indicated (steps 1–16). A transient microtubular structure, manchette, is shown in blue. The Golgi complex is depicted as a darker gray structure in all cells. **B)** The immunofluorescence image (left) shows a typical germ granule staining of a stage VII-VIII seminiferous tubule cross-section from a wildtype mouse testis. PIWIL2 antibody (yellow) labels the IMC in pachytene spermatocytes and DDX25 (pink) labels the CB in round spermatids. Nuclei (white) are stained with DAPI. The electron microscopy images (middle and right) visualize the electron dense appearance of the IMC and the CB. The IMC (blue arrows) appears as a dense material between the mitochondrial clusters. The CB presents as electron-dense irregularly shaped large (~1 μm in diameter) structure surrounded by small vesicles (purple arrows) that are also often found within its lobes. Scale bars for electron microscopy images: 250 nm. Nu, nucleus; M, mitochondria *(Modified from Lehtiniemi and Kotaja[236])*.

2.4.1   The dynamics of germ granules

During spermatogenesis, germ granules undergo regulated changes in composition, morphology, and localization (Figure 4).

The IMC, via electron microscopy, appears as rich electron-dense material associated with clustered mitochondria with no limiting membranes. The IMC is present in many cell types like fetal prospermatogonia and postnatal spermatogonia but is particularly prominent in mid-to-late pachytene spermatocytes. As mitochondria are dispersed during and after meiotic divisions, and the IMC disappears and is no longer detectable in haploid cells[42,237,238].

CB precursors co-exist with the IMC for a short time, in very late pachytene spermatocytes just before the first meiotic division. There the initial CB material, small electron-dense granules, intermingled with small vesicles, but not with mitochondria, associate with the nuclear envelope. By the late diplotene stage, the IMC is disintegrated, while the CB precursors condense to form a few large (0.5 µm) electron-dense perinuclear bodies. After meiosis, a single big (~1 µm) CB arises for the first time in step 1 round spermatids. The CB can thereafter be detected throughout round spermatid differentiation (steps 1-8)[227,239,240].

The CB, much like the IMC, appears as an electron dense mass often seen by the nuclear membrane. On closer examination the CB is an accumulation of exceedingly thin filaments that form a singular compact structure or a network of dense strands of varying thickness. These strands bound interstices or irregular shapes that are occupied by the cytoplasm and small vesicles that are also frequently observed around the periphery of the organelle[237]. The CB appears at the time of active transcription during spermatogenesis. The largest CBs are observed from steps 4 to step 6. In step 7 round spermatids, the CB starts decreasing in size and moving towards the basis of the flagellum[226,237]. The size is dramatically reduced in elongating spermatids, its protein composition changes[241] and during elongation, the CB splits into two: one fragment forms a dense sphere discarded with most of the cytoplasm in the residual body[237,242,243] but the other forms a ring around the basis of the flagellum. The late CB then moves along the flagellum together with the annulus which is a ring-shaped structure separating the middle piece and principal piece of the tail. To date the biological role of this late CB is a mystery but as mitochondria are seen associated with the axoneme on coattails of the CB, its role in the formation of the mitochondrial sheath has been suggested[237,243]. At step 16, in elongating spermatids, the CB is no longer visible but the details regarding its disintegration are not yet understood (Figure 4).

Constant remodelling is a characteristic feature of many germ granules. The CB is a dynamic granule that continually receives and exports new material, is under continuous structural reformation and can be seen moving to different cellular locations continuously[244–246]. The movement of the CB is microtubule-dependent and

can be disrupted by using microtubule-depolymerizing drugs, which also cause the CB to break into smaller fragments[247]. The CB is usually found next to the nuclear membrane where it continuously moves, reshapes, and travels along the nuclear envelope making frequent contacts with it. In particular the CB enjoys the areas with accumulations of nuclear pores and there seems to be active material transfer between the nucleus and the CB[237,248,249]. While in early round spermatids, the CB tends to maintain its perinuclear position, during the later steps the CB often dissociates from the nuclear envelope to move more widely in the cytoplasm. The CB has even been observed in the cell periphery, close to the intercytoplasmic bridges where CB-derived particles can be transported from one haploid cell to another one through the bridges[247]. As for most of their "lifespan" the CBs are detected at perinuclear regions in close association with nuclear pores their function may be to surveil and process nascent mRNAs as they exit the nucleus.

2.4.2   Autophagy and germ granules

As discussed, germ granules are, by definition, not limited by any membranes. However, while the IMC is found intermingled with mitochondria clusters and therefore in close association with mitochondrial membranes[250], the CB is always seen in close communication with several membranous structures of the endomembrane system. In addition to the nuclear envelope the CB frequently associates with the Golgi complex, the ER and multivesicular bodies (MVBs). Furthermore dozens of small vesicular structures are seen both in the immediate CB periphery and embedded inside of its interstices and lobes[251] (Figure 4). The late CB in elongating spermatids is, in fact, completely covered with vesicles[252]. CB-associated vesicles have been linked to the autophagy-lysosomal pathway[253].

Autophagy is an evolutionarily conserved catabolic pathway that ensures nutrient recycling and removal of unwanted substrates thus helping maintain cellular homeostasis. Autophagy occurs constitutively at basal levels but can be rapidly upregulated, enabling adaptation to changing cellular demands and protection from stress. Autophagy constitutes a collection of processes by which a cargo of cellular components is targeted for degradation by the lysosomes. Three distinct pathways depending on a cargo's delivery route to the lysosome can be described. In chaperone-mediated autophagy proteins containing a specific motif are recognized by chaperone proteins, and guided to the lysosome where the lysosomal-associated membrane protein 2A (LAMP2A) facilitates their translocation across the lysosomal membrane[254]. During microautophagy, the autophagic cargo is directly captured by membrane protrusion and invagination by lysosomes and late endosomes, and then degraded in the endolysosomal lumen[255]. Macroautophagy (hereafter: autophagy) is the predominant and most extensively studied form of autophagy.

The initiation of autophagy is regulated by two kinases. When nutrient levels are low or growth factors decline, the mammalian target of rapamycin (mTOR) is inhibited, which promotes the onset of autophagy until the resulting release of recycled molecules, including amino acids, derived from increased autophagy, reactivates mTOR to inhibit autophagy[256,257]. The energy-sensing AMP-activated protein kinase (AMPK) on the other hand promotes autophagy by promoting the activity of the Unc-51-like autophagy-activating kinase (ULK1) complex. The active ULK1 complex initiates autophagosome nucleation by translocating to the autophagosome formation site with the transmembrane spanning ATG9. This activates the PI3K complex class III, formed by VSP34, VSP15, Beclin1 and ATG14, resulting in the phosphatidylinositol 3-phosphate (PI3P) production and consequently recruitment of proteins with PI3P-binding domains, such as FYVE domain-containing proteins. The cup-shaped phagophore elongates, through the recruitment of membrane from different sources and bends into a spherical shape to form a double-membrane autophagosome sequestering autophagic cargo within itself. Two ubiquitin-like reactions are required for completing elongation, the ATG12/ATG5–ATG16L1 complex formation and the conjugation of the cytosolic LC3-I protein to the membrane via lipid anchors forming LC3-II. Membrane-bound LC3-II controls autophagosome closure and is also involved in later steps, movement of autophagosomes, fusion with lysosomes, and degradation of the autolysosome's inner membrane[258]. As LC3-II is incorporated to autophagosomal membranes, the number of autophagosomes can be determined by measuring LC3-II. After LC3-II incorporation, autophagosome undergoes further maturation through fusion with endocytic vesicles to form amphisomes. Autophagosomes/amphisomes are transported along microtubules to lysosomes. The degraded cargo is thereafter released for cellular recycling[259].

The selective autophagy concept emerged after the initial view that autophagy is a non-selective bulk degradation process. For example, ribosomes were initially believed to be subject for bulk autophagy as they were often seen within autophagic structures in starved cells[260], but more recently selective autophagy mechanisms called ribophagy[261] that relies on specific adaptor proteins was reported[262]. Selective autophagy has, to date, been described for many cellular components including mitochondria (mitophagy)[263], the ER (reticulophagy)[264], lysosomes (lysophagy)[265–267] and protein aggregates (aggrephagy)[268] among others. Selective autophagy relies on autophagy receptors and specific adaptor proteins that link the cargo with the autophagy machinery. Several adaptor proteins have been reported and more are being discovered constantly[269]. For example p62/SQSTM1[270,271]is a widely studied adaptor involved in *e.g.* aggrephagy and mitophagy that recognizes cargo through its ubiquitin-binding domain and interacts with LC3 which, apart from its functions in initial autophagosome membrane dynamics, is a key protein for adaptor recognition in selective autophagy.

RNA catabolism via autophagy involves the degradation of RNA by RNases such as RNase T2 and lysosomal acidic hydrolases within the lumen of lysosomes. Even though the classical autophagy studies have focused on autophagy-mediated protein catabolism, RNA, RBPs and RNP granules can also be degraded by autophagy. As mentioned earlier, ribosomes are regularly eliminated by autophagy both in non-selective and selective ways. Ribophagy constitutes an important example of RNA catabolism through autophagy as ribosomal RNA (rRNA) is the primary component of ribosomes and roughly 80% of total cellular RNA is derived from ribosomes[272,273]. Other examples include RNautophagy[274], in which mRNA molecules are bound directly by LAMP2C or SID1 transmembrane family member 2 (SIDT2) proteins and, in an ATP-dependent manner, transferred inside lysosomes. RNautophagy does not require the formation of a double-membrane vesicle and thus resembles the chaperon mediated autophagy[275,276].

Defected autophagy has been linked to various pathologies[277] including cancer[278], renal disease[279], pulmonary disorders[280], heart disease[281], neurodegenerative disorders[282,283], reproductive dysfunctions[284,285] and age-related illnesses such as cataract[286]. Currently, the role of autophagy in ageing and age related conditions is under particularly active investigations. [287,288] At the heart of several of these studies are a type of RNP granule known as the stress granule. Stress granules are assembled during a stress response. They are transient structures that function as sites for the sequestration and storage of mRNAs that can be cleared by several mechanisms once cellular conditions have become favorable again. Stress granules may be removed via disassembly by molecular chaperones[289], clearance by the ubiquitin–proteasome system[290] or via granulophagy[291]. Dysregulation of stress granule formation, dissolution, or composition has been associated with several diseases including neurodegenerative disorders[282,283]. Apart from pathological conditions, RNP clearance via autophagy is also linked to physiological contexts.

Maternal germ granules, also known as P granules, are specialized structures that contain RNA and proteins necessary for germ cell development in embryos. During embryogenesis, maternal germ granules are essential for the specification and differentiation of germ cells but as development progresses, the clearance of germ granules becomes necessary for the proper formation of somatic cells and the restriction of germline potential to the appropriate cells. Autophagy has been identified as one of the mechanisms involved in this process[292]. In *Caenorhabditis elegans*, for instance, autophagy plays a role in the elimination of P granule components during embryogenesis. P granule components in somatic cells form PGL-1-positive granules that are selectively removed by autophagy with the help of autophagy adaptor, *suppressor of ectopic P granule in autophagy* 1 (SEPA-1)[293]. The potential connection of male germ granules and autophagy is largely unexplored

although the tenuous link discovered in the CB proteome analysis described below initiated one of the main projects that are the subject of this thesis work.

2.4.3   Chromatoid body proteome and beyond

In recent years, there has been a significant advancement in our knowledge of the molecular characteristics of germ granules, specifically the CB[236]. Through the use of mutant mouse models, important insights into the function of germ granules have been discovered. In particular, their importance for male fertility has been highlighted as any core component loss-of-function mutation has usually lead to defected spermatogenesis. Another step towards unravelling their mystique, a protocol to isolate CBs from mouse testis enabled their full molecular composition to be discovered and analyzed[26,240].

An autophagy adaptor, FYVE and coiled-coil domain-containing protein 1 (FYCO1), was found among the roughly 90 proteins identified by mass spectrometric analysis of isolated CBs. FYCO1 is a large protein (~170kDa mice) that contains a FYVE domain, which allows it to bind to PI3P and an LC3-Interacting Region (LIR) enabling its interaction with LC3 proteins[294–296]. FYCO1 has been linked to the maturation of early phagosomes into late LAMP1-positive phagosomes, the formation of tubular lysosomes in macrophages upon lipopolysaccharide treatment, and transport of late endosomes along the microtubule network[294,297,298]. In recent years the role of FYCO1 in several human pathologies has gained interest, especially congenital cataract[299–302], but no link to large RNP granules has yet been reported.

However, apart from FYCO1, most proteins in the CB proteome did not represent a link to the autophagy pathway but were, instead, RBPs and other proteins involved in RNA regulation, processing, translation and splicing[26]. The CB includes a plethora of pre-mRNA binding and processing proteins that are ubiquitously expressed, but also several germ cell-specific proteins. The most prominent molecular pathway seems to be the piRNA pathway and the most abundant proteins in addition to the piRNA-binding PIWI proteins PIWIL1 and PIWIL2 include several Tudor-domain containing proteins (TDRD) and the DEAD-box helicases DDX4 and DDX25[303–307]. The structural scaffolding mesh of the CB seem to consist of Tudor domain-containing proteins, including TDRD1, TDRD3, TDRD5, TDRD6, TDRD7, RNF17 and STK31[308–313] and, in fact, the morphology of the CB has been shown to depend on at least TDRD6 or TDRD7 as in their absence the CB disintegrates[304,309]. The CB also accumulates NMD pathway components, such as SMG1, SMG6, UPF2 and UPF3.

Considering the plethora of RNA-binding proteins, it is somewhat unsurprising that the CB also accumulates large quantities of diverse RNAs. In fact, a considerable

portion of the round spermatid mRNA transcriptome is found in the CB transcriptome[26]. There is a constant flow of RNA to the CB and the morphology of the CB actually depends on active transcription[244]. Apart from mRNAs the CB accumulates non-coding RNAs such as thousands of non-annotated intergenic non-coding transcripts, piRNA precursors and piRNAs[26].

2.4.4   Chromatoid body accumulates piRNAs

In germ cells of mammals, small non-coding RNAs of 24–35 nucleotides in length PIWI-interacting RNAs (piRNAs) guide PIWI proteins to diverse protective processes[25,314,315]. Distinct groups of piRNAs direct DNA and histone methylation of transposon sequences during embryogenesis[316–318] and silence transposons during spermatogenesis[319] and regulate gene expression, ensure completion of meiosis and maintain successful spermatogenesis[320,321]. Unlike miRNA and siRNA that are derived from double-stranded RNA precursors, piRNA production begins with long single-stranded piRNA precursors, that are transcribed from dedicated genomic loci called piRNA clusters by the RNA polymerase II [322–324]. Based on their expression profile piRNAs are categorized to two broad classes: pre-pachytene and pachytene piRNAs.

piRNA biogenesis in the mouse begins as PIWI proteins guided by existing piRNAs cleave piRNA precursor transcripts, creating pre-pre-piRNAs on which the piRNA biogenesis initiates. The 5′ end of the pre-pre-piRNA is monophosphorylated which enables a PIWI protein to bind to it. On the outer mitochondrial membrane, the endonuclease PLD6 cleaves the pre-pre-piRNA 3′ to the footprint of the PIWI protein, releasing a PIWI-bound pre-piRNA and a new 5′ monophosphorylated pre-pre-piRNA that can bind yet another PIWI protein. Successive cycles of binding by PIWI proteins and cleavage by PLD6 chop the original piRNA precursor into pre-piRNAs. PNLDC1 exoribonuclease defines the mature piRNA's lenght, within limitation set by the PIWI protein to which the piRNA is loaded. Finally, the 3′ end of the precursors are trimmed and 2′-O-methylated by S-adenosylmethionine-dependent methyltransferase (HENMT1) producing mature piRNAs[325,326].

Transposable elements are in a ceaseless battle in the genome of every organism as parasitic elements that seek to integrate into the host DNA. Protecting the integrity of the germ line genome from these attacks is the function of the piRNA pathway representing the ancestral role of piRNAs. In the fetal mouse testis, these piRNAs also known as prepachytene piRNAs silence invading active transposons together with their associate PIWI proteins, PIWIL2 and PIWIL4[327].

Pachytene piRNAs are the second class of piRNAs in mammals. They are produced in vast quantities from transposon-depleted, unique non-coding sequences transcribed by RNA polymerase II. Postnatal mouse germ cells first produce pre-pachytene piRNAs that are PIWIL2-bound and 26–27 nucleotides in length. They are

derived from the coding sequences or 3′ UTRs of diverse mRNAs. After the onset of the pachytene stage of meiosis, pachytene piRNA precursor transcription is induced. Thereafter pachytene piRNAs largely replace the pre-pachytene piRNAs in number and in the adult testis the pachytene piRNAs account for ~95% of all piRNAs[328]. The transcription factor that initiates pachytene piRNA biogenesis, A-MYB, drives the coordinated transcription of ~100 pachytene piRNA precursors. It also regulates the expression of proteins required for pachytene piRNA pathway such as PIWI proteins PIWIL1 and the previously mentioned PIWIL2. PIWIL2 expression is maintained up to early round spermatid stage while PIWIL1 appears slightly later in late pachytene spermatocytes and persists through round spermatid differentiation [329,330]. In pachytene spermatocytes roughly 84% of pachytene piRNAs are PIWIL1-bound and rest PIWIL2-bound[328,331]. While prepachytene piRNAs have a well-known purpose in the maintenance of genome stability, the functions of pachytene piRNAs appear more diverse and include translational control and destabilization of mRNA and long non-coding RNA targets [321,330,332,333]. In any case, the importance of proper and functional piRNA pathway for spermatogenesis is undeniable and has been demonstrated by mouse models targeting the piRNA pathway[334–336].

Germ granules, such as the IMC and the CB, are strongly linked to the function and biogenesis of piRNAs[236]. The appearance of the IMC coincides with the massive production of pachytene piRNAs and it closely associates with mitochondrial membranes hosting the previously mentioned MitoPLD (PLD6). Furthermore, PIWIL2 strongly accumulates to the IMC and its interactome was recently shown to include several proteins with known functions in piRNA biogenesis[337]. In round spermatids, piRNAs and the proteins they are bound by localize to the CB together with several proteins indicated in the piRNA pathway[26]. Current evidence suggests that the production of pachytene piRNAs from precursor transcripts takes place in the IMC, and PIWI protein-loaded piRNAs are then transferred to the CB (Figure 5). In *Drosophila* germ plasm piRNAs use partial base-pairing to bind mRNAs randomly, acting as adhesive traps that capture mRNAs[338]. It remains to be elucidated whether the CB-localized PIWIL1/PIWIL2 loaded piRNAs could similarly lure and tether mRNAs to the CB for downstream actions. In addition, several other mysteries remain in the piRNA field and are under active study. One of the main questions is how piRNA pathway executes its ultimate functions. Several possible ways have been proposed such as PIWI protein-catalysed target RNA cleavage guided by piRNA[339], miRNA-like destabilization of target RNA, translation repression without degradation of mRNA targets and translation activation of specific mRNAs by PIWIL1[332]. However, none of these models currently have adequate experimental evidence to back them up.

The importance of both germ granules and the piRNA pathway for male fertility is highlighted by the numerous KO mouse models that have resulted in impaired spermatogenesis. The deletion of some factors has been shown to cause a block of spermatogenesis at the meiotic phase and other factors have been shown to be critical for the haploid differentiation as manifested as the spermatogenic defect occurred later at the round spermatid or elongating spermatid phase. Figure 6 summarizes the mouse models with a pathway or biological process that has been affected by the deletion/mutation and the stage in which the spermatogenetic defect was shown to occur. Also included in Figure 6 are the two models created in this thesis that will be described and discussed next.
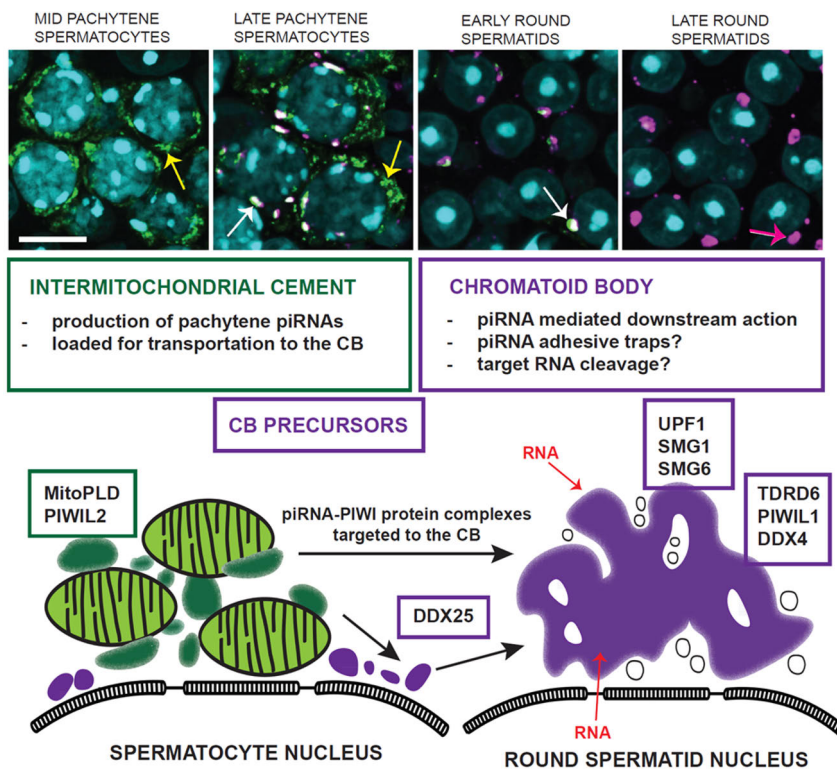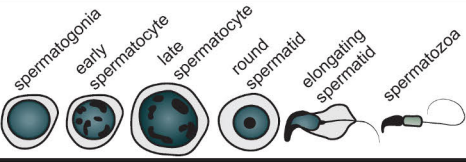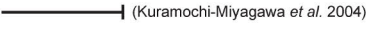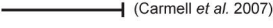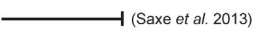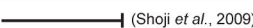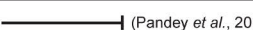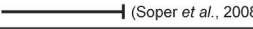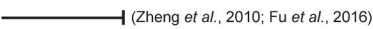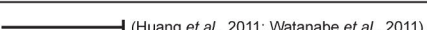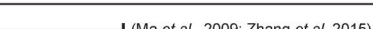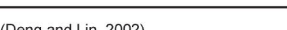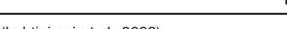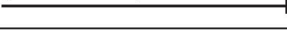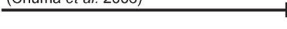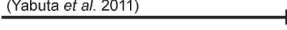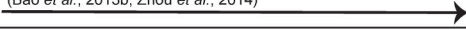
Figure 5. Germ granules and the piRNA pathway. Pachytene piRNA primary processing from precursors takes place in the IMC (green) followed by their delivery to proteins the CB (purple). Some of the key proteins involved in this process are indicated inside the green and purple boxes. In the IF images, the IMC, CB precursors and CBs are shown as they emerge during spermatogenesis in pachytene spermatocytes and round spermatids whose nuclei are stained by DAPI (light blue). PIWIL2 (green) stains the IMC in mid and late pachytene spermatocytes and the CB in early round spermatids but not late round spermatids, while DDX25 (magenta) is found only in CB precursors of late pachytene spermatocytes and the CBs in early and late round spermatids. Yellow arrows indicate the IMC in one of the spermatocytes, pink arrow the CB of one late round spermatid and the co-localization of PIWIL2 and DDX25 in CB precursors and early CBs is indicated by white arrows. Scale bar: 10 μm *(Modified from Lehtiniemi and Kotaja[25])*

MOUSE MODEL / MUTATED PROTEIN	spermatogonia / early spermatocyte / late spermatocyte / round spermatid / elongating spermatid / spermatozoa	MOLECULAR FUNCTION/ BIOLOGICAL PROCESS	GERM GRANULE
MILI	(Kuramochi-Miyagawa et al. 2004)	(pre-pachytene) piRNA binding protein, piRNA pathway	IMC, early CB
MIWI2	(Carmell et al. 2007)	(pre-pachytene) piRNA binding protein, piRNA pathway	IMC, P-bodies
DDX4/ MVH	(Tanaka et al. 2000)	RNA helicase, piRNA pathway	IMC, CB, small germ granules
TDRD2/ TDRKH	(Saxe et al. 2013)	primary piRNA biogenesis	IMC
TDRD9	(Shoji et al., 2009)	binds MIWI2, piRNA biogenesis, piRNA pathway	CB, P-bodies
TDRD12	(Pandey et al., 2013)	secondary piRNA biogenesis	
MAEL	(Soper et al., 2008)	piRNA pathway	CB
MOV10L1	(Zheng et al., 2010; Fu et al., 2016)	primary piRNA biogenesis, binds piRNA precursors, interacts with PIWI proteins	IMC
MITOPLD	(Huang et al., 2011; Watanabe et al., 2011)	IMC formation, piRNA biogenesis, piRNA pathway	mitochondrial outer membrane
GASZ	(Ma et al., 2009; Zhang et al. 2015)	mitofusion, piRNA pathway	IMC
MIWI	(Deng and Lin, 2002)	(pachytene) piRNA binding protein, piRNA pathway	CB
SMG6*	(Lehtiniemi et al., 2022)	nonsense-mediated decay	CB
TDRD7	(Tanaka et al., 2011)	CB/RNP structure maintanance, LINE1 retrotransposon repression	CB
TDRD1	(Chuma et al. 2006)	molecular scaffold, binds MILI, piRNA biogenesis	IMC,CB
TDRD5	(Yabuta et al. 2011)	CB/RNP structure maintanance, LINE1 retrotransposon repression	IMC, CB
DDX25	(Tsai-Morris et al., 2004)	RNA helicase	IMC, CB, small germ granules
RNF17	(Pan J. et al., 2005)	suppressor of secondary piRNA production	
UPF2 Ddx4Cre	(Bao et al., 2016)	nonsense-mediated decay	CB
UPF2 Stra8Cre	(Bao et al., 2016)		
TDRD6	(Vasileva et al. 2009)	CB/RNP structure maintanance, nonsense-mediated decay	CB
TDRD8/ STK31	(Bao et al., 2013b; Zhou et al., 2014)	interacts with MIWI	IMC, P-bodies
EXD1	(Yang. et al., 2016)	secondary piRNA biogenesis, LINE1 retrotransposon repression	IMC
FYCO1*	(Da Ros et al., 2017)	autophagy	IMC, CB, vesicles

*model presented in this thesis work

Figure 6. Many germ/piRNA granule components are required for normal spermatogenesis. The figure summarizes the spermatogenic phenotype of selected mouse models with arrows or blunt end lines indicating the progression or arrest in spermatogenesis. P-bodies; processing bodies *(Modified from Lehtiniemi and Kotaja[25])*

3 Aims of the Present Study

While the importance of germ granules to male fertility is widely accepted their role in specific functions during spermatogenesis has remained obscure. The main objective of this thesis work was to elucidate how these enigmatic germ granules maintain germ cell differentiation and to discover new molecular pathways residing in these granules. The two main projects of this thesis each consider the CB from a distinct perspective. One observes the CB in its cellular environment, surrounded by vesicles and reveals its connection to autophagy through a peripheral CB protein, FYCO1. Then diving deep into the core of the CB, a link between the components of the nonsense mediated RNA decay pathway and the piRNA pathway is uncovered and their collaboration in regulating the transcriptomic balance of male germ cells studied. In addition, a secondary objective of this thesis was to develop new methods to facilitate firstly our own research but also to introduce easy and feasible germ cell research tools for a wide scope of researchers. Subsequently the method developed was used in both of the main research projects.

The specific objectives of this study are as follows:

I.   To develop a simple BSA gradient based method to isolate round spermatids and spermatocytes from mouse testis without the need for expensive specialized equipment.

II. To uncover the role of FYCO1 in spermatogenesis and germ granules using a *Fyco1*-cKO mouse model.

III. To uncover the role of SMG6 in spermatogenesis and germ granules using a *Smg6*-cKO mouse model.

4 Materials and Methods

Complete information on the catalog codes of the reagents used is provided in the original publications (I–III).

4.1 Animal work and ethics (I-III)

The genetic background of all the mice used in this study was mixed background with C57Bl/6J and SV129. Transgenic mouse lines were created together with Turku Center for Disease Modeling (TCDM). All mice were maintained and housed at the central animal facility of the University of Turku, Finland, under controlled pathogen-free conditions (12 h light/12 h dark, temperature: $21 \pm 1°C$), following local laws and regulations (Finnish Act on the Protection of Animals Used for Scientific or Educational Purposes [497/2013], Government Decree on the Protection of Animals Used for Scientific or Educational Purposes [564/2013]). Mice were euthanized by CO_2 inhalation followed by cervical dislocation. The Laboratory Animal Care and Use Committee of the University of Turku approved all the animal experiments.

4.2 Mouse models

4.2.1 Generation of *Fyco1* conditional knockout mice (II)

The construct for the generation of the *Fyco1* conditional knockout (MGI:107277) was purchased from the International Mouse Phenotyping Consortium (IMPC), and validity confirmed by restriction enzyme digestion and sequencing. G4 embryonic stem cells (ES, derived from 129S6/C57BL/6Ncr mice) were cultured on neomycin-resistant primary embryonic fibroblast feeder layers, and 106 cells were electroporated with 30 µg of linearized targeting construct. After electroporation, the cells were plated on 100 mm culture dishes and with G418 (300 µg/ml; Sigma). After 7-9 days selected colonies were grown on 96-well plates. To delete *Neo* cassette in the targeted ES cells, they were re-electroporated with plasmid pCAGGS-Cre and plated on 100 mm culture dishes. After 3-5 days colonies were picked and

moved to 96-well plates. Targeted ES clones with *Neo* deletion were detected by PCR and sequencing and subsequently used for blastocyst injection to create chimeras. Male chimeras were bred with wild-type females to determine the germline transmission. To achieve selective male germ cell-specific inactivation of *Fyco1* in germ cells, homozygous *Fyco1* floxed mice were first bred with *Cre*-expressing mice. *Cre* was expressed under the *Neurogenin3* (*Ngn3*) promoter, the expression of which begins at postnatal day 5. *Fyco1*(fx/wt);*Ngn3Cre+* and *Fyco1*(fx/wt);*Ngn3Cre−* mice were thus obtained. Of these the *Fyco1(fx/wt);Ngn3Cre+* heterozygous males were chosen for mating with *Fyco1*(fx/fx) females to produce *Fyco1*(fx/fx);*Ngn3Cre+* cKO mice, as well as *Fyco1* (fx/fx);*Ngn3Cre−* and *Fyco1* (fx/wt);*Ngn3Cre−* littermates that were used as controls in all experiments. Genotyping of *Ngn3Cre* transgene was performed as reported before[340] and floxed *Fyco1* allele was genotyped using specific primers flanking the flox site (Table 1).

4.2.2   Generation of *Smg6* conditional knockout mice (III)

The targeting construct for the generation of the *Smg6*-cKO mice (PG00253_Z_1_B03) was purchased from IMPC, and validity was confirmed by restriction enzyme digestion and sequencing. G4 ES (derived from 129S6/C57BL/6Ncr mice) were cultured on neomycin-resistant primary embryonic fibroblast feeder layers and 107 cells were electroporated with *Asi*SI linearized targeting construct. After electroporation cells were plated on 100 mm culture dishes with G418 (300 μg/ml; Sigma). After 7-9 days selected colonies were grown on 96-well plates. To delete *Neo* cassette in the targeted ES cells, the cells were re-electroporating the ES cells with plasmid pCAGGS-Cre and plated on 100 mm culture dishes. After 3-5 days before colonies were picked and moved to 96-well plates. Three targeted ES clones and several ES clones with the right *Neo* deletion were determined by PCR (Table 1) and sequencing. Two of the right targeted ES clones with *Neo* deletion were used for blastocyst injection to generate chimeras. Chimeric male mice from both lines were bred with C57BL/N6 wild-type mice to test germline transmission. To achieve selective inactivation of *Smg6* in early postnatal germ cells, transgenic *Ngn3Cre* male mice[340,341] were first mated with homozygous *Smg6* floxed females, *Smg6*(fx/fx) in order to generate *Smg6*(fx/wt);*Ngn3Cre+* mice. *Smg6*(fx/wt);*Ngn3Cre+* heterozygous males were then crossed with *Smg6*(fx/fx) females to produce *Smg6*(fx/fx);*Ngn3Cre+* cKO mice, as well as *Smg6*(fx/fx);*Ngn3Cre−* and *Smg6*(fx/wt);*Ngn3Cre−* littermates that were used as controls in all experiments. Genotyping of *Ngn3Cre* transgene was performed as reported before[340], and floxed *Smg6* allele was genotyped using specific primers flanking the flox site (Table 1). The phenotype of *Smg6*-cKO was

confirmed from both clones before choosing one line to use for the following experiments.

Table 1. Primers used for genotyping *Smg6*-cKO and *Fyco1*-cKO mouse lines.

Smg6	Amplicon size (bp)	Forward primer (5´-3´)	Reverse primer (5´-3´)
WT allele	178	GTTACTCTATCTCTGTCAGA	AAGACTCAGTGAGTGGACAG
Floxed allele	377	AAGGCGCATAACGATACCAC	AAGACTCAGTGAGTGGACAG
Floxed and Null alleles	1277	AAGGCGCATAACGATACCAC	CCCAAGAGGAACATTCAAAC
	262		
Fyco1	Amplicon size (bp)	Forward primer (5´-3´)	Reverse primer (5´-3´)
WT allele	216	AGTGAGAAAGAGGGGAAGGC	GGTACTGACTCTGTGGTAGG
Floxed allele	353	AAGGCGCATAACGATACCAC	TCACTCTTGCTCCTCTTTCC
WT and Floxed alleles	377	GCCCAATTAGGAAAGTATGGATAG	TCACTCTTGCTCCTCTTTCC
	519		

4.3 Fertility (II-III)

4.3.1 Breeding strategy

In each experimental group, adult male mice were bred with two wild-type females of the same genetic background. Breedings were continued for at least 48h and the number of pups and sex were recorded.

4.3.2 Sperm count and morphology

Sperm from the epididymis was released by placing one tail section (cauda) in 1 ml of 1xPBS, cutting it 10 times with scissors and incubating for 30 min in 37 degrees. Samples were then pipetted up and down to extract all sperm from the cauda to PBS. 20 µL of each sample was then counted in a Bürker chamber and results were extrapolated. For sperm morphology analysis, another sample of 20 µL was pipeted onto a glass slides, air-dried, and stained with hematoxylin according to standard protocols. Images were acquired with the microscope slide scanner Pannoramic P1000 (3D Histech) for bright field imaging with 40X objective.

4.4 Stainings and imaging (I-III)

4.4.1 Tissue preparation for stainings

For histology, immunohistochemistry, and immunofluorescence analysis entire organs (mice), tissue pieces (mice and human) and squash preparation of seminiferous tubules (mice) were collected for downstream stainings.

Tissues were directly fixed in 4% paraformaldehyde (PFA) (all tissues) or in Bouin fixative (for testis only) overnight at RT in gentle rotation. After washes, tissues were embedded in blocks of paraffin. Then, 4 µm thick sections were cut, placed on microscopy slides, incubated at 37 degrees overnight and stored at +4 degrees.

Squash slides of stage specific sections of mouse seminiferous tubules for tubule cultures and immunofluorescence labelling were prepared according to protocol[41,342]. Briefly, testes from adult mice were decapsulated and sections representing specific stages of the seminiferous epithelium were isolated based on the light absorption pattern with the help of a stereomicroscope. The sections of the seminiferous tubules were then transferred to a glass slide with the use of a pipette and a glass coverslip deposited on top to allow the germ cells to form a monolayer. The glass slide was then snap-frozen in liquid nitrogen, coverslip removed, and slide placed for fixing in 100% ice-cold acetone for 10 min. Slides were then air-dried overnight at room temperature.

4.4.2 Histology

Paraffin-embedded tissue section slides were dehydrated using an ascending gradient of ethanol and xylene: sections were deparaffinized and rehydrated by incubation 3×5 min in xylene, 2×10 min in 100% ethanol (EtOH), 2×10 min in 96% EtOH, 2×10 min in 70% EtOH and then washed in milliQ water 2×2 min. Testis were stained with periodic acid-Schiff (PAS) and epididymis with hematoxylin-eosin (HE) according to standard protocols. Images were acquired with the microscope slide scanner Pannoramic P1000 (3D Histech) for bright field imaging with 40X objective.

4.4.3 Immunohistochemistry

Paraffin-embedded tissue section slides were deparaffinized and rehydrated as described above (4.5.2). Antigens were retrieved by pressure cooking in 10 mM sodium citrate (pH 6.0) for 10 min and cooled to RT. Non-specific binding was blocked with 30 min incubation in 3% BSA in 0.5% PBST (immunohistochemistry

blocking solution). Primary antibodies were diluted in blocking solution (1:200 for anti-SMG6, 1:300 for anti-FYCO1) and sections were incubated at +4°C overnight. Slides were washed 2 x 5 min with 0.05% PBST and endogenous peroxidase activity was blocked with 20 min incubation in 3% H_2O_2. Secondary antibody incubation was done using Envision+ system with HRP labeled polymer anti-rabbit (Dako) for 30 min at room temperature. DAB-color formation was detected with 3,3′-diaminobenzidine (liquid DAB+, Dako) and the color reaction was stopped with 3 x 3 min dH2O washes. Sections were stained with 10 sec incubation in Mayer's Hematoxylin and washed under running water for 5 min. Sections were dehydrated with 2 x 5 min in 70% EtOH, 2 x 10 min in 96% EtOH, 2 x 5 min in 100% EtOH and 3 x 5 min in xylene and mounted with PERTEX medium. Images were taken with digital slide scanner Panoramic 250 Flash III (3DHistech) and processed using Adobe Photoshop.

4.4.4 Immunofluorescence

Pre-treatment for tissue samples: Paraffin-embedded testis sections (mouse and human) were deparaffinized and rehydrated by incubation 3 × 5 min in xylene, 2 × 10 min in 100% ethanol, 2 × 10 min in 96% ethanol, 2 × 10 min in 70% ethanol and then washed in milliQ water 2 × 2 min. Antigen retrieval was performed by incubation in sodium citrate solution (10 mM sodium citrate, 0.05% Tween 20 [Sigma, P2287], pH 6.0) or in Tris-EDTA solution (10 mM Tris Base, 1 mM EDTA Solution, 0.05% Tween 20, pH 9.0) for 20 min, at 1 atmosphere at 120°C. After cooling down to room temperature for at least 2 h slides were washed 4 × 3 min in milliQ water and 5 min in PBS.

Pre-treatment for squash samples: Slides were postfixed in 4% paraformaldehyde in PBS for 10 min, washed 5 min in PBS, incubated 5 min in 0.2% Triton X-100 in PBS and washed 3 × 5 min in PBS before proceeding with staining.

Staining protocol: Slides were incubated at 10% normal donkey serum (Jackson Immunoresearch, 017–000–121) and 3% bovine serum albumin (Sigma, A2153) in PBST (0.1% Tween-20) (=blocking solution) for 1 h. Primary antibody was diluted in blocking solution (1:100-1:500) and incubation was performed for 1 h at room temperature or overnight at 4°C. Slides were washed 3 × 5 min with PBST. Alexa Flour conjugated secondary antibodies were used in dilution of 1:500 for 1 h at room temperature. Acrosome labeling was done with Rhodamine-conjugated peanut agglutinin (PNA, RL-1072). Blocking and incubations blocking performed in a humidified environment protected from light. Slides were washed 3 × 5 min in PBST, incubated 5 min in DAPI (Sigma-Aldrich, D9542; 5 mg/mL stock) diluted 1:20,000 in PBS, washed 5 min in PBS followed by 5 min with milliQ water and mounted with Vectashield HardSet Mounting Medium (Vector Laboratories, H-1400) or ProLong Diamond Antifade Mountant (Life Technologies, P36970). Slides were left for 24 h at

room temperature and moved to +4 for longer storage. 3i CSU-W1 Spinning disk (objective 40x, 63x or 100x) and Pannoramic Midi Fluorescence slide scanner (3D Histech) were used for obtaining images. Acquired images were processed with Image J 1.8.0 software version (National Institute of Health, USA) and Adobe Photoshop.

4.4.5 Terminal deoxynucleotidyl transferase dUTP nick end labeling assay (III)

Apoptotic cells were detected using the terminal deoxynucleotidyl transferase dUTP nick end labeling (TUNEL) assay. Paraffin-embedded testis sections were deparaffinized by incubation 3×3 min in xylene, 2×2 min in 100% ethanol, 2×2 min in 96% ethanol, 2×2 min in 70% ethanol and then washed in TBS (Tris-Buffered Saline, pH 7.5) 1×5 min. Sections were subjected to antigen retrieval in sodium citrate solution as described above. After cooling down the slides, autofluorescence was blocked by incubating the slides in 100 mM NH_4Cl for 10 min. After washing the slides with TBS 3×5 min in TB, slides were incubated for 10 min in 100 mM NH_4Cl and TBS washes were repeated. Slides were incubated for 1 h at 37ºC in humidified conditions with TUNEL (TdT-mediated dUTP nick end labeling) mixture: TdT buffer with terminal transferase (03333566001, Roche) 1U/µl, CoCl2, and 1 µM biotin-16-dUTP (11093070910, Roche) in milliQ. Positive control sections were incubated with DNAase I, grade I (30 U/ml DNAase1 Invitrogen) for 30 min at 37ºC and negative control sections were incubated without terminal transferase (03333566001, Roche). The reaction was stopped by incubating slides for 15 min RT with 300 mM NaCl, 30 mM Na Citrate in milliQ, and washed 4×5 min with TBS. Slides were blocked, incubated with specific antibodies, PNA and secondary antibodies as described above. The slides were then mounted and imaged as described above (4.6.4).

4.4.6 Immunofluorescence of testicular cryosections (II)

Cryosections were treated as described above (4.6.4) with some modifications: Dissected testes were fixed in 4% PFA overnight at RT, dehydrated in 20% sucrose solution in PBS, and embedded into an optimal cutting temperature compound. Notably, 10 µm thick sections were used for staining. Paraffin-embedded testis sections were deparaffinized in xylene and descending ethanol series. Sections were subjected to antigen retrieval in sodium citrate solution as described above. Slides were rinsed with PBS and sections were then incubated in 5% normal donkey serum and 5% BSA in 0.2% Tween 20 in PBS for 1 h at RT. Primary antibodies were diluted in 1% BSA in 0.2% Tween 20 in PBS and incubated overnight at 4°C. After the incubation of the primary antibodies, the slides were washed in 0.2% Tween 20 in PBS 3 x 5 min. Alexa

Flour 488/546/647 conjugated secondary antibodies (Life Technologies) were used in dilution of 1:500 in 1% BSA in 0.2% PBST and incubated for 1 h at 37°C in the dark. The slides were then mounted and imaged as described above.

4.5 Electron microscopy and tomography

4.5.1 Electron microscopy (II-III)

Testis samples were fixed in 5% glutaraldehyde and treated with a potassium ferrocyanide-osmium fixative. The samples were embedded in epoxy resin (Glycidether 100, Merck), sectioned, post-stained with 5% uranyl acetate and 5% lead citrate, and visualized on a JEOL 1400 Plus transmission electron microscope (JEOL Ltd., Tokyo, Japan).

4.5.2 Electron tomography (II)

For electron tomography samples were prepared similar to electron microscopy samples (described above) except that uranyl acetate *en-bloc* staining was performed before plastic embedding. Serial semithick 220 nm sections were cut and placed on single slot grids. Colloidal gold particles of 10 nm in diameter were placed on top and below the grids to serve as markers for the alignment of the tilt series. Dual axis tilt series were acquired using SerialEM software (http://bio3b.colorado.edu/serialEM) running on a Tecnai FEG 20 microscope (FEI, the Netherlands) operating at 200 kV. Images from 3 consecutive sections were recorded at 1-degree intervals over a tilt range of ± 62 degrees. Tilt series were acquired with Ultrascan 4000 CCD camera (Gatan Corp., Pleasanton, CA, USA) at nominal magnification of 11.5 k providing a 2X binned pixel size of 1.94 nm. IMOD software (http://bio3d.colorado.edu/imod) was used to create 3D reconstructions. The images were segmented using Microscopy Image Browser, developed by the Electron Microscopy Unit, University of Helsinki [343] 3D rendering of selected cytoplasmic vesicles was performed with BioimageXD version 1.56.

4.6 Chromatoid body isolation (II-III)

Chromatoid body immunoprecipitation was performed as described previously with modifications[344]. Briefly, germ cells were released from four testes of adult C57BL/6 mice, six testes of adult *Smg6*-cKO mice or three testes of control mice from Smg6 mouse line and fixed in 0.1% PFA in PBS (Electron Microscopy Sciences, Hatfield, PA, USA). After fixation cells were lysed by sonication (UCD-200; Diagenode, Liege, Belgium) in 1.5 mL of RIPA buffer [50 mM Tris-HCl pH 7.5, 1% Triton-X, 0.5% w/v

sodium deoxycholate, 0.05% w/v sodium dodecyl sulphate, 1 mM EDTA, 150 mM NaCl, 1X complete protease inhibition cocktail (Roche, Basel, Switzerland), 0.2 mM PMSF and 1 mM DTT] and the CB-enriched pellet fraction was separated by centrifugation at 500 × g for 10 min. The CBs were immunoprecipitated using Dynabead Protein G (Thermo Fisher Scientific, Watham, MA, USA) coupled to anti-MVH antibody in rotation at 4°C overnight. Rabbit IgG coupled Dynabeads were used as control (NC-100-P; Thermo Fisher Scientific, Watham, MA, USA). For western blotting, samples from each isolation step (lysate of cross-linked cells; supernatant after low-speed centrifugation; CB-containing pellet fraction; CBs isolated by anti-DDX4 IP; and control IP using rabbit IgG) were diluted in Laemmli buffer and incubated 5 min at 95°C before loading them on the gel. For RNA-seq crosslinks of the isolated CBs were reversed by incubation at 70°C for 45 min.

4.7 Protein extraction and co-precipitation analysis

4.7.1 Protein extraction from tissues (II-III)

Tissue samples were homogenized in radioimmunoprecipitation assay (RIPA) lysis buffer (50 mM Tris-HClL at pH 7.5, 1% Triton X-100, 0.5% w/v sodium deoxycholate, 0.05% w/v sodium dodecyl sulfate, 1 mM EDTA, 150 mM NaCl) supplemented with 1 mM DTT, 0.2 mM PMSF and 1X protease inhibitor cocktail, and the lysates were cleared by centrifugation at >14000 × g for 5-10 min. For tissue expression and ontogenesis studies, protein concentration was measured using Pierce BCA protein assay kit (Life Technologies, 23227); absorbance was measured with a Victor2 plate reader (Wallac, Turku, Finland).

4.7.2 Protein extraction from isolated cells (I)

Protein was extracted from enriched germ cell fractions using RIPA lysis buffer supplemented with protease inhibitors by adding 500-1500μl of supplemented ice-cold RIPA on each cell pellet and pipetting vigorously up and down. Lysates were left to lyse on ice for 15min before clearing as described above. For tissue expression and ontogenesis studies, protein concentration was measured using Pierce BCA protein assay kit (Life Technologies, 23227); absorbance was measured with a Victor2 plate reader (Wallac, Turku, Finland).

4.7.3 Immunoprecipitation (I-III)

Three testes from adult mice were collected in 1.7 ml of isotonic nondenaturing lysis buffer (150 mM NaCl, 5 mM EDTA, 50 mM Tris-HCl, pH 8.0, 1% Triton X-100,

1X complete mini mix [Roche, 4693124001], 0.2 mM PMSF and 1 mM DTT). Samples were homogenized with TissueLyser LT (Qiagen) homogenizer for 90 sec and kept on ice for 30 min. Lysates were cleared by centrifugation at $14000 \times g$ for 10 min. Supernatant was divided to equally three parts, pre-cleared using 10 µl of Dynabead Protein G and incubated with either anti-SMG6, anti-SMG7 or rabbit IgG at 4°C overnight. Protein complexes were immunoprecipitated using 30 µl of Dynabead Protein G for 1 h RT. The Dynabeads-antibody-antigen complexes were washed 3 times in 1 ml of the non-denaturing lysis buffer.

4.7.4   Western blotting (I-III)

Protein samples were diluted in Laemmli buffer and incubated 5 min at 95°C before Western blotting. Proteins were separated by 10% SDS-PAGE and transferred to PVDF membranes (Amersham, RPN303F) with wet-blotting system (Bio-Rad). After blotting the PVDF membranes were incubated in 100% methanol for 15 seconds and air-dried for 30 min at 37°C or at room temperature overnight. Membranes were incubated in primary antibodies diluted in 5% skimmed milk, 0.1% Triton X-100, 1X TBS or 1x PBS (=TBST/PBST) for 1h at room temperature or overnight at +4°C, washed 3×5 min with TBST/PBST. Horseradish Peroxide (HRP)-conjugated anti-rabbit or anti-mouse IgG was used as a secondary antibody (dilution of 1:1000 in PBST/TBST). Proteins were detected using western lightening ECL pro (Ne112200IEA, Perkin Elmer, Netherlands. The chemiluminescence signal was recorded with LAS4000 (FujiFilm), saved as 16-bit TIFF files, and processed with image J 1.8.0 software version 1.8.0 (National Institute of Health, USA) and Adobe Photoshop.

4.8   Mass spectrometry

4.8.1   LC-ESI-MS/MS (II)

Dynabeads-antibody-antigen complexes with FYCO1/IgG were washed 2×1 mL of 25 mM NH_4HCO_3 buffer and 2×200 µL of 6 M urea in 25 mM NH4HCO3 buffer. Samples were loaded on a Criterion XT Bis-Tris precast 12% SDS-PAGE gel (Bio-Rad) and run with constant 200 V for 9 min. MOPS buffer was used as a running buffer. Three pieces from the upper part of the SDS-PAGE gel were cut.

Samples were submitted to Turku Proteomics Facility where the Liquid Chromatography Electrospray Ionization Tandem Mass Spectrometric (LC-ESI-MS/MS) analyses were performed on a nanoflow high performance liquid chromatography (HPLC) system (Easy-nLCII, Thermo Fisher Scientific) coupled to the LTQ Orbitrap Velos Pro mass spectrometer (Thermo Fisher Scientific) equipped with a nano-electrospray ionization source. Peptides were first loaded on a trapping

column and subsequently separated inline on a 15-cm C18 column (75 μm × 15 cm, Magic 5 μm 200 Å C18). The mobile phase consisted of water/acetonitrile (98:2 [v/v]) with 0.2% formic acid and acetonitrile/water (95:5 [v/v]) with 0.2% formic acid. A linear 30 min gradient from 5% to 35% B was used to elute peptides. MS data was acquired automatically by using Thermo Xcalibur 3.0 software (Thermo Fisher Scientific). An information dependent acquisition method consisted of an Orbitrap MS survey scan of mass range 300 to 2000 m/z.

The data files were searched for protein identification using Proteome Discoverer 1.4 software (Thermo Fisher Scientific) connected to an in-house Mascot server running the Mascot 2.4.1 software (Matrix Science). Data were searched against the SwissProt database (release 2014_08). The following search parameters were used. Type of search: MS/MS Ion Search, Taxonomy: Mus musculus, Enzyme: Trypsin, Fixed modifications: Carbamidomethyl (C), Variable modifications: Oxidation (M), Mass values: Monoisotopic, Peptide Mass Tolerance: ± 5 ppm, Fragment, Mass Tolerance: ± 0.5 Da, Max Missed Cleavages: 1, Instrument type: ESI-TRAP. Results from ProteomeDiscoverer were exported and saved as Excel files. Only proteins assigned at least with 2 peptides were accepted.

4.8.2   LC-ESI-MS/MS (III)

Dynabeads-antibody-antigen complexes from IP with SMG6/ SMG7/ IgG or CB-IP/IgG were washed with 3 x 1 ml of Tris-HCL (pH 8.0).

Samples were submitted to to Turku Proteomics Facility where the LC-ESI-MS/MS analyses were performed on a nanoflow HPLC system (Easy-nLC1200, Thermo Fisher Scientific) coupled to the Orbitrap Fusion Lumos mass spectrometer (Thermo Fisher Scientific) equipped with a nano-electrospray ionization source. Peptides were first loaded on a trapping column and subsequently separated inline on a 15 cm C18 column (75 μm x 15 cm, ReproSil-Pur 5 μm 200 Å C18-AQ). The mobile phase consisted of water with 0.1% formic acid or acetonitrile/water (80:20 (v/v)) with 0.1% formic acid. A linear 30 min gradient from 8% to 39% B was used to eluate peptides. MS data was acquired automatically by using Thermo Xcalibur 4.1 software (Thermo Fisher Scientific). An information dependent acquisition method consisted of an Orbitrap MS survey scan of mass range 300–1750 m/z followed by higher-energy C-trap dissociation (HCD) fragmentation for most intense peptide ions.

4.9   Cell culture (II)

HeLa cells (American Type Culture Collection, CCL−2) were cultured in DMEM/F12 media (Gibco) supplemented with 10% fetal calf serum (PromoCell),

50 IU/ml penicillin and 50 μg/ml streptomycin supplemented at 37°C in humidified atmosphere with 5% CO2. To induce autophagy, cells were amino acid- and serum-starved for 1 h. Cells were collected, lysed with RIPA buffer and cell debris pelleted by centrifugation (17,000 × g, 5 min, 4°C). Supernatant diluted with Laemmli buffer was used in Western blot analysis as described.

4.10   Preparation of testicular vesicle fraction (II)

Testes from 3 C57Bl/6J adult mice were collected, tunica albuginea removed, and seminiferous tubules minced with scissors. The solution containing the seminiferous tubule fragments was divided into 2 tubes containing 25 mL collagenase solution (0.1% glucose in PBS with 22.5 mg collagenase type I and 5 μg DNase I). Cells in collagenase solution were incubated at 34°C for 30 min with gentle shaking. Cells were centrifuged 5 min 500 × g at 4°C and the cell pellets washed twice with ice-cold 0.1% glucose PBS. Cells were combined to one tube and after a final 500 × g at 4°C centrifugation, supernatant was discarded and 1,500 μl of HEPES buffer (0.25 M sucrose, 10 mM HEPES, pH 7.2, 1X complete protease inhibitor cocktail) was added. Cells were disrupted by nitrogen cavitation (Parr Instruments, 500 p.s.i, 5 min at room temperature). Cell lysate was centrifuged 5 min, 17,000 × g at 4°C. FYCO1 complexes were immunoprecipitated using Dynabead Protein G coupled to either rabbit anti-FYCO1 antibody (Sigma) or rabbit IgG at 4°C overnight.

4.11   Isolation of germ cells (I-III)

Round spermatids and spermatocytes were isolated according to the protocol published by us[345] and included in this thesis "Enrichment of Pachytene Spermatocytes and Spermatids from Mouse Testes Using Standard Laboratory Equipment". Briefly, testes were decapsulated and digested using consecutive collagenase IV (C5138, Sigma) and DNase I (DN25, Sigma-Aldrich) supplemented trypsin digestions (LS003703, Worthington) in 1× KREBS buffer (prepared as described in[345]). Cells were washed with 1× KREBS filtered with 100μm filter and loaded on a BSA gradient. After a 2 h sedimentation, cells were collected, washed, and purity of fractions verified with DAPI staining.

4.12   Seminiferous tubule cultures (II-III)

4.12.1   Tissue preparation for seminiferous tubule cultures

Stage specific sections of mouse seminiferous tubules for tubule cultures were prepared according to protocol[41,342]. Briefly, mouse testes were decapsulated in

DMEM and sections representing specific stages (II-V and VII-VIII) of the seminiferous epithelium were isolated based on the light absorption pattern with the help of a stereomicroscope.

4.12.2   Studying autophagy in seminiferous tubule cultures (II)

Segments of the seminiferous epithelial cycle representing stages II-V and IV-VI were dissected from adult mice. Tubules were cultured in 50 µL final volume of DMEM with a drug (for stage II-V: wortmannin (Sigma, W1628) rapamycin (Santa Cruz Biotechnology, sc-3504) or bafilomycin A1 (Santa Cruz Biotechnology, sc-201550); for stage IV-VI: nocodazole (Sigma, M1404)) and vehicle (DMSO) or the vehicle alone for 6 h in a humidified incubator at 34°C, 5% CO2. For immunofluorescence analysis, squash slides were prepared after incubation and samples imaged as described. For protein expression quantification, sections of seminiferous tubules were collected by centrifugation $500 \times g$, 5 min in 4°C, homogenized in RIPA buffer with a TissueLyser LT (Qiagen, Hilden, Germany) 50 Hz for 30 seconds. Cells were left to lyse 30 min on ice, centrifuged to clear the supernatant and supernatant analyzed by western blot as described above.

4.12.3   EU labelling in seminiferous tubules, click reaction (III)

Segments of the seminiferous epithelial cycle representing stages VII–VIII were dissected. Tubules were placed on glass slides in 30 µl of DMEM supplemented with 1 mM ethynyl uridine (EU) at 34◦C for 10 h in a highly humidified atmosphere containing 5% CO2. Spermatogenic cells were spread out of the cultured seminiferous tubules to monolayers using the squash technique described above, snap frozen in liquid nitrogen, and fixed in 96% EtOH for 3 min. The nascent RNA was visualized using the Click-iT RNA Alexa Fluor 488 Imaging Kit (Molecular Probes, Invitrogen, C10329). Mounting was done using ProLong Diamond Antifade Mountant with DAPI (P36962, Life Technologies).

4.13   Antibodies (I-III)

- Rabbit polyclonal antibody against TSKS was a kind gift from Prof. J.A. Grootegoed, Department of Reproduction and Development, Erasmus MC - University Medical Center Rotterdam.

- Rabbit polyclonal antibody against UPF3B was a kind gift from Prof. Miles F. Wilkinson, UCSD, San Diego, USA

- Secondary antibodies conjugated with Alexa Fluor 488, 546, 594 and 647 made in donkey and streptavidin conjugated with Alexa Fluor 488 or 647 were

purchased from Thermo Fisher Scientific (A-21202, A-21206, A-11055, A10036, A10040, A-11056, A-21203, A-21207, A-11058, A-31571, A-31573, A-21447, S32354, S32357).

- ECL anti-mouse IgG HRP-linked whole antibody made in sheep (NA931) and ECL anti-rabbit IgG HRP-linked made in donkey (NA934) were purchased from GE Healthcare Life Sciences.

Table 2.   Antibodies.

Target	Species, Type	Cat. #	Company	WB	IF	IHC	Study
DDX25	goat, polyclonal	sc-51271	Santa Cruz		1:200		I,II,III
Hiwi	goat, polyclonal	sc-22685	Santa Cruz		1:100		III
ACTA2/ α actin	mouse	sc-32251	Santa Cruz		1:200		II
TUBA/ α tubulin	mouse	14-5698-82	Thermo Fischer		1:1000		II
DDX4	rabbit, polyclonal	ab13840	Abcam	1:500	1:200		I,II,III
LAMP1	rat, monoclonal	ab25245	Abcam		1:200		II
EIF4A3	rabbit, polyclonal	ab32485	Abcam	1:500	1:300		II,III
RUVBL2	rabbit, polyclonal	ab36569	Abcam		1:200		II
SMG6	rabbit, polyclonal	ab87539	Abcam	1:500	1:200	1:200	III
DCP1A	rabbit, polyclonal	ab47811	Abcam		1:100		II
ESPIN	mouse, monoclonal	611656	BD Bio-sciences		1:400		III
SOX9	rabbit, polyclonal	ab5535	EMD Millipore		1:400		III
PIWIL2 clone 13E-3	mouse	MABE363	Millipore		1:200		I,II,III
GAPDH	mouse, monoclonal	5G4	HyTest	1:1000			I,II,III
SMG7	rabbit, polyclonal	A302-170A	Bethyl Lab.	1:500	1:200		III
μH2AX	mouse, monoclonal	05-636	Millipore		1:100		I,II,III
hVasa	goat, polyclonal	AF2030-SP	R&D systems		1:200		III
PLZF	rabbit	sc-22839	Santa Cruz		1:400		II, IV
RUVBL1	rabbit, polyclonal	HPA019948	Sigma-Aldrich		1:200		II
FYCO1	mouse, polyclonal	H00079443-A01	Abnova		1:200		II
FYCO1	rabbit, polyclonal	HPA035526	Sigma-Aldrich	1:500	1:200		II,III
TDRD1	rabbit, polyclonal	PA5-58079	Thermo Fischer		1:200		III
UPF1	rabbit, monoclonal	D15G6	Cell Signaling		1:100		III
pUFP1	rabbit, polyclonal	07-1016	Millipore		1:100		III
PNA		RL-1072	Vector Lab.		1:2000		I,III
SMG1	rabbit, polyclonal	ab30916	Abcam		1:300		III
PIWIL1	rabbit, polyclonal	G82	Cell Signaling	1:500	1:200		I,III
LC3B	rabbit, polyclonal	2775	Cell Signaling	1:500	1:200		II

4.14   RNA sequencing (II-III)

4.14.1   RNA isolation

Total RNA was isolated from mouse testis at different time points postpartum, round spermatids, spermatocytes and isolated CBs using TRIsure (Bioline, BIO-38033) following standard protocols and manufacturer's instructions. Isolated RNA was analyzed using a NanoDrop (Thermo Scientific) and Bioanalyzer (Agilent). For the RNA profile of *Smg6*-cKO and control 24 dpp testes and CBs, the isolated RNA was separated in 10%–15% denaturing urea-polyacrylamide or 1–2% agarose gels, poststained with SYBR Gold (Invitrogen), and visualized using Chemidoc Imaging (BioRad).

4.14.2   Germ cell RNA sequencing and data analysis from *Fyco1*-cKO mice(II)

Two biological replicate samples from isolated round spermatids from adult *Fyco1*-cKO and control mice were submitted for RNA sequencing (Finnish Functional Genomics Centre, Turku Bioscience). PolyA RNA was enriched using standard protocols and sequencing performed with HiSeq 3000 sequencing system (Illumina, San Diego, CA, USA).

4.14.2.1   Differential expression analysis

Transcript analysis was performed using the *Mus musculus* genome as a reference (Ensembl built 82). Mapping of the transcripts was performed using STAR (Version 2.4.2a). Fragments per kilobase of transcript per million mapped reads quantification was performed with RSEM (RNA-Seq by Expectation-Maximization, Version 1.2.22) and count data was obtained with HTSeq (Version 0.6.1p1). Differential expression (DE) analysis was performed using the edgeR package[346]. piRNA precursor coordinates were from Li et al.[328]. and the coordinates for CB-associated novel transcripts from Meikar et al.[347]. Nonexpressed genes were filtered from the data. Only genes with ≥2 counts per million mapped reads were considered. Trimmed Mean of M-values (TMM) normalization was applied to account for the compositional bias. Transposons were quantified using the piPipes pipeline that uses the RepBase database for the transposon sequence information[348]. Cufflinks and Cuffmerge (Version 2.1.1)[349] were used to predict novel intergenic transcripts. Individual counts for the consensus loci were again obtained using HTSeq and the DE analysis was then performed with the edgeR package.

4.14.3 Germ cell RNA sequencing from *Smg6*-cKO mice(III)

Three biological replicate samples from isolated round spermatids and spermatocytes from adult *Smg6*-cKO and control mice (3x *Smg6*-cKO RS, 3x control RS, 3x *Smg6*-cKO SPC, 3x control SPC) were submitted for RNA sequencing (Finnish Functional Genomics Centre, Turku Bioscience). Libraries were created using Illumina TruSeq Stranded mRNA polyA library preparation kit and sequencing performed with HiSeq3000 sequencing system (Illumina, San Diego, CA, USA).

4.14.3.1 DE analysis of genes, TEs and piRNA precursors

For gene-level DE analysis, reads were trimmed off adapter contents using cutadapt (v2.8) and mapped to the mouse genome (Ensembl: Grcm38) using STAR (v2.7.3a). Reads were assigned and counted using featureCounts (v2.0.0) against reference gtf file (Ensembl: Grcm38) in paired-end mode. First, raw read counts were filtered to keep genes with ≥10 counts in at least three individual samples among six samples (RS or SPC). **For TEs,** reads were assigned and counted using TEtranscripts[350] and for piRNAs the 214 piRNA precursors[328] using featureCounts. Raw read counts were filtered to keep genes with ≥10 reads across all samples. Raw counts were normalized and DE calculated using DESeq2 in R (v4.1.3). **For transcript-level** DE analysis, the procedure was similar except raw read counts were filtered to keep only transcripts with ≥20 counts in at least three individual samples. GO plots were generated using clusterProfiler. Expression clustering was based on normalized counts extracted from each sample using DESeq2. The genes were filtered according to DE analysis and further normalized counts were scaled and averaged to finally use hclust() function in R for hierarchical clustering.

4.14.3.2 NMD-inducing features and stability

For analysis of NMD-inducing features, sequences were obtained using the UCSC Table Browser. To identify putative NMD features, a custom program was used[154,351]. Only Ensembl-defined transcripts harboring both 5'UTR and 3'UTR regions were considered. To find dEJs, exon junction positions for each transcript were identified and dEJs were defined as EJs ≥50 nt from the PTC. The 5'UTR sequences identified through the annotation process were used to scan for uORFs that contained particular nucleotides from the Kozak consensus sequence critical for initiating translation. In particular, we only considered uORFs ≥ 30 nt long that had a purine at the −3 position or a guanine at the +1 position (relative to the A in the AUG initiation codon [+1]). To reduce the probability of identifying uORFs that can re-initiate translation (and thus escape NMD), one additional criterion is that the uORF must not contain the main

ORF. To infer the RNA stability, we used the REMBRANDTS program[352] following the tutorial (https://github.com/csglab/REMBRANDTS).

4.14.3.3   3' UTR analysis

Transcripts were assembled (Cufflinks v2.2.1) and transcripts assemblies were merged (Cuffmerge). 3'UTR genomic locations were retained from cuffmerge output and a new gtf file was produced. Subsequently, a DE analysis was run using Cuffdiff in order to identify lowly expressed 3'UTR transcripts and filter merged transcripts. In parallel, Cuffmerge was used to merge transcripts assemblies from control and *Smg6*-cKO samples separately. Merged transcripts were trimmed to keep only 3'UTR locations and transcripts ≥1 FPKM.

4.14.3.4   *Smg6*-cKO vs. *Piwil1*-KO

The datasets for *Piwil1*-KO: GSE42004 and GSE64138 were downloaded. Reads were trimmed off adapter contents and low-quality bases were cut using trimmomatic (v0.39). The clean reads were mapped to the mouse genome (Ensembl: Mus musculus. GRCm38.101) using STAR (v2.7.1a), assigned and counted using featureCounts in R after mapping. After filtering the raw data to keep genes with reads above or equal to 10, reads were normalized and DE calculated using DESeq2. piRNA targets were predicted without filtering '–distance-from-canonical-cut-site' with GTBuster (https://github.com/weng-lab/GTBuster) and NCBI-BLAST. The piRNA species in RS with normalized read counts ≥ 1 were kept. piRNA target sites were predicted at the transcript-level, and the potential piRNA targeted transcripts were combined to genes according to their locations. The putative piRNA targets were identified based on two rules: (i) perfect pairing at g2–g7 of the piRNA molecule, and (ii) varying number of additional base pairing (8, 10, 12 or 14 matches) after the seed sequence at g8–g21.

4.14.3.5   Small RNA sequencing (III)

Small-RNAseq from the same samples was conducted using QIAseq miRNA library preparation kit and HiSeq2500 Rapid run sequencing platform (1 × 75 bp). SPORTS1.1[353] was used to map small RNA reads successively rRNA-derived small RNAs (rsRNA), miRNA, and transfer RNA-derived small RNAs (tsRNA) sequences extracted from mm10 UCSC genome files originating from rRNAdb, miRBase (v.22), and GtRNAdb (v.2.0) using SPORTS default settings. Using a pre-compiled Perl script from SPORTS1.1, the original locations of all sequences were identified and analyzed whether they originated from 5'end, 3'end or 3'CCA end of tRNA.

Then rsRNA, miRNA, and tsRNA sequences were extracted from SPORTS output text file using R. Repeats from repeatMasker and piRNA precursor locations[328] were mapped to the mouse genome (UCSC: mm10) using HISAT2 (v2.1.0); then, reads were assigned and counted using featureCounts (v2.0.0) against reference gtf files. Raw read counts were filtered to keep only genes with ≥1 occurrence per sample. FPM (fragment per million) was calculated after raw counts normalization using SPORTS output in R. Raw read counts were normalized and DE calculated using DESeq2.

4.14.4 Chromatoid body RNA sequencing (III)

Three *Smg6*-cKO and four control CB RNA samples were submitted for total RNA sequencing without ribosomal RNA removal (Novogene). Total RNA libraries were prepared by NEBNext® Ultra™ Directional RNA Library Prep Kit without fragmentation. Sequencing was performed with NovaSeq6000 (PE150) platform (Illumina). Gene and transcript level DE analysis, as well as the analysis for NMD-inducing features were performed as for germ cell samples.

4.15 RT-qPCR (II-III)

After DNase I treatment (AMPD1, Sigma) one microgram of extracted RNA was reversed transcribed using sensiFAST cDNA synthesis Kit (BIO-65054, Meridian bioscience). Before cDNA synthesis, RNA was treated with DNase I (Sigma-Aldrich, AMPD1). cDNA was synthesized with DyNAmo cDNA Synthesis Kit (Thermo Scientific, F-470), DyNAmo HS SYBR Green qPCR kit (Thermo Scientific, F-410) RT-qPCR was performed using SsoAdvanced Universal SYBR Green Supermix (Bio-Rad Laboratories, catalog no. 1725270), following manufacturer's instructions. Expression data were normalized to housekeeping genes. All RT-qPCR reactions and analysis were performed following MIQE guidelines.

4.16 Statistical analysis of the data (II-III)

For colocalization studies, Manders coefficients were calculated using BioimageXD and data analysis was done using MS Excel 2016. For other data analyses, R 4.1.3 or GraphPad Prism 9.0.0.JMP or GraphPad Prism 5/7/9 software (GraphPad Software, San Diego, CA, USA) was used. P values ≤ 0.05 were considered significant. All values are presented as mean ± standard error of the mean unless stated otherwise.

5 Results and Discussion

The following are the main results of studies I–III:

I. A method to enrich spermatids and pachytene spermatocytes from mouse testes using standard laboratory equipment was developed, published, and utilized in the studies II and III to discover novel aspects of germ granules.

II. Chromatoid Body component FYCO1 regulates the integrity of germ granules via autophagy.

III. Chromatoid Body component SMG6 is pivotal for the maintenance of male fertility and the transcriptomic balance of developing male germ cells.

5.1 A new enrichment method for germ cells

Over the past few decades, different techniques such as fluorescence-activated cell sorting (FACS)[23], centrifugal elutriation[21], and STA-PUT[24] have been successfully applied for the isolation of different germ cells from mouse testes. However, all these methods require dedicated devices and specialized training. In this study we wanted to create a protocol to isolate germ cells using only standard laboratory equipment and a minimal number of mice.

This method, named "**MDR**" (Modified Density gradient for Round spermatids), is a simple velocity sedimentation protocol to isolate elongating spermatids, round spermatids and pachytene spermatocytes from mouse testes. MDR requires minimal starting material, only standard laboratory equipment and reagents and very little training. This protocol has been used in both of the published research articles[354,355] included in this thesis. In addition several groups have recently published papers citing MDR as their method of choice for germ cell isolation[356–358].

5.1.1 The motivation for developing the MDR method

Much is still unknown about the molecular events taking place during mammalian spermatogenesis. As described in detail above (2.1.) the testis contains a mixture of germ cells, including spermatogonial stem cells, spermatogonia, spermatocytes at different stages, round spermatids, elongating spermatids and condensing spermatids as well as somatic Sertoli cells which are intermingled with germ cells and surrounded by peritubular myoid cells that form walls of the tubules, not to forget testosterone producing Leydig cells in the interstitial space between tubules. As each of these cell types have a distinct biochemical and molecular profile, any analysis placed on the entire testis does not necessarily provide the answers one is looking for (discussed under 2.4.). Therefore, the proper study of spermatogenesis often requires the separation of a germ cell population from the complex mixture prior to analysis.

Many different strategies exist for cell enrichment. The most successful methods to date are centrifugal elutriation based on counterflow centrifugation[21], FACS sorting[22,23] which is based on DNA content or specific markers and the STA-PUT velocity sedimentation by unit gravity[24]. These methods are widely used by experts in the spermatogenesis field, and they produce highly enriched germ cell populations. However, these techniques are all limited by the requirement for specialized, expensive instruments and training and, in the case of elutriation and STA-PUT, a substantial amount of starting material.

The principal goal of this study was to develop a method that allows for the isolation of a highly enriched round spermatid population from mouse testes using as little starting material as possible. Later, during the optimization phase, elongated spermatids and spermatocytes were found to isolate nicely as well. Importantly, an additional key criterion for the method was its flexibility when using genetically modified mice *i.e.* successful enrichment should be possible when using mice that have a reduced number of (certain) cells or mice that lack certain cell types altogether. The method should also be simple and produce easily reproducible results *i.e.* one would not require extensive training to master this technique. Finally, the aim was to create accessibility for such a method *i.e.* one would not need to invest significant funds towards particular instrumentation.

5.1.2 MDR method development and optimization

The optimized MDR method consists of four main steps: preparing of a single-cell suspension from testes, constructing a layered BSA gradient onto which the cell suspension is loaded, manual collection of 1 ml cell fractions after sedimentation and analysis of the fractions. The overall flow of the method, the time needed for the main steps and main outcomes are presented in the original publication (I, Figure 4)

5.1.2.1 Single-cell suspension

Developing the pretreatment protocol – separating germ cells from the seminiferous epithelium (I, Figure 2A) – was the first optimization step aiming for fast and gentle yet efficient procedure able to produce a homogenous single-cell suspension allowing for a reliable separation of cells on the gradient. Sequential enzymatic digestions were chosen: collagenase IV followed by trypsin, combined with use of a bicarbonate buffer (KREBS buffer) which has been shown to improve the separation and viability of the germ cells[359].

Collagenase IV digestion is done to remove interstitial cells. This digestion untangles the tubules detaching them from their environment but leaving them intact (Figure 7). If digestion at this step is incomplete, the eventual yield will suffer as the enzymes in following steps cannot perform at optimal level. And on the other hand, a prolonged digestion can lead to the premature release of spermatids from tubules and their loss during the wash steps. By carefully observing the tubules and by analyzing the contents of the supernatant after collagenase treatment, a three-minute incubation in 37 °C water bath was chosen. Before moving to the next steps, the tubules are carefully washed, a pivotal step, which when omitted would lead to significant contamination of the final cell fractions by interstitial cells.

Trypsin digestion is done to release germ cells from the seminiferous tubules and each other. The key to optimizing the digestion time was balancing efficient digestion with cell lysis that occurs after a cell has been released from the protective environment of the seminiferous tubule. At this step, visual observation of the suspension is telling: optimal digestion turns the spaghetti-like tubules into small pieces and the liquid from clear to cloudy (Figure 7). Due to occasional cell lysis, and subsequent release of genomic DNA, slight clumping is acceptable as the following filtering steps remove irregularities from the solution. To combat clumping, DNAse I was added to this step. The appearance of substantial clumps even with DNAse I implies the cellular state is compromised due to excessive cell lysis, which cannot be compensated with more DNAse I. Instead, one should double check the incubation environment and enzyme activity (which may vary between batches and/or during storage) for the following MDR isolations so optimal cell yield and viability of the cells is achieved.
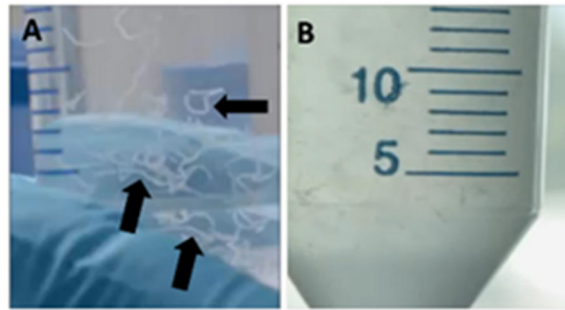
Figure 7. Testicular sample after collagenase IV (A) and trypsin (B) treatments. Arrows indicate pieces of seminiferous tubules after collagenase treatment, during the first subsequent wash. At this point germ cells are still inside the seminiferous tubules The liquid changes from clear to cloudy during trypsin treatment due to the release of germ cells from the seminiferous tubules. (*Modified from Da Ros et al.*[360])
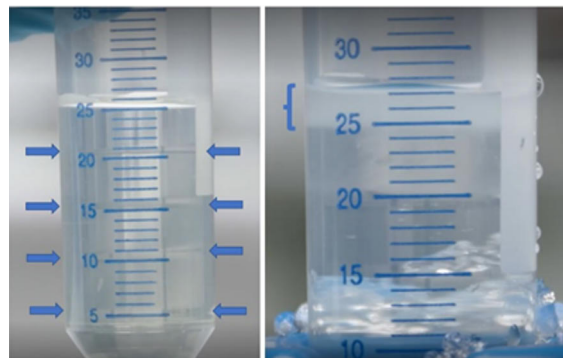
Figure 8. Freshly prepared BSA gradient (left) and the gradient with cells loaded (right). The layers between the different BSA solutions are clearly visible (arrows) as well as the cloudy layer of cells on top of the gradient between (indicated). Furthermore, the following layer (1%, between 20-25 ml lines) is slightly cloudier as cells have begun to sediment. (*Modified from Da Ros et al.*[360])

5.1.2.2 The gradient

For MDR, the underlying principle of the STA-PUT[24] method was downscaled and modified. Instead of a linear gradient in large chambers, a discontinuous gradient is built inside a standard 50 ml conical tube. The five layered gradient is build using standard pipettes and cut pipette tips by starting from the densest BSA solution (5%) in 5ml sections until reaching 1%. The cells are then loaded on top in a 0,5% solution which is just dense enough to layer the cells on top of the gradient without piercing the structure. Different sedimentation times were tested, and the protocol optimized to 1h30min which is enough to obtain good separation of all three cell types: elongating spermatids, round spermatids, and spermatocytes. As the gradient is built by hand, pipetting each layer on top of each other, a mechanical pipette with a

smooth piston and a steady hand are required. When the construction of the gradient has been successful, one can clearly tell the line between different BSA solutions in the ready gradient although with time the layers will begin to diffuse (Figure 8). The gradient should be produced directly prior to use on a stable surface before the diffusion takes place. After loading the cells, a clear layer of cloudy suspension should be visible on top of the gradient before the cells being to sediment.

5.1.2.3   Fractions collection and analysis

Instead of using a fraction collector, the cells are manually collected as 1 ml fractions of BSA solution using standard pipettes with cut pipette tips moving from the top of the gradient toward the bottom (I, Figure 1). The cells in each fraction are then washed and samples taken before one can proceed with downstream analysis or before moving samples to storage.

Careful analysis of each cell fraction is pivotal to ensure proper enrichment and should be done before combining fractions and moving to downstream analysis. Therefore, alongside the MDR method, we introduce a quick staining protocol for the user. Samples from each fraction are quick-fixed on a standard microscopy slide with 4% PFA and stained with DAPI to visualize the nucleus of each cell. Then a fluorescence microscope is used to assess the enrichment percentage by observing nuclear morphology and quantifying cells based on the hallmarks of different cell types. Mainly, the round spermatid nucleus is often symmetrically round, small (6−7 µm in diameter), and contains a single round heterochromatin structure, the chromocenter. Nuclei of elongating spermatids are typically elongated, curved in shape, and smaller due to chromatin condensation. The nuclei of pachytene spermatocyte are by comparison larger (>10 µm in diameter) and more irregular in shape, with dense areas of packed chromatin distributed throughout.

For the confident user, DAPI staining should suffice (I, Figure 2A). However, another protocol containing IF staining steps with specific markers, such as PNA for acrosome staining (Figure 3) was added (I, Figure 2C,D) to ensure that all researchers, in addition to true germ cell aficionados, could reliably tell the purity of the fractions obtained. In fact, it is always recommendable to collect a second set aside of the quick DAPI staining for later analysis to double-check the enrichment percentage as any results obtained from the fractions in the downstream analysis should be considered in the light of what cells were, in fact, obtained. This method is routinely used by several researchers in our laboratory and regardless of the user, the enrichment pattern remains the same: elongating spermatids fractions 1-2, round spermatids 5-8 and pachytene spermatocytes 14-15. Nevertheless, it is absolutely pivotal to carefully check the success of each MDR round. Arguably, this is the approach anyone should take with any cell enrichment method whenever possible.

5.1.3   Representative results: Enrichment level

As mentioned, this method is regularly used in our laboratory and enriched round spermatids representing >90% of all cells in the appropriate fractions are routinely obtained. For pachytene spermatocytes and elongating spermatids enrichment level of ~75% and ~80% respectively is usually reached. Results from one representative MDR enrichment are shown in Figure 9. In this example, fraction 1 contains ~80% of elongating spermatids of which most have condensed nuclei. The following fractions contain round spermatids and the enrichment was above 90% for fractions 2-4, and more than 80% altogether in seven fractions (2−8). Pachytene spermatocytes of ~75% purity were obtained in fractions 14 and 15.

5.1.4   Representative results: Quantity

In the representative enrichment example presented in Figure 9, round spermatid fractions (5−8) when combined contained >10 million cells. The best pachytene spermatocyte fractions (14 and 15) contained $1.5−2.0 \times 10^6$ cells per fraction and the best elongating spermatid fraction 0.75×10^6 cells. In our experience this example MDR enrichment is in line with our usual results as typically the method performs best for round spermatids. In the example, the range of RNA obtained from each fraction was 0.5−2.5 µg and the amount of protein varied from 20−140 µg which are also in line with our usual RNA and protein yields. Therefore, most downstream RNA and protein analysis can be performed from each individual fraction. See the original publication for examples of quantities obtained (I, Figure 3A-B) and for examples of downstream protein work (I, Figure 3C-D). See publication III[34] for examples on RNA work where 2-3 fractions of RS and SPC were combined for RNAseq, small RNAseq and qRT-PCR.
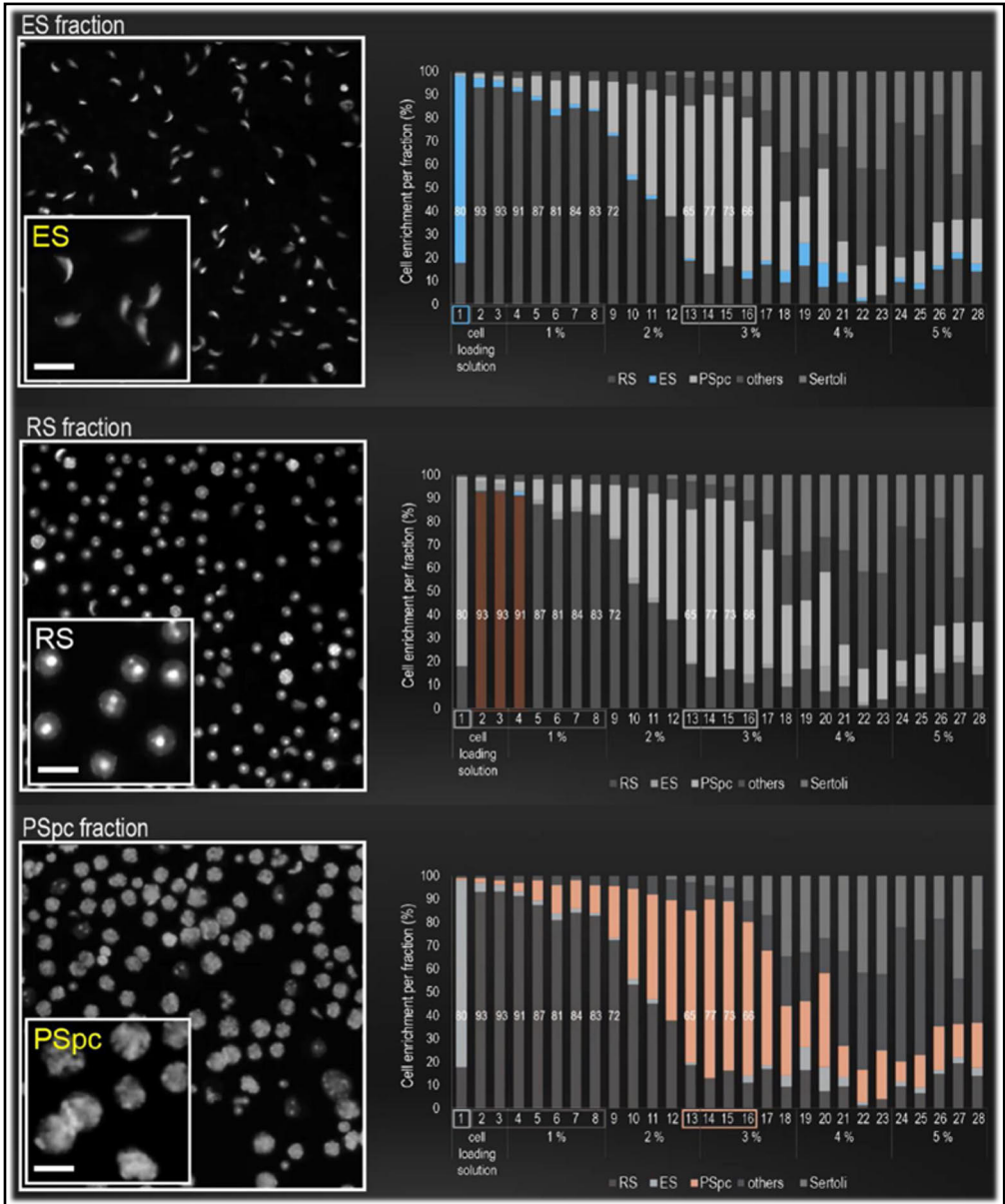
Figure 9. Relative quantification of different germ cells per collected 1 ml fraction starting from fraction 1 that is collected first from the top of the gradient and continued until fraction 28. Cells were categorized to elongated spermatids (ES, blue), round spermatids (RS, brown), pachytene spermatocytes (PSpc, orange), Sertoli, and other cells (containing all other germ cells and somatic cells, including Leydig cells). The fraction numbers and respective percentages of BSA in the gradient are indicated on the x-axis. (*Modified from Da Ros et al.[360]*)

5.1.5   The advantages and limitations of MDR

The main advantages of the MDR method are its feasibility, simplicity, and speed. No special equipment or specialized training is needed making MDR feasible for any researchers working in a standard molecular medicine laboratory setting. The basis for the enrichment technique is simple and thus easy to troubleshoot if needed. After euthanizing the animal, fractions of enriched germ cells are collected in 3,5h. A fast-track method to assess the purity of fractions is also provided as part of the protocol. Finally, the MDR method was optimized to collect enriched fraction of germ cells form a single mouse while still obtaining a sufficient number of enriched cells for downstream analyses. This helps reducing costs and the number of animals, which is highly important not only considering animal work ethics and 3Rs but also considering the cost and limited availability of genetically modified mice. Standard STA-PUT[361] protocol recommends using as much as 12 adult mice, although from experience I can tell that successful isolation can be done from 3-4 adult mice. The lowest amount of starting material reported to be sufficient for centrifugal elutriation is 6 mouse testes (3 mice).

Like any technique, the MDR method has its limitations. The method was optimized using two testes of an adult mouse (80-120 mg/testis) as starting material. Successful enrichment from the reduced amount of starting material has been performed. Specifically, during sample collection for the publication III[34] successful germ cell enrichment of round spermatids and spermatocytes was routinely performed from *Smg6*-cKO mice that have smaller testes (40-65 mg/testis), have increased germ cell apoptosis and lack elongating spermatids. Therefore, downscaling the method down to two testes has proven to be efficient. However, upscaling by increasing the starting material (>2 adult testis) is not recommended. The cells are meant to be loaded on top of the gradient in solution of given density that allows for the cells to remain on top and "line-up" before descending. However excess number of cells can severely interfere with this part of the protocol, saturating the gradient and causing the cells to remain stuck rather than gravitating downwards. Therefore, one can only upscale the procedure by building additional gradients. When large quantities of cells are needed, one should consider the previously mentioned methods such as the STA-PUT[361].

The most important limitation, however, is that there are several testicular cell types that cannot be enriched using this protocol. As mentioned, this protocol was developed to isolate round spermatids and while a good number of elongating spermatids and spermatocytes with decent enrichment are obtained as well, several other cellular types are not obtained as enriched fractions as illustrated by the cell count in Figure 9.

5.1.6   Future perspectives and final remarks

Recently, isolated germ cells are on demand, particularly since the discovery of male germ cell-predominant piRNAs and their role in pathologies and since the paternal epigenetic inheritance of acquired disorders has gained more interest. While our motivation for the development of MDR was to add a fast low-starting-material method to our own repertoire, the motivation for publishing it was to provide a feasible method for the research groups new to the germ cell field as well as the groups not focusing on spermatogenesis. In addition, MDR provides a convenient tool for established germ cell groups who, like us, can use it alongside other techniques such as FACS or STA-PUT as each method has their advantages and disadvantages. This protocol has been used in both of the published research articles [354,355] included in this thesis and discussed next. In addition, several groups have recently published papers citing MDR as their method of choice for germ cell enrichment and have successfully used it in their downstream analysis[356–358,362].

5.2   Two novel germ granule components

FYCO1 and SMG6 were previously identified as highly-enriched CB components[26]. Both proteins were found to be ubiquitously expressed proteins in adult mouse tissues. Both also had particularly prominent expression patterns in testes. Expression study in juvenile mice, during the first wave of spermatogenesis, at time points reflecting the initial appearance of specific spermatogenic cells revealed a similar pattern. FYCO1 and SMG6 are expressed at low level at postnatal week 1, when only somatic cells and spermatogonia are present, and at week 2, when spermatogonia have just differentiated to form spermatocytes. Their expression increases at week 3, when spermatocytes undergo meiosis and split to round spermatids, and further increases from week 4 onwards. Both proteins appear as granular material highly concentrated to cytoplasmic sites in developing germ cells, particularly pachytene spermatocytes and round spermatids. After co-localization studies with known CB markers, it was determined that both are indeed novel germ granule components.

These two proteins, FYCO1 and SMG6, were chosen as the two target proteins of this thesis. Using a similar strategy, both projects started with the creation of a mutant mouse model lacking the target protein. Thereafter initial discoveries and the phenotypes of *Fyco1*-cKO and *Smg6*-cKO led the two projects to two separate directions and thus, will be discussed separately, until final conclusions.

5.3 FYCO1

The CB is in close communication with several membranous structures of the endomembrane system, the nuclear envelope, the Golgi complex, the ER and MVBs[251,252,363]. But it were the dozens of mysterious small vesicles in the immediate CB periphery that became the focus of this study. These vesicular structures of unknown function are always detected in the immediate CB periphery of and were shown by us[364] to also reside inside its cavities. A previous study had tentatively suggested a connection between CBs and autophagy[253], and as the only autophagy related protein in the CB proteome was FYCO1, we launched this study to see whether this relatively large adaptor protein is the missing link between the CB and a key cellular homeostasis maintenance process, autophagy.

5.3.1 FYCO1 is a peripheral CB component

Immunofluorescence analysis showed that FYCO1 co-localizes with known CB markers from late pachytene spermatocytes to round spermatids. FYCO1 is present all the way to elongating spermatids where it localizes to the uncharacterized late CBs and co-precipitates with late CB markers TSSK1 and TSSK2 (II, Supplementary Table 1). Detailed imaging of round spermatid CBs demonstrated that FYCO1 localizes to the peripheral regions of the CB rather than "the core" of the structure. FYCO1 appears to extend over the surface of the CB and is often also observed in areas outside of the main CB matrix (II, Figure 2).

In line with this, we found that the FYCO1 interaction partners identified via mass spectrometric analysis extend beyond CB proteins such as DDX4 and DDX25 (II, Figure 4). In HeLa cells, FYCO1 has been implicated in the plus end-directed microtubule-dependent vesicle transport as its overexpression induces peripheral redistribution of lysosomes, autophagosomes and autolysosomes[294]. Presumably, FYCO1 interfaces with plus end-directed kinesin motor proteins. In the mouse testis, FYCO1 interacted with several kinesin proteins (such as kinesin heavy chain isoform KIF5C, kinesin-like proteins KIFC2, KIFC3, KIF3A, KIF3B, and kinesin light chain 3) which indicates that FYCO1's role as an autophagy adaptor protein is retained in germ cells. FYCO1 interactome also included proteins involved in the ubiquitination pathway including E3 ubiquitin protein ligases HERC2, TRIM36, UBR4 and several CULLIN proteins (CUL9, CUL7, CUL4A), which are components of the ubiquitin-protein ligase complexes. Therefore, the results suggest that FYCO1 acts as an adaptor between the CB and cellular processes, in particular processes regulating protein turnover and the maintenance of cellular homeostasis. (II, Supplemental Table1).

5.3.2   *Fyco1*-cKO male mice are fertile

All previous (published) KO models where a CB core component such as PIWIL1, PIWIL2, DDX4, TDRD6 or TDRD7 was depleted resulted in spermatogenic failure[236] (Figure 6). Nonetheless *Fyco1*-cKO (*Fyco1(fx/fx);Neurog3 Cre+*) mice displayed normal testis size and histology, normal spermatogenesis, produced morphologically normal spermatozoa and delivered pups at equal number to control (*Fyco1(fx/fx);Neurog3 Cre-*) mice. For details on generating and validating the mouse model, see original publication II. In line with our results, another FYCO1 KO mouse model was also recently published and reported to have macroscopically and microscopically normal organs and tissues with no fertility issues declared[365]. Therefore, to date, FYCO1 is the only CB component whose depletion has not led to impaired male fertility.

5.3.3   FYCO1 inactivation disrupts CB structure

FYCO1 has been shown to bind phosphatidylinositol 3-phosphate (PI3P) via its FYVE domain[294]. PI3P is a central phospholipid to autophagy that is generated by phosphatidylinositol 3-kinase (PI3K). Inhibition of PI3K effectively inhibits autophagy as, among other things, PI3K controls the activation of a key autophagy regulator, mTOR. In seminiferous tubule cultures, PI3K inhibitor treatment[366] clearly impacted the CB morphology and created FYCO1 positive and FYCO1 negative domains within the CB (II, Figure 3). The morphology of the CB is therefore subject to change upon external stimuli.

A dramatic change in the CB morphology was further seen upon FYCO1 depletion, in *Fyco1*-cKO mice. Instead of one large perinuclear granule, several smaller CBs appeared in the cytoplasm of *Fyco1*-cKO early (stage I) mid (stage II-V) and late (stage VII-VIII) round spermatids. While the CB of *Fyco1*-cKO was clearly fragmented into smaller pieces than a full CB, the total quantified area occupied by CB material per nuclei was increased. Several CB protein components were analysed and apart from PIWIL2 whose expression seemed reduced, most were unaffected by FYCO1 depletion (II, Figure 8B). This indicates that though the CB structure was disrupted, its core functions are intact.

5.3.4   FYCO1 inactivation disrupts CB-vesicle associations

EM analysis revealed that in mice the CB is associated with cup-shaped double-membrane vesicles of 100-200nm in diameter (II, Figure 6A,B). Large perinuclear LC3B-positive areas were also detected by immunofluorescence (II, Figure 6C). In the absence of FYCO1 the association of LC3B with the fragmented CB (detected by DDX25) was clearly reduced from ~30% of overlap to only ~10% and larger

LC3B-positive areas were completely absent (II, Figure 6D). Furthermore, the overall number of CB-associated vesicles was greatly reduced throughout round spermatid development. FYCO1 interaction with LC3B in tissue, previously shown in Hela[294], was demonstrated by anti-FYCO1 immunoprecipitation from round spermatid vesicle-containing fractions. Both LC3-I and LC3-II were shown to co-precipitate with FYCO1 (II, Figure 6E). The aforementioned results indicate that FYCO1 is directly involved in the recruitment of LC3 positive vesicles to the CB.

5.3.5   CB-vesicle associations and autophagy

Apart from LC3B, LAMP1-positive vesicles were also detected in the cytoplasm of stage II-V round spermatids. While under physiological conditions some LAMP1 positive vesicles were detected in the CB vicinity, a clear increase took place after the tubules were exposed to rapamycin – a well-characterized autophagy inducer – or bafilomycin A1 – an autophagy inhibitor[367] (II, Figure 7A). However, in the absence of FYCO1, rapamycin did not induce an accumulation of LAMP1-positive vesicles onto the CB nor did bafilomycin A1 have any detectable effect either (II, Figure 7A). Curiously, treatment with rapamycin, but not bafilomycin 1A, led to the downregulation of PIWIL2 levels in the presence, but not in the absence of FYCO1 (II, Figure 8C). Overall, a clear link between CB components, CB associated vesicles and autophagy was established.

5.3.6   Discussion of FYCO1

While searching for the missing link between the CB and the vesicles around it, FYCO1 was identified. FYCO1 is among the most abundant CB-proteins and as one of the few linked to vesicular transport among the CB proteome, it was chosen as a promising candidate for this investigation. FYCO1 is an autophagy adaptor protein that can interact with LC3 and RAB7, two autophagy membrane-associated proteins. This complex can further interact with kinesin motor proteins and mediate microtubule plus-end-directed autophagosome transport[294,295]. In the mouse testis, FYCO1 was found to interact with several kinesin proteins (II, Figure 4) as well as LC3 (II, Figure 6) indicating that FYCO1's role as an autophagy adaptor protein could be retained in germ cells. Thereafter two different techniques were used to study the effect of FYCO1 depletion on the "CB vesicles" and with both approaches a similar observation was made. Via immunofluorescence the LC3 positive cloud usually residing close to the CB dispersed in the absence of FYCO1 and very little overlap between LC3 and the CB was detected. And via EM nearly all small cup-shaped vesicles in the CB vicinity disappeared in the absence of FYCO1 (II, Figure 6). Together these results indicate that LC3 positive autophagic vesicles are normally

present in the CB vicinity and that FYCO1 is the adaptor protein directly involved in their recruitment there.

Manipulating the autophagy pathway resulted in diverse phenotypes in the mouse testis. FYCO1 had previously been shown to bind PI3P, a central phospholipid to autophagy generated by PI3K[294]. To explore the connection between the CB and autophagy in the testis, seminiferous tubule cultures were set to inhibit autophagy by using wortmannin, a PI3K inhibitor[366]. Using this well-characterized autophagy inhibitor that specifically targets the phosphatidylinositol 3-kinase that produces PI3P needed for autophagosome formation, the FYCO1 signal moved from around the CB to a distinct domain that only partially covered the DDX25 positive CB area much like a Venn diagram with some overlapping components (II, Figure 3). The significance of this curious phenotype remains to be investigated but regardless, this experiment clearly demonstrated that the morphology of the CB is sensitive to changes in the autophagy pathway. And indeed, by then removing FYCO1, an autophagy adaptor protein from postnatal germ cells, an even more dramatic CB phenotype emerged. The morphology of the CB was consistently and evidently fragmented. Instead of one large perinuclear granule several smaller CBs appeared in the cytoplasm of round spermatids (II, Figure 5).

Drawing from our evidence it seems that autophagy may be required for the maintenance of germ granule integrity. As autophagy is a negative regulatory pathway, one could expect its targets to become accumulated if an important factor (here: adaptor) is removed. Therefore, the increase in DDX25-positive CB material in *Fyco1*-cKO round spermatids could indicate a defective turnover of the germ granule material and suggest FYCO1 participates in granulophagy that removes RNP granule material (II, Figure 5). While this would explain the increased granular material, we were unable to show a quantifiable accumulation of any single CB protein via western blot analysis from total testis extracts and instead found all studied CB components at comparable levels to controls except for one well-established CB component which was detected at lower levels.

PIWIL2 was shown to be expressed at reduced levels in the absence of FYCO1 (II, Figure 8). While PIWIl2 was seen correctly localized to CB fragments, its expression in total testis western blot analysis was significantly reduced. Importantly, the PIWIL2 protein level responded to autophagy induction in control cells but not in *Fyco1*-cKO where PIWIL2 was already expressed at a lower level (II, Figure 8 A-C). This indicates that the PIWIL2 downregulation is tied to autophagy as upon autophagy induction it is downregulated but only if the autophagy adaptor, FYCO1, is present. Therefore, the downregulation of this piRNA pathway component during autophagy induction appears to be dependent on FYCO1. However, while a link between PIWIL2 expression and autophagy in male germ cells is indicated by these results the mechanism governing these events is unknown. It is

possible that the absence of FYCO1 leads to the activation of another molecular pathway that in turn induces PIWIL2 downregulation. Or perhaps PIWIL2 is required for a function that becomes redundant due to the altered CB morphology seen in *Fyco1*-cKO (II, Figure 5). Either way as FYCO1 mice exhibit normal spermatogenesis and fertility, it is unlikely that the piRNA pathway is compromised or defected but rather the downregulation of PIWIL2 is linked to a secondary activity of this protein.

Nocodazole treatment to inhibit microtubule polymerization in wildtype mice caused a similar fragmentation to that of FYCO1 depletion (II, Figure 5E). A functioning microtubule network is therefore required for correct CB structure assembly and maintenance. While a microtubule defect in *Fyco1*-cKO seemed unlikely due to the mild phenotype of the mice, the status of the microtubule network in *Fyco1*-cKO was examined. As expected, no abnormalities in microtubules were found (II, Figure 5F). Importantly, nocodazole treatment of *Fyco1*-cKO did not alter the CB morphology further indicating that the required pathway to structural CB maintenance was already disrupted in *Fyco1*-cKO (II, Figure 5E). Presumably, FYCO1 acts as the adaptor between the CB "core" components and microtubule climbing kinesin proteins both of which it was shown to interact with in co-immunoprecipition studies (II, Figure 4). This suggests that functioning FYCO1-mediated autophagosome trafficking is required for CB integrity.

Discovering that autophagy related processes are taking place in the immediate CB surroundings raises the question whether autophagy is required for round spermatid homeostasis and furthermore fertility. The CB is well-recognized as a pivotal granule for male fertility maintenance demonstrated repeatedly by numerous KO models where a CB component has been inactivated (Figure 6). It was therefore surprising that *Fyco1*-cKO mice appeared to have completely normal fertility. In fact, *Fyco1*-cKO mice were successfully bred for dozens of generations and for several years (beyond the duration of our fertility trials) with no observable delayed or accumulative effects on their fertility (II, Supplemental Figure S3). Even more curious is the notion that while no effect on male fertility was observed the removal of FYCO1 did not leave the testicular phenotype untouched but instead several clear consequences of its removal were detected on a molecular level. Not only was the structure of the CB altered but most noticeably the relationship with the CB and small vesicles had dramatically changed as vesicles appeared to have deserted the CB. Furthermore, the expression level of PIWIL2 was reduced in *Fyco1*-cKO testis. And yet, no observable effects on male fertility were detected. However, while spermatogenesis was thoroughly assessed with each cell type placed under the microscope, so-to-speak as well as literally, spermatozoa were not scrutinized to great detail. As *Fyco1*-cKO sperm was functional and intact enough to produce equivalent number of pups to control mice

throughout this 5-year projects lifetime the detailed analysis of spermatozoa was beyond the scope of this study. Therefore, while crude morphological comparison found no differences compared to control sperm, there is a small chance that subtle differences in spermatogenetic capacity or optimal fertility could have been overlooked.

Spermatogenesis of *Fyco1*-cKO - normal under normal conditions. A recent study with a similar KO model, demonstrated that FYCO1 is essential for adaptation to cardiac stress in mice[368]. FYCO1 deletion did not affect basal autophagy in isolated cardiomyocytes but only under glucose deprivation. Likewise, while *Fyco1*-deficient mice did not display differences in cardiac function under basal conditions, a 48h food deprivation experiment demonstrated that starved KO mice had significantly impaired cardiac parameters compared to controls. FYCO1 overexpression on the other hand was able to induce autophagy in isolated cardiomyocytes and transgenic mouse hearts, rescuing cardiac dysfunction[368]. Assuming that FYCO1 main function is connected to its previously identified role as an adaptor protein in autophagy in germ cells as well, its role in maintaining spermatogenesis might not have been evident under physiological conditions. It is possible that FYCO1-dependent processes are dispensable for the normal progression of spermatogenesis under physiological conditions but become needed if autophagy is induced as response to cellular stress. In our studies *Fyco1*-deficient mice were not subjected to adverse conditions and this therefore remains to be seen. Further studies involving toxicological and aging-related mouse models could elucidate the potential role of FYCO1 in mediating autophagy responses induced by stress in spermatogenic cells.

Finally, in recent years FYCO1 has been gaining interest among eye researchers. FYCO1 was discovered to have a role in lens development and transparency in humans, where some mutations were directly linked to congenital cataracts, which is a significant cause of vision loss in children[301,302,365,369–371]. FYCO1 has also been implicated in other pathologies such as osteoporosis[372] and, as mentioned, heart disease[368]. However, no human studies linking spermatogenesis and FYCO1 have so far been reported.

5.4   SMG6

The exceptionally diverse transcriptome of developing germ cells creates a demand for effective RNA regulatory mechanisms. Components of two RNA regulatory pathways, the piRNA pathway and the NMD pathway, as well as different RNA species and RBPs accumulate to the CB that creates a granular platform for diverse interactions. As SMG6 has a particularly prominent CB localization and it is the sole

endonuclease found in the CB proteome[26], deciphering its functional role in spermatogenesis became the aim of this study.

5.4.1 SMG6 is a core CB component

SMG6 co-localizes with known CB markers in mice (III, Figure 1F) and human round spermatids (III, Figure 1G). In addition, in mouse late pachytene spermatocytes, SMG6 partially co-localizes with DDX4 and PIWIL1 both of which localize to the CB and IMC. SMG6 also fully co-localizes with DDX25 which is only associated with the CB precursors (and not the IMC). Therefore, SMG6 is accumulated specifically to the CB where it resides with other NMD components such as UPF1 and UPF3B (III, Supplemental Figure S2A,B). However, SMG7, which represents another branch on NMD, did not accumulate to the CB (III, Fig. 2A, Supplemental Fig. S2C) and SMG7 was absent from CB-immunoprecipitation as well (III, Figure 2B). In testis, there is a partial overlap of SMG6 and SMG7 interactomes but the majority of binding partners are unique to either SMG6 or SMG7 (III, Figure 2D). SMG7 interactome contained its well-known partner SMG5 and many proteins indicated in the ubiquitination pathway. SMG6 interacts with CB-associated proteins, such as DDX4, PIWIL1 and TDRD3 (III, Supplemental Table S1).

5.4.2 *Smg6*-cKO male mice are infertile

In breeding trials *Smg6*-cKO (*Smg6(fx/fx);Neurog3Cre+*) mice did not reproduce when co-caged with wildtype females. Furthermore *Smg6*-cKO testes were significantly smaller in size (III, Figure 3F, Supplemental Figure S3C), cauda epididymides from *Smg6*-cKO appeared abnormally translucent (III, Figure 3I) and histological examination revealed a complete absence of mature spermatozoa (III, Figure 3H). Instead, the epididymides were filled with atypical round cells, indicating the release of immature germ cells from the seminiferous epithelium (III, Figure 3H, Supplemental Figure S3D). Histological examination of *Smg6*-cKO testis revealed that in the absence of SMG6 spermatogenesis arrests at the round spermatid stage (III, Figure 4A,B, Supplemental Figure S4). Quantification of cell types showed no difference for SOX3-positive undifferentiated spermatogonia or SOX9-positive Sertoli cells (III, Figure 4A, Supplemental Figure S5A) but the sex body-containing pachytene spermatocytes were significantly decreased and, most notably, the number of round spermatids was dramatically reduced, and no elongating spermatids were found in any histological examinations (III, Figure 4A, Supplemental Figure S5B). No phenotype was observed for heterozygous

(*Smg6(fx/wt);Neurog3 Cre+*) mice (III, Figure 3E,F). For details on generating and validating the mouse model, see original publication III.

5.4.3 SMG6 inactivation leads to transcriptome imbalance

SMG6 inactivation is expected to compromise the NMD pathway and lead to the upregulation of SMG6's targets. More than 2000 misregulated genes in spermatocytes and more than 6000 misregulated genes in round spermatids were identified in the absence of SMG6. More specifically, the differential expression (DE) analysis identified 808 up- and 1392 downregulated genes in *Smg6*-cKO spermatocytes, and 2971 up- and 3121 downregulated genes in round spermatids (III, Figure 5A, B,5A, B, Supplementary Table S3A, B). The vast majority of the upregulated genes (~90%) in round spermatids were protein-coding and the rest corresponded to pseudogenes and other non-coding RNAs (III, Supplementary Table S3A, B).

By grouping the genes based on their expression patterns, 6 groups emerged: genes downregulated solely in *Smg6*-cKO spermatocytes (P1; ~210 genes), round spermatids (P3; ~3070 genes), or both (P2; 60 genes), and genes upregulated solely in *Smg6*-cKO spermatocytes (P4; ~570 genes), round spermatids (P6; ~1250 genes), or both (P5: ~1540 genes) (III, Figure 5C). GO analysis linked the downregulated genes to processes related to fertilization and spermiogenesis, such as flagellum biogenesis (III, Figure 5D) which might simply reflect the spermatogenic arrest phenotype of *Smg6*-cKO. The upregulated genes, on the other hand, were significantly enriched for biological processes unrelated to spermatogenesis, such as immune functions.

5.4.4 SMG6 is required for the meiotic-to-postmeiotic molecular switch

SMG6 expression peaks during the meiotic-to-postmeiotic transition (III, Figure 1, Supplementary Figure S1) which is the phase right before the detrimental effects of SMG6 depletion occur in spermatogenesis (III, Figure 3 and 4, Supplementary Figure S3). Hierarchical clustering of meiotic and post-meiotic cells isolated from *Smg6*-cKO and control testis revealed that *Smg6*-cKO round spermatids cluster closely not with control round spermatids but rather with spermatocytes. SMG6 inactivation thus appears to interfere with the spermatocyte-to-round spermatid differentiation inhibiting the SMG6 deprived cells to switch to correct molecular programs and proceed in haploid differentiation (III, Figure 5E).

According to our clustering analysis (III, Figure 5 F), a large group of genes (3899 genes, all groups combined) are normally downregulated during the meiotic-

to-postmeiotic transition *i.e.* expressed to a higher degree in spermatocytes compared to round spermatids. However, in the absence of SMG6 a different pattern was observed. While two thirds of these genes (group 1) followed the trend, a third resisted downregulation (groups 2 + 3). Of these 25% remained stable (group 2) and additional 7% (=281 genes) were, in fact, upregulated in round spermatids compared to spermatocytes (group 3), reversing the normal trend. The genes that resisted downregulation in *Smg6*-cKO postmeiotic cells were associated with a diverse set of processes e.g., transport, cell growth, and signaling (III, Supplementary Figure S5C) according to our GO term analysis. In contrast, the processes required for meiotic progression (e.g., chromosome segregation) were enriched in group 1 genes and thus unaffected by SMG6 inactivation. These results indicate that SMG6 is required for the degradation of meiotically expressed genes and its absence impairs the haploid differentiation program.

5.4.5   SMG6 inactivation disrupts haploid cell differentiation

Unsurprisingly, considering the reduced number of round spermatids in *Smg6*-cKO testis, the TUNEL analysis revealed a significant increase in apoptosis in *Smg6*-cKO testis (III, Figure 4D). The percentage of *Smg6*-cKO tubules containing at least one apoptotic spermatocyte was >5-fold increased (from 13% to 70%) and the percentage of tubules with at least one apoptotic round spermatid was 10-fold increased (from 3% to 31%, III, Figure 4C). The overall number of apoptotic cells per tubule was increased as well (III, Figure 4D,E). During spermatogenesis, apoptotic spermatocytes are usually observed at two 'checkpoints' at stage IV and stage XII[373]. In the absence of SMG6, however, spermatocyte apoptosis was observed throughout the seminiferous epithelial cycle in addition to stages IV and XII where increased numbers of apoptotic cells were detected (III, Supplementary Figure S4D). Furthermore, while apoptosis of the haploid spermatids at any stage of spermatogenesis is an extremely rare event, in *Smg6*-cKO testis apoptotic spermatids were frequently detected (III, Supplementary Figure S4D).

In addition to apoptosis, the reduced number of round spermatids is explained by extensive sloughing from the epithelium, accompanied by the discovery of spermatid-appearing cells in the epididymal lumen (III, Supplemental Figure S5D). ESPIN antibody staining pattern demonstrated that the apical ectoplasmic specialization these junctions between germ cells and Sertoli cells were disorganized in *Smg6*-cKO testes (III, Figure 4G). Together, the results show that SMG6 deletion leads to increased apoptosis and early cellular detachment during the meiotic-to-postmeiotic transition.

As the number of especially haploid cells is clearly impacted by the SMG6 inactivation, the status of the remaining cells was next examined. The acrosome

transforms step-by-step during haploid differentiation and can therefore be used as an indicator of round spermatid's developmental status. In the Golgi phase, acrosome biogenesis appears normal in early *Smg6*-cKO round spermatids as a single large acrosomal granule is detected per spermatid. However, from early cap phase on, the acrosomes appear abnormal. Instead of elongation, the acrosomes appear to developmentally stall, become fragmented and eventually disintegrate which becomes particularly evident during the late cap phase and the early acrosome phase. Finally, during the late acrosome phase, from stage IX of the seminiferous epithelial cycle onwards, no acrosomes are detected, reflecting the loss of spermatids from the epithelium.

5.4.6 *Smg6*-cKO CBs - not all they seem to be

Morphological analysis of the CBs by electron microscopy from the remaining population of round spermatids found no obvious structural defects. A single perinuclear dense material construct with interstices of irregular shapes and sizes intermingled with small vesicles was found in the cytoplasm of *Smg6*-cKO round spermatids, as in control cells (III, Figure 5G). Furthermore, even after an extensive panel of CB proteins were investigated, all studied proteins were correctly localized to the CB in *Smg6*-cKO (III, Figure 5H) and the CB proteome in mass spectrometric analysis detected DDX4, DDX25, PIWIL1 and PIWIL2, several Tudor domain-containing proteins, and overall the main CB components were present apart from, expectedly, SMG6 (III, Supplemental Table S5D). Furthermore, SMG6 inactivation did not have a measurable effect on the accumulation of RNA into the *Smg6*-cKO CBs[26] as, just like in the control, the nucleotide analog 5-ethynyl uridine labeled the SMG6 depleted CBs after a 10 h incubation in seminiferous tubule cultures (III, Supplementary Figure S5E).

However, high-throughput sequencing of isolated CBs identified more than 2000 significantly misregulated genes. More specifically, 844 upregulated and 1242 downregulated genes (III, Figure 5I, Supplementary Table S3C). The majority of the upregulated (~60%) and the downregulated (~80%) genes were among the upregulated and downregulated genes in round spermatids, respectively (III, Supplementary Figure S5F). Though, importantly, the two datasets produced either from CBs or round spermatids were analyzed using different library preparation protocols and thus the overlap detected by our analysis may be an underestimate. Regardless, while the loss of functional SMG6 did not measurably disrupt CB formation, morphology, RNA import, or protein composition, the RNA profile was significantly altered in a similar way as the transcriptome of the cell itself. This connection both emphasizes CB's central role in RNA regulation and indicates that SMG6-dependent processing of haploid cells transcriptomes is linked to the CB.

5.4.7   SMG6 inactivation leads to long 3′UTR accumulation

SMG6 inactivation has a profound effect on spermatogenesis cells during the meiotic-to-haploid phase which is reflected by both cellular and transcriptomic imbalance. As SMG6 is well-characterized in the NMD pathway which promotes the decay of specific subsets of mRNAs, this imbalance may be brought on by defective NMD. To examine this possibility our data was compared to previously published gene lists of putative NMD target RNAs. Specifically an overlap between the genes upregulated in *Smg6*-cKO (as NMD is a negative regulatory pathway degrading its targets) was compared with an assembled a list of previously discovered likely NMD substrates from different mouse cells and tissues[374]. The analysis revealed that 8%, 17% and 20% of the protein-coding genes that are upregulated in *Smg6*-cKO spermatocytes, round spermatids, and CBs, respectively, were among the putative NMD target mRNAs (III, Supplementary Table S3). Further comparison was done with a high-confidence NMD target list consisting of 202 experimentally validated target RNAs. At this added level of scrutiny, a modest overlap of only 38 out of the possible 202 was reached by round spermatids and 16 by CBs confirming that while NMD is defective in *Smg6*-cKO germ cells, male germ cells likely have many undiscovered NMD target mRNAs (Supplementary Table S3B,C).

To investigate whether the SMG6-mediated NMD in germ cells is particularly sensitive to specific RNA features, NIF analysis was conducted. Unlike other features, one NIF – a long 3'UTR – was significantly enriched among the upregulated transcripts compared to downregulated or unchanged transcripts, an accumulation that was only detected in round spermatids but not spermatocytes (III, Supplementary Figure S5G, Supplementary Table S4A, B). Three groups according to 3' UTR length – <350, 350-1500 and >1500 nt – were defined and each transcript's expression in *Smg6*-cKO vs. control round spermatids was plotted against these groups revealing that the median log2FC values of the long and medium 3′UTR groups (0.48 and 0.29, respectively) were significantly higher than that of the short 3′UTR group (–0.74). A striking 3′UTR length bias was also observed in round spermatids and the CB (III, Figure 6B, Supplementary Table S4C). To validate the 3′UTR length findings that until this point relied on UTR length information obtained from external databases, an independent analysis where 3′UTR lengths of transcripts were assembled from our own datasets using the Cufflinks program, was performed. This analysis confirmed that the median 3′UTR length is significantly increased in up- versus down-regulated transcripts in both round spermatids and CBs but not in spermatocytes (III, Figure 6C). The mis-regulation of mRNAs in SMG6 deficient round spermatids correlates with an accumulation of transcripts carrying long 3' UTRs.

Together, these results strongly suggest that one NMD-inducing feature that commonly elicits mRNA decay in round spermatids is the long 3′UTR. Furthermore, our data raise the possibility that the CB is a specific site where long 3′UTR-mediated mRNA decay occurs. While the exact purpose of this is unknown, one possibility concerns the genes identified important for the meiotic-to-postmeiotic transition. Notably, of the transcripts resisting the normal meiotic-to-postmeiotic gene downregulation in *Smg6*-cKO postmeiotic cells, more than 40% contained a long 3′UTR. These findings together link the meiotic-to-postmeiotic molecular program switch, CB and 3′UTR length induced SMG6-mediated NMD (III, Figure 5F, Supplementary Table S4D, E).

5.4.8   Selective upregulation of piRNAs in *Smg6*-cKO

Since the CB contains a significant number of components not only from the NMD pathway but also the piRNA pathway, the potential effect that the inactivation of one could have on the other, was investigated. Of note, the temporal expression and localization pattern of the pachytene piRNA-binding protein PIWIL1 in testis is almost identical to that of SMG6 (III, Figure 1, Supplementary Figures S1,S6). Like SMG6, PIWIL1 co-localizes with DDX25 in CB precursors and CBs (III, Supplementary Figure S6) and neither proteins' localization pattern is perturbed by the deletion of other. Furthermore, the deletion of either leads to similar defects in spermatogenesis[305] (III, Figure 7B, Supplementary Figure S6). The two proteins also appear to interact when co-precipitated from mouse testis where their interaction is, at least in part, mediated by RNA (III, Figure 7A).

A functional piRNA pathway requires piRNAs which are ~30 nucleotides-long germline-specific RNAs normally present in enormous amounts[314], enough to detect as a clear band on polyacrylamide gels stained with SYBRGold (III, Figure 7C). Gel electrophoresis analysis showed that pachytene piRNAs are expressed in SMG6 depleted testis. To study the piRNA population in detail, small-RNAseq was performed. The majority of reads mapped to known piRNA clusters[328] in both *Smg6*-cKO and control round spermatids (III, Figure 7D) and spermatocytes (III, Supplementary Figure S7A). The overall size distribution of piRNAs was unaffected by SMG6 inactivation (Figure 7E, Supplementary Figure S7B), suggesting that the processing of mature piRNAs is intact in *Smg6*-cKO testes. The small-RNA-seq reads were divided to piRNA clusters classified according to their temporal expression patterns during spermatogenesis: 'pre-pachytene' (expressed from 10.5 dpp), 'pachytene' (expressed from 12.5 dpp), and 'hybrid'[328]. Unlike other clusters, almost a quarter of pre-pachytene piRNA clusters were significantly upregulated in *Smg6*-cKO round spermatids thus revealing a selective effect of SMG6 inactivation (III, Figure 7F, Supplementary Figure S7C,D, Supplementary Table S5). This

finding was not explained by changes in piRNA precursor expression – as observed in our long RNA seq data – and is thus unlikely to result from a piRNA processing defect. (Supplementary Figure S7E-H, Supplementary Table S6A-C).

5.4.9   Novel link between SMG6 and PIWIL1

A significant upregulation of piRNAs could indicate a potential disturbance of the piRNA pathway and therefore misregulation of its targets. To examine whether *Smg6* deletion had, in fact, resulted in the misregulation of the piRNA pathway, known targets of the pathway were examined. Due to the well-characterized role of piRNAs in safeguarding genome integrity from TEs[314], their expression in *Smg6*-cKO germ cells was first examined. While some misregulated TEs were found in *Smg6*-cKO spermatocytes, rounds spermatids and CBs, there were no indications of major defects in transposon silencing (III, Supplementary Table S6D–F). Next *Smg6*-cKO round spermatid transcriptome was compared to two *Piwil1*-KO round spermatid datasets available in public repositories which were reprocessed to allow for maximum comparability. Differential expression analysis identified roughly ~1000 significantly upregulated genes in both of the datasets and in both cases one-in-four common upregulated genes were found between *Piwil*-KO and *Smg6*-cKO. Importantly, these overlapping transcripts were enriched for long 3'UTRs and ~40% of them contained a long 3′UTRs which is more than the percentage of 3'UTR containing transcripts upregulated in *Smg6*-cKO round spermatids only (III, Figure 7H). Similarly, the median 3′UTR length of these these shared upregulated transcripts increased when compared to transcripts upregulated only in the *Smg6*-cKO round spermatids (III, Figure 7I). Finally, yet another important clue to the emerging SMG6-PIWIL1 connection was discovered as predicted piRNA-target sites in genes differentially expressed in *Smg6*-cKO round spermatids were analyzed. The proportion of predicted piRNA targets among the genes upregulated in *Smg6*-cKO round spermatids was higher than for downregulated genes. Furthermore, the proportion of predicted piRNA-targeted genes was dramatically higher for genes upregulated in both *Smg6*-cKO and *Piwil1*-KO round spermatids (III, Figure 7J). Together, this data indicates that PIWIL1 participates in SMG6-mediated long 3′UTRs containing RNA regulation.

5.4.10   Discussion of SMG6

SMG6 is the sole endonuclease in the NMD pathway. According to recent view, SMG6 is the primary executor of mRNA degradation on this pathway[162]. NMD serves to remove pathogenic RNA species containing a premature termination codon but also regulates normal mRNA levels in several other contexts with the help of

SMG1, UPF1, UPF2, and UPF3B[375]. Knockdown of Smg6 in zebrafish[376] and KO of *Smg6* in mice[172] results in early embryonic lethality. Circumventing this detrimental phenotype, a conditional Smg6 KO in postnatal germ cells model was created in this study.

As SMG6 expression peaks in late spermatocytes and round spermatids, pronounced spermatogenesis defects at the meiotic-to-postmeiotic transition were expected to occur in the *Smg6*-cKO. Consistently, a dramatic phenotype of full haploid arrest was observed and as discovered by differential expression analysis, was accompanied by a massive transcriptomic imbalance that seemed to target a specific developmental program. According to our expression analysis of the meiotic and postmeiotic control cells – enriched pachytene spermatocytes and round spermatids – around 3900 genes should be downregulated during the meiotic transition. However, in the absence of SMG6 only ~2600 genes followed this pattern while more than 30% did not follow the pattern or were even upregulated. In fact, cluster analysis placed *Smg6*-cKO round spermatids markedly close to control (and KO) spermatocytes as if their development was stalled and instead of reaching their haploid identity, they were unable to move past the meiotic character. Among the transcripts that lingered past their normal elimination date were genes linked to processes with no connection to spermatogenesis, including wound healing, gliogenesis, and osteoclast differentiation. The failure to eliminate these transcripts suggests that SMG6 functions in clearing mRNAs synthesized as a result of the 'leaky transcription'[173,187]. Fitting with the general scope of NMD to protect cells from dangerous gene products, SMG6 destabilizes the products of these genes prohibiting the production of proteins that could at the very least waste the cellular resources and at worst be detrimental by initiating a wrong differentiation program. Either way, due to the evident identity confusion in SMG6 depleted round spermatids, differentiation at this point comes to a halt and elongation becomes impossible. Instead, round spermatids begin to undergo apoptosis and detach from the seminiferous epithelium prematurely. At this point syncytium with multiple nuclei of round spermatids are frequently detected in the seminiferous epithelium. The apical ectoplasmic specialization[83] appears disorganized and junctions between the nursing Sertoli cells and round spermatids are coming undone. Evident increase in apoptosis of both spermatocytes and round spermatids is detected, and as the result of all of this, the epididymis fills with immature germ cells instead of spermatozoa.

Phenotypes closely resembling that of *Smg6*-cKO mice have been reported. Among the genes whose deletion results in similar phenotypes are *Crem*, which serves as the master transcription factor for spermiogenesis[377–379]; *Grth/Ddx25*, encoding an RNA helicase and a well-established CB component [26,380]; *Tlf/Trf2*, a testis-specific factor related to TATA-binding protein[381]; *Tpap*, encoding a testis-specific cytoplasmic poly(A) polymerase[382–384]; *Rnf17*, that associates with pachytene piRNA

precursors, partakes in piRNA biogenesis, and represses secondary piRNA amplification[312,313]; *Boule,* member of the DAZ (Deleted in AZoospermia) family of genes encoding an RNA-binding protein with unknown function; *Tdrd1*, that encodes a molecular scaffold that partakes in piRNA biogesis[308]; *Tdrd7* and *Tdrd5* whose expression is required for CB/RNP structural maintenance and LINE1 transposon repression[304,311]; *Piwil1*, encoding a well-established CB-component that binds pachytene piRNAs, regulates mRNA elimination mRNAs and activates translation of an mRNA subset; and *Ck137956/Tssa* that binds *Piwil1* and regulates its mRNA stabilizing function[385]. In all these studies, spermatogenesis was arrested by the beginning of the elongation phase. While inactivation of SMG6 leads to a similar phenotype RNA-seq did not reveal any of these genes to be significantly downregulated in *Smg6*-cKO round spermatids although a modest reduction of *Crem* was indicated. As a master transcription factor in spermatogenesis downregulation of *Crem* and its downstream targets could contribute to the phenotype[381,386]. This cannot be ruled out especially as *Tnp1, Tnp2, Prm1* and *Prm2*, known downstream targets of cAMP responsive element moderator (CREM) encoding transition proteins and protamines were all significantly downregulated in *Smg6*-cKO spermatocytes and round spermatids (III, Supplemental Table 3C). If a connection between SMG6 and CREM exists, it would certainly be interesting as CREM is one of the very few genes that, in humans, have been reported to cause azoospermia due to arrest in round spermatids[387] while no spermatogenesis compromising mutations related to SMG6 in human have been identified thus far. However, based on our data a connection between the two cannot be confirmed.

Of note, another conditional *Smg6* loss-of-function mouse model was created around the same time as the *Smg6*-cKO presented in this thesis and reported by Katsioudi et al.[388]. This loss-of-function Smg6 model was created to study the circadian clock, a system known to require rapid mRNA turnover, and demonstrated that functional loss of SMG6 affects the peripheral circadian clocks, rhythmic gene expression, and food entrainment of the liver oscillator in mice. The study also showed that the stability of specific mRNA transcripts, including the core clock component Cry2, is regulated by SMG6-mediated NMD and suggested that NMD-mediated regulation of gene expression oscillations plays an important role in maintaining circadian rhythms[388].

A peculiarity of spermiogenesis is that transcription of many mRNAs takes place several days prior to their translation. This presents a challenge in terms of ensuring that these mRNAs are translated precisely at the appropriate time. For example, *Tnp1, Tnp2, Prm1* and *Prm2* are transcribed already in late pachytene spermatocytes, but are translated only during elongation, about a week later[389–391]. To address this issue, a complex network of translational regulation is required. This regulation is believed to occur at the CB, which serves as a platform for RNAs and

RNA binding proteins to interact. The two most prominent molecular pathways localized to the CB are the SMG6-mediated NMD pathway and the PIWI-protein led piRNA pathway. This co-localization suggests close communication and potential functional cooperation between these pathways.

Deciphering the potential for direct interaction between SMG6 and PIWIL1 was one of the aims, and also technical challenges, in this study. SMG6 and PIWIL1 localize to a large ribonucleoprotein granule and though co-immunoprecipitation consistently showed their interaction, the CB environment is expected to fortify the interaction with any CB components while the CB is intact. Several approaches using RNAse treatments were attempted to test whether SMG6-PIWIL1 interaction is RNA dependent with inconclusive results. RNAse treatment weakened the SMG6-PIWIL1 interaction but did not dissolve it completely even under stringent conditions. As RNA's are protected from RNAse inside RNP complexes, especially within as large a granule as the CB, and no positive control for this experiment exists, RNA participation in the SMG6-PIWIL1 interaction cannot be ruled out.

Regardless of the nature of the interaction, much of our data supports a close collaboration between the NMD and the piRNA pathways. As stated, the phenotype of *Piwil*KO and *Smg6*-cKO mice is similar, with both of them experiencing a block at the round spermatid stage. Reviewing the (short) list of other mouse models with this phenotype, it became evident that most depleted genes on this list are linked to either the piRNA pathway, NMD, germ granules or all of the above[142,304,313,392–394]. This indicates that a quality control process that regulates male fertility takes place at the CB involving components of these to RNA-centered pathways. Whether the CB can be an active site for RNA processing and for example the NMD pathway is a key question to answer. Considering the components that are required for SMG6-mediated endonucleolytic cleavage of mRNA, several proteins have been shown pivotal. According to functional assays, protein–protein interaction studies and *in vitro* experiments, SMG6 activity has been shown to specifically require SMG1 and UPF1 both of which are highly accumulated in the CB[395]. Furthermore, as described above, several other NMD components are within the CB proteome which strengthens the hypothesis that active NMD takes place in the CB. However, active translation is a pre-requisite for the NMD pathway and this has not, yet, been proven to take place in the CB. In our analysis, a plethora of ribosomal proteins were found in the CB proteome indicating ribosomes may, in fact, reside witthin the CB structure. A careful imaging analysis will likely reveal ribosomes, polysomes in or on the CB structure, in the future.

As for the piRNA pathway, the CB could either function as a site of piRNA biogenesis or take part in downstream actions. The former is unlikely as the CB does not associate with piRNA biogenesis relevant enzymes[396]. It is well-established

that the main piRNA biogenesis factors associate with mitochondrial membranes that connect with another germ granule, the IMC, in spermatocytes[397]. Furthermore, although mature piRNAs from several pre-pachytene piRNA clusters were misregulated, the production of piRNAs was not compromised by SMG6 inactivation. Therefore, in a more likely scenario, the initial steps of pachytene piRNA processing occur in mitochondria-associated germ granules and subsequently the PIWI protein-loaded piRNAs move to the CB.

Long 3'UTRs appear to be the prevailing NMD inducing feature in the CB. While a few different NMD triggering features have been characterized and analyzed from the RNAseq data, only the long 3'UTR feature was accumulated in the absence of SMG6. The 3'UTR may play a crucial role in SMG6-dependent NMD during germ cell development. Accumulation of transcripts with long (>1500 nt) 3'UTRs in *Smg6-cKO* particularly in round spermatids was detected. Moreover, the median length of 3'UTRs was significantly longer in upregulated transcripts compared to downregulated and non-regulated transcripts. This trend was consistent with the conditional loss of another NMD factor, UPF2, in male germ cells, which also resulted in the upregulation of transcripts with long 3'UTRs[143]. Similarly, TDRD6 depleted germ cells preferentially upregulate long 3'UTR-containing transcripts in round spermatids[142]. UPF1 is not detected in *Tdrd6*-null CB remnants and could explain the phenotype as SMG6-mediated NMD is dependent on UPF1. It is worth noting that germ cells, including spermatocytes and spermatids, typically possess transcripts with shorter 3'UTRs compared to somatic cells. This has been attributed to germ cell-specific early polyadenylation site usage. However, an alternative explanation could be that mRNAs with long 3'UTRs are more efficiently degraded by NMD in germ cells compared to somatic cells, leading to a selective accumulation of mRNAs with short 3'UTRs. In summary, our findings highlight the importance of long 3'UTRs in SMG6-dependent NMD during germ cell development. The accumulation of transcripts with long 3'UTRs in specific genetic contexts, such as the loss of SMG6 or TDRD6, suggests a regulatory role for NMD in shaping the transcriptome of germ cells, potentially allowing the preferential accumulation of mRNAs with short 3'UTRs.

Arrest at the haploid stage in *Smg6*-cKO mice. Spermatogenesis progressing through meiosis, producing round spermatids that are then unable to elongate and condense is a rare phenotype. Previous studies resulting in a similar phenotype include mutations in genes transcribing PIWIL1[305], TDRD1[398], TDRD4/RNF17[313], TDRD5[310], TDRD7, DDX25 and Ck137956/Tssa[385]. Incidentally all these proteins accumulate to the CB[26]. PIWI proteins, such as PIWIL1 are conserved proteins with central roles in germ granules across species. In *Drosophila,* Piwi is required for the maintenance of both male and female germline stem cells, while in the mouse PIWIL1 and PIWIL2 are essential for the postnatal germ cell differentiation in males only[305,306] PIWIL1 is highly expressed by round spermatids and when removed or catalytically inactivated,

spermatogenesis arrests at the round spermatid phase[305,306]. Similarly, in Drosophila Tudor domain-containing proteins (TDRDs) are crucial for the germ line in females while *Tdrd1* inactivation in mice leads to infertility in male only[308,394,399–401]. Tudor proteins have been shown to act as molecular scaffolds[402] and in the absence of TDRD6 or TDRD7 the CB morphology is disrupted[304,309]. Tudor proteins are known to interact with proteins containing symmetric dimethylarginines such as PIWIL1[394,401]. TDRD5 binds piRNA precursors and enhances pachytene piRNA processing in mice. TDRD6 and TDRD7 have both been linked to the piRNA pathway as well. In the absence of TDRD6, the localization of UPF1, but not UPF2, to the remnants of CB was disrupted. Moreover, the interaction between UPF1 and UPF2 was significantly affected in the testes of Tdrd6-null mice. Considering that UPF1 helicase activity is known to depend on the presence of UPF2, it is likely that NMD is substantially impaired in these mice. Analysis of UPF2 mutant mice revealed that transcripts with long 3' UTRs derived from ubiquitous genes were upregulated in the absence of UPF2, while the levels of transcripts containing premature termination codons remained unaffected[143]. Importantly, transcriptome analysis of *Tdrd6*-null germ cells supported these findings, indicating that the NMD pathway stimulated by long 3' UTRs was indeed impaired in these cells, possibly due to disrupted interactions within the NMD machinery[142]. Based on these results, it is plausible that NMD in male germ cells preferentially targets transcripts containing long 3' UTRs.

Altogether, the aftermath of SMG6 depletion is not simple to interpret. Among the potential secondary effects of the deletion and other noise, important groups of transcripts arose, especially among the upregulated genes. It seems that there are specific genes whose correct expression level depends on the CB-localized SMG6. The overlap and link to the piRNA is particularly interesting. In the *Drosophila* germ plasm, PIWI protein loaded piRNAs have been shown to use partial base-pairing to bind mRNAs, thus collecting them to the germ plasm for unknown downstream actions[403]. In our analysis, piRNA targeting sites were enriched among the mRNAs upregulated in *Smg6*-cKO round spermatids especially among the group upregulated in both *Smg6*-cKO and *Piwil1*-KO. The CB accumulated piRNAs could perhaps act as RNA sponges in the mice as well. This scenario would merge the piRNA pathway acting as an adhesive trap to the CB where in close proximity several RBPs could regulate the fate of the RNAs. For ones with and NMD inducing feature, degradation by SMG6 would then be in the cards.

In summary, the transcriptome of meiotic and post-meiotic germ cells is misregulated in the absence of SMG6 with three partially overlapping groups particularly impacted: transcripts derived from genes normally silenced during meiotic-to-postmeiotic transition, putative NMD targets and transcripts regulated by PIWIL1. The misregulation leads to a detrimental phenotype of round spermatid arrest in development and complete male sterility.

5.5   The Ins and Outs of the Chromatoid Body

The two main projects of this thesis work focused on two CB components, FYCO1 and SMG6. Up until here the projects have been separately presented and discussed in view of their respective results. In this last chapter, the CB is considered in view of all the evidence and the overall nature of the CB is discussed with emphasis in what remains to be discovered and proven.

Phase separation occurs when molecules at a given location surpass the concentration threshold at which they condense to form a body effectively parting themselves from the cytoplasm at large[234]. The CB appears at a time of active transcription when the number of RNAs of all sizes peaks in male germ cells[404]. Considering the perinuclear localization of the CB, phase separation could well be the force driving its formation. In other words, the CB may arise in response to the accumulation of newly synthesized RNAs and RNA binding proteins at the nuclear membrane first at several specific sites (as CB precursors) in spermatocytes and merging to one large condensate moving along the nuclear membrane in round spermatids.

While some germ granule condensates exist in a solid-like state with little component exchange such as the Balbiani body[231], others exhibit liquid-like dynamic behavior like P granules[232]. The CB falls to the latter group for several reasons. The CB is known to actively exchange material with its environment, to constantly receive RNA, to replace protein components with others and to be under constant remodeling. At least 90 proteins have been detected within the CB proteome but during spermatogenesis different CB proteins take to the CB at different times. For example, PIWIL2[405] is present in the CB precursors of pachytene spermatocytes and early CBs whereas RNA binding protein SAM68 is only transiently seen in the secondary spermatocyte's CBs and very early round spermatids[406]. And here we demonstrated that one of our study subjects, SMG6, localizes to the CB from precursors to the beginning of elongation only while FYCO1 is detected even at the enigmatic late CB. Therefore, one can hardly speak of one CB with defined composition but rather several different CB condensates that form and transform as the cell undergoes maturation from diploid to haploid on their journey towards the formation of spermatozoa.

Another feature often linked to dynamic biomolecular condensates is that they are non-uniform and distinct sub-domains or compartments within a condensate can be detected[233]. While FYCO1 is consistently co-precipitated as a CB-component[26], detailed 3D imaging revealed that FYCO1 is not homogenously mixed in the CB matrix but rather covers its surface (II, Figure 2). And at least sometimes tends to focus more on one surface rather than encircling the entire structure. This FYCO1-positive "CB domain" was shown to be in close association with small LC3 positive vesicles and link the CB to the autophagy pathway (II, Figure 6). Therefore, for the first time, we demonstrated that some CB components localize to specific areas of the granule

forming a surface domain with likely distinct functions from the core functions of the CB (II, Figure 2). Furthermore, we showed that this specific CB domain's structure is responsive to specific external triggers. Observation of CBs in tubule cultures experiments demonstrated that the FYCO1 positive CB domain can re-shape to globular form on one side of the CB upon Wortmannin treatment (II, Figure 3). The biological relevance of this phenomenon to spermatogenesis is unclear, but it demonstrates that CB acts as a dynamic condensate.

Even though the disintegration of the CB structure due to TDRD6 or TDRD7 deletion has led to impaired fertility, FYCO1 depleted CBs underwent morphological changes without an evident effect on fertility. This suggests that not all CB functions are directly required for fertility and the main functions of the CB are able to continue even when disintegrated to several entities within a cell. While FYCO1 appears on the CB surface, SMG6 and PIWIL2, appear to localize deep in the core of the CB as they do not fully overlap with DDX25-positive CB (Figure 10). Future quantification and detailed imaging will likely confirm this preliminary finding and uncover further proof that the CB consists of domains that are responsive to external stimuli and that are in dynamic interaction with each other.
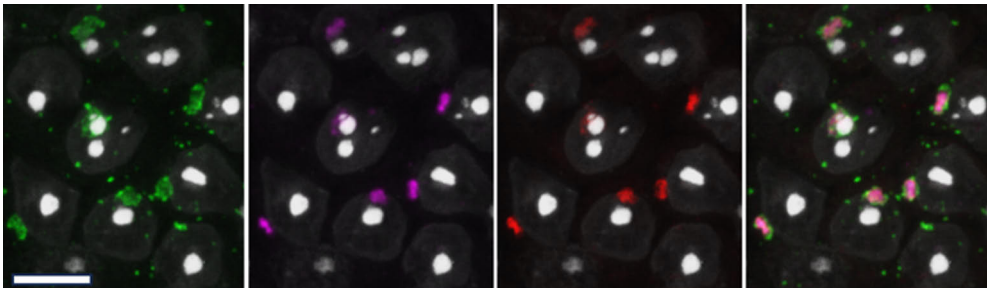
Figure 10. From left to right: CB-marker DDX25 (green) co-localizes with NMD endonuclease SMG6 (purple) and piRNA pathway's PIWIL2 (red) in wildtype male mouse's round spermatids as demonstrated by the last, merge image. Each germ granule marker is presented together with DAPI stained nuclei (left and middle). The overlay of all channels (right) demonstrates that DDX25 signal exceeds the area covered by either SMG6 or PIWIL2 alone. Scale bar: 5 µm. (Unpublished data)

While the phenotype of FYCO1 depleted CBs contained obvious morphological aspects, SMG6 depleted CBs appeared unaffected at first glance. No obvious changes in morphology, proteome or RNA dynamics (RNA accumulated to the CB normally) were discovered in SMG6-less CBs. However, RNAseq revealed that the RNA composition had undergone significant changes due to SMG6 depletion. As the CB's were pulled from the entire testis, it is possible that the altered status of the round spermatids from which the CBs are extracted may affect their RNA content. One possibility is that the round spermatids that remain in SMG6 depleted testis are

stuck at an early step of the round spermatid differentiation. While this possibility cannot be excluded, observing the transient CB proteins PIWIL2 and SAM68 showed that the *Smg6*-cKO CB's follow the same patterns of expression as controls (unpublished). Whether the observed changes in the RNA profile are a direct outcome of the SMG6 depletion or they reflect of the altered cellular state, it is clear that the CB demonstrates a dynamic responsive nature in the *Smg6*-cKO testis even when no obvious morphological defects are detected.

Cytoplasmic RNP granules have been linked to mRNA storage and translational repression in several context. In stress granules environmental stress drives the storage of mRNAs to a translationally repressed state until stress is alleviated. During spermatogenesis active transcription takes place from early spermatogonia onwards peaking at meiotic spermatocytes and round spermatids. However, as nuclear condensation soon renders the cells transcriptionally inactive, mRNAs required for the final steps of spermatogenesis need to be produced much earlier and then maintained inert for several days[177–180]. The CB could be the entity that provides the mRNAs a stabilizing environment, a compressed storage of sorts.

To date it is not understood how the translation of germ granule mRNAs is activated at appropriate times. It was recently shown that translation is activated after an mRNA exits from germ granules (P granules) in *C. elegans*[407] suggesting that the action of exiting from the germ granule environment may be required for translation activation. While that may be the case for some mRNAs, other studies have proposed a link between germ granule components and translation activation themselves. PIWI protein PIWIL1 has been shown to activate translation by recruiting translation initiation factors to germ granules in mice[408] a finding that was soon supported by a similar study in *Drosophila*[409]. Another interesting finding recently came from studying Fragile X mental retardation syndrome–related protein 1 (FXR1) in mouse spermatids. The translational activation of FXR1 was found to depend on the capacity of FXR1 to form RNP granules. FXR1 associates with the translation factors EIF4G3 (eukaryotic translation initiation factor 4γ3) and PABPC1 [poly(A) binding protein C1] and recruits them to granules in late spermatids. While FXR1 is not a bona fide CB component, interestingly, we identified it as one of the interaction partners of SMG6 is our MS analysis (III, Table S1) and validated the interaction via WB (unpublished). EIF4G3 and PABPC1 were also among the SMG6 interactome according to our MS analysis (III, Table S1). Future studies exploring the connections between SMG6, CB proteins and the other interactome partners of SMG6 may end up revealing more about the lifespan of the CB functions. It is tempting to speculate that the early CB, fully formed CB and the enigmatic late CB fragments contain very distinct functions in male germ cells transcriptome maintenance. While mRNAs can be initially protected and safeguarded in the CB environment, they are likely also screened for quality, regulated accordingly at

specific time points and ultimately, at least to some extent, released for downstream action and translation. Which CB form and function support each undertaking is something yet to be confirmed and while several important clues were obtained, importantly, the data acquired in the projects included in this thesis often overlook the late CB due to methodological restrictions and therefore the results presented here focus mainly on the early CB in pachytene spermatocytes to the CB in its most prominent state in round spermatids.

Finally, to that end, the evidence presented here supports a model where the CB is formed in response to massive RNA production in germ cells. The CB consists of at least two main "condensate domains", the SMG6-positive core and the autophagy linked FYCO1-positive surface. Based on the evidence obtained from transcriptomic studies (III) the core function of the CB is to maintain the transcriptome of germ cells likely by a system that employs the endonuclease SMG6 and the piRNA pathway components. While SMG6 is clearly pivotal, it remains to be determined whether the transcriptome control is performed via SMG6-mediated NMD or by another SMG6 dependent function. Based on our results, all components required for NMD are present in the CB environment. At minimum NMD requires SMG1, UPF1 and SMG6 all of which are found in the CB proteome, furthermore both us and Fanourgakis et al[142]. have shown that several NMD components are highly concentrated to the CB with little available elsewhere in the cytoplasm. NMD is widely accepted as a translation dependent process and while active translation has not been demonstrated to take place in the CB, a plethora of ribosomal proteins were recurrently detected in our recent CB analysis (III).

Combined, this body of work changed our perception of the CB in many ways. Against all prior knowledge, we found that an intact CB is not a pre-requisite for male fertility. It appears that the CB is about function above formation and the loss of its usual morphology in *Fyco1*-cKO is survivable for the developing germ cells. And on the other hand, as demonstrated by the other model *Smg6*-cKO, a structurally sound CB is not a guarantee for a successful spermatogenesis. Unlike the loss of its autophagy adapter protein, FYCO1, the loss of the endonuclease SMG6 is not survivable even though the CB's morphology is unaffected and all other components are present. Therefore, we determine that the role of SMG6 is at the heart of CB's inner functions in the maintenance of the male germ cell transcriptome and male fertility. Overall, two different CB components were studied, and the combined results increased our understanding of both the ins and outs of the Chromatoid Body.

6   Conclusion

Collectively, this thesis study addressed the role of selected germ granule proteins in controlling specific events during spermatogenesis. Together, the main results and accomplishments of this thesis include key information on the molecular processes that govern male fertility and reproduction as well as a new method for the field of spermatogenesis.

The main results and findings:

I.   A modified density gradient for the isolation of germ cells with minimal starting material was developed. This method provides any research group the means to isolate both haploid and diploid cells from mouse testis using standard laboratory equipment. Moreover, this protocol was used to isolate germ cell populations from both KO mouse models used in the other two studies presented in this thesis.

II. A novel peripheral CB component, FYCO1 was discovered to be important for CBs granular integrity.

III. The relationship between vesicles and the CB was elucidated. The CB's association with autophagic activity was clarified and the FYCO1-dependent recruitment of lysosomal vesicles to the CB discovered.

IV. The core CB component SMG6 was found to be pivotal for spermatogenesis and male fertility, in mice.

V.   The endonuclease SMG6 was found to collaborate with the piRNA pathway to regulate the male germ cell transcriptome.

VI. The nature and form of the CB as a dynamic and reactive germ cell condensate was elucidated.

VII. The pertinence of the CB as a platform for RNA processing pathways required for the maintenance of male fertility was confirmed.

Acknowledgements

First and foremost, my deepest gratitude goes to my supervisor, Professor Noora Kotaja. I do not have the words to describe what an excellent supervisor you truly are. I feel lucky and privileged to have had these years to work with you and your research team. From the beginning you entrusted me with the most fascinating projects and with all the challenges we faced, you never let us stop or compromise. Your determined, unwavering, positive attitude and persistence are something I deeply admire. No matter how busy you have been, you always found time for me, and I never left your office feeling worse (about my results) than when I came in. Not sure how that is possible, yet it is true. I also wish to thank you for trusting so many younger researchers under my lab mentorship and for giving me many opportunities to teach as well as to present my work at conferences. Those have given me so many fond memories and have allowed me to learn and grow. Overall, this thesis would not exist without you.

Next acknowledgement goes to Professor Emeritus Martti Parvinen, for his pioneering work in the field. When I was just getting started, I was inspired by your passion for science and genuine curiosity regarding the mysterious Chromatoid Body. I thank you for sharing your stories and for your encouragement.

I am very grateful to the esteemed reviewers of this thesis. I thank Mikko Frilander for his insightful comments and detailed review that led to great improvements of this book and Renata Prunskaite-Hyyryläinen, for her meticulous review and encouragement to take parts of this book a step further.

I want to thank Professor Jorma Toppari, Petra Sipilä, PhD and Riikka Lund, PhD, for being the members of my thesis committee: you helped me with thorough comments and contributed to improving the quality of my scientific work. All my co-authors and collaborators are also kindly acknowledged for their contribution to this work. The work described here was much improved due to kind contributions from generous fellow scientists. To that end, a special mention to Geert Hamer.

Next, I would like to thank all alumni and current members of the Kotaja research team. Our weekly meetings with encouragement, feedback and troubleshooting really demonstrate what kind of a team we are and I for one feel very lucky to have been a part of it. First, I must thank the ever smart and beautiful Karin Sõstar, for introducing me to the group and for being my friend ever since. I must thank Matteo Da Ros for all the hours you spent showing me the ropes and for your continuous support when I was just getting started. I thank Oliver Meikar, a boy unmatched in energy, the admirably meticulous Ram Prakash-Yadav and kind Hanna Hyssälä for welcoming me with open arms and making my integration easy. I extend my gratitude for peer support and friendship to Mari Lehti, Matthieu Bourgery, Lin Ma, Anna Eggert and Juho-Antti Mäkelä. It has been an absolute joy to work and collaborate with you.

A special mention to Freja Hartman, Margareetta Mäkelä, Juho Asteljoki, Jan Lindstrom and Helena Matilainen for the intense work you put in and for spending long hours in the lab by my side, making them go by much faster. An especially happy greeting to Opeyemi Olotu, our ray of sunshine. Your kindness and your good heart are unmatched. Elina Louramo, Samuli Laasonen, Sini Leskinen, Anna Puisto and Olli Heikkinen are acknowledged for the work they have put in to advancing our common goal and I also wish to acknowledge and remember Elina Palonen. Finally, I congratulate all the new members of the research team for your excellent choice! I cannot wait to read your publications so keep pipetting and getting data. Ammar Ahmedani, that means you. The little overlap we had was all laughs and I always enjoy our discussions, scientific or otherwise. Good luck to you and all members of the group that strive to reveal the inner workings of male reproduction!

During these past years, I have also had the privilege to belong to the Turku Doctoral Programme of Molecular Medicine. Not only am I grateful for the funding and the training I was provided but also for having been entrusted a position at the steering group. As such, my most joyful thanks go to Eeva Valve and Kati Elima who trusted me to establish a student council with whom we planned many unforgettable events. Thereafter a special greeting goes to all my fellow TuDMM researchers and especially to the council members, past, present and future!

My sincerest gratitude to all the members of the former Department of Physiology for providing all the equipment, support and expertise that enabled me to reach the finish line. To that end I also wish to thank all the past and present technical personnel for your help and assistance in pushing our scientific objectives forward. A special consideration to Tuula Hämäläinen for keeping us all in line and for keeping us together. A special mention also to Minna Lindroth, Johanna Järvi, Taina Kirjonen, Pauliina Toivonen and Marko Tirri, for your help with the day-to-day tasks and for always being there and not letting us despair in times of crisis.

This thesis project would not have been successful without the meticulous work and guidance by Mona Niiranen and Jonna Palmu. For excellent maintenance and dedicated care, a special acknowledgement is given to Terhi Hiltula-Maisala and her team, especially Sanna Poretie. This work would have been impossible without your support. The expertise of the Histocore has been invaluable and I thank Erica Nyman and Marja-Riitta Kajaala for your help with my many histological samples over the years. The wonderful TCDM team is given all the credit for their hard and meticulous work. Your expertise has been pivotal for the success of the projects presented in this thesis. The inputs of Leena Karlsson, Ida Hyötyläinen, Heidi Liljenbäck, Nina Messner, Heli Niittymäki, Jenni Airaksinen, Janne Sulku, Merja Leppiaho, Madeleine Latvala, and Clara-Theresia Kolehmainen are equally acknowledged. Your support both material and immaterial is deeply valued.

From my first day at the Department of Physiology I enjoyed the warm and collaborative work environment. I would like to thank everyone for creating this supportive atmosphere among the different research groups. I especially wish to acknowledge our Professors, Docents, and Senior Researchers Jorma Toppari, Matti Poutanen, Noora Kotaja, Nafis Rahman, Jukka Kero, Petra Sipilä, Manuel Tena-Sempere, Ilpo Huhtaniemi, Lauri Pelliniemi, Antti Perheentupa, Marko Kallio, Harri Niinikoski as well as Adolfo Rivero-Müller, Leena Strauss, Helena Virtanen, Pirjo Pakarinen and the talents of all the scientist I have had the pleasure to work with, including Marcin Chruschiel, Mirja Nurmio, Mari Vähä-Mäkilä, Heli Jokela, Jaakko Koskenniemi, Arttu Junnila, Laura Mairinoja, Guillermo Martinez Nieto, Sofia Pruikkonen, Christoffer Löf, Donata Ponikwicka-Tyszko, Janne Hakkarainen, Matias Knuutila, Ashutosh Trehan, Mahesh Tambe, Jaakko Koskenniemi, Sergey Sadov, Valeriy Paramonov, Mehrad Mahmoudian, Konrad Patyra, Wiwat Rodpraset, Kamila Pulawska, Krisztina Kukoricza, Luís Crisóstomo, Andrea Usseglio Gaudi and the ever classy Gabriela Martínez Chacón.

I am immensely grateful to my former office mates which all made the time working on this thesis much more enjoyable. First, I want to thank Julian Undeutsch for your friendship and continuous support through the years. You are one of my ultimate favorite people. A particularly happy greeting goes to all other B607 folk including Milena Doroszko, Ida Björkgren, Emmi Rotgers, Heidi Kemiläinen and Jenni Mäki-Jouppila in addition to the ones mentioned earlier. Thank you for all the silly times we shared and the fun we had! B607 forever.

I have also had the pleasure to meet many fellow testis enthusiasts and germ cell aficionados through the Network for Young Researchers in Andrology. I thank my fellow board members, past and present for all the fun we have had at conferences and for all the scientific discussions we have enjoyed. May all young germ cell researchers find this network and enjoy it as I have.

Words cannot express how lucky I am for the group of clever, weird and fun people I have in my life and I want to take this opportunity to acknowledge them all. My love and gratitude goes to Michael Gabriel. Thank you for all the discussions, debates and dancing. Thank you for having my back and for sharing my taste in music. I promise to always have yours and to never stop showing you off at the dancefloor. Hanna Heikelä, it has been an absolute pleasure knowing you and working side by side during this long thesis writing process. Thank you for the peer support and all the tea we shared during the evenings or weekends in Medisiina when everyone else was having a life. Sheyla Cisneros Montalvo, you are a force to be reckoned with.

Dear friends outside the lab, thank you for bearing with me all these years while I worked insane hours. I start by sincerely thank the A-team of Jenna, Make, Michael and Jouni. A special mention for Jenna and her wonderful creative brain. And Jouni, thank you for all your help these last few months. All three of us value it so much. I am grateful to have met and befriended the likes of Krista, Moona, Eerika, Terhi and Siina, during the very first steps towards this thesis at Arcanum. I thank you all for so many fond memories from travels to lunch hours, from ordinary things to so many not ordinary parties. I also thank you for your patience during this endeavor and hope to see a lot more of you in coming days, weeks and months. Avi, I thank you for your unwavering support over the years. I am lucky to have you and Nitin in my life. Camilla, thank you for all your friendship and happy 30th birthday (see I did not forget)! Reetta, Sari and Megha, I have shared unique experiences with all of you and am grateful to call you my friends. Sannilotta, I am never not laughing with you and would almost move to France for you. Anna, I thank you for all your sage advice and support. Maria and Elina, my oldest friends, I am lucky to have you in my life after all these years. May there be endless number still to come. To all my friends, my sincerest thank you.

Finally, I want to express my deepest gratitude to my family. I first wish to acknowledge and remember my grandmother, Tyyne Lehtiniemi, my ultimate spirit guide, mentor, and beacon of inspiration. And my utmost gratitude goes to her daughter, my mother, Leena Lehtiniemi, to whom I owe everything. Thank you for making me believe I could do anything. Thank you for introducing me to the worlds of music and art, for giving me the freedom to explore, for letting me find my passion for science and for encouraging me every step of the way.

And last but not least, I extend my love to my boys. My 1-year-old Artturi Onni Vesanpoika Paakkanen, maailman söpöin pikku patkula, thank you for being the happiest, funniest, charming little boy you are. Thank you for lighting my mornings up with your smile. And, importantly, thank you for sleeping through enough nights to have allowed me to write this thesis. And to that end, a special thank you to Vesa Paakkanen for staying up when Artturi did not. This thesis could not have been

completed without your support. I would simply not have survived. I could not have asked for a better partner in both reproduction and life. Thank you.

Advancements in science are always the result of innumerable small contributions from every individual involved, ranging from undergraduate students attempts to produce beautiful western blot images to the senior researchers and professors tirelessly pursuing grants while fostering a good work environment. In this collaborative tapestry of efforts, I extend my heartfelt gratitude to each person dedicated to advancing science. Thank you for your passion, perseverance and best of luck in all your endeavors!

Tiina Lehtiniemi

25.9.2023

References

1. Infertility Prevalence Estimates, 1990–2021. https://www.who.int/publications/i/item/978920068315.
2. Leslie, S. W., Soon-Sutton, T. L. & Khan, M. A. Male Infertility. *StatPearls* (2023).
3. Agarwal, A. *et al.* Male infertility. *Lancet (London, England)* **397**, 319–333 (2021).
4. Sun, H. *et al.* Global, regional, and national prevalence and disability-adjusted life-years for infertility in 195 countries and territories, 1990-2017: results from a global burden of disease study, 2017. *Aging (Albany. NY).* **11**, 10952–10991 (2019).
5. Barratt, C. L. R. *et al.* What advances may the future bring to the diagnosis, treatment, and care of male sexual and reproductive health? *Fertil. Steril.* **117**, 258 (2022).
6. Adamson, G. D. *et al.* International Committee for Monitoring Assisted Reproductive Technology: world report on assisted reproductive technology, 2011. *Fertil. Steril.* **110**, 1067–1080 (2018).
7. Kabeya, Y. *et al.* LC3, a mammalian homologue of yeast Apg8p, is localized in autophagosome membranes after processing. *EMBO J.* **19**, 5720–8 (2000).
8. Chambers, G. M. *et al.* Population trends and live birth rates associated with common ART treatment strategies. *Hum. Reprod.* **31**, 2632–2641 (2016).
9. Tekayev, M. & Vuruskan, A. K. Clinical values and advances in round spermatid injection (ROSI). *Reprod. Biol.* **21**, (2021).
10. Hanson, B. M., Eisenberg, M. L. & Hotaling, J. M. Male infertility: a biomarker of individual and familial cancer risk. *Fertil. Steril.* **109**, 6–19 (2018).
11. Glazer, C. H. *et al.* Male factor infertility and risk of death: a nationwide record-linkage study. *Hum. Reprod.* **34**, 2266–2273 (2019).
12. Salonia, A. *et al.* Are Infertile Men Less Healthy than Fertile Men? Results of a Prospective Case-Control Survey. *Eur. Urol.* **56**, 1025–1032 (2009).
13. Ventimiglia, E. *et al.* Infertility as a proxy of general male health: results of a cross-sectional survey. doi:10.1016/j.fertnstert.2015.04.020.
14. Ding, G. L. *et al.* The effects of diabetes on male fertility and epigenetic regulation during spermatogenesis. *Asian J. Androl.* **17**, 948 (2015).
15. Amaral, S., Oliveira, P. J. & Ramalho-Santos, J. Diabetes and the impairment of reproductive function: possible role of mitochondria and reactive oxygen species. *Curr. Diabetes Rev.* **4**, 46–54 (2008).
16. Ornellas, F., Carapeto, P. V., Mandarim-de-Lacerda, C. A. & Aguila, M. B. Obese fathers lead to an altered metabolism and obesity in their children in adulthood: review of experimental and human studies. *J. Pediatr. (Rio. J).* **93**, 551–559 (2017).
17. Craig, J. R., Jenkins, T. G., Carrell, D. T. & Hotaling, J. M. Obesity, male infertility, and the sperm epigenome. *Fertil. Steril.* **107**, 848–859 (2017).
18. Krausz, C. & Riera-Escamilla, A. Genetics of male infertility. *Nat. Rev. Urol. 2018 156* **15**, 369–384 (2018).
19. Lehtiniemi, T. & Kotaja, N. *The Genetics of Postmeiotic Male Germ Cell Differentiation from Round Spermatids to Mature Sperm. Monographs in Human Genetics* vol. 21 (2017).

20. Komeya, M., Sato, T. & Ogawa, T. In vitro spermatogenesis: A century-long research journey, still half way around. *Reprod. Med. Biol.* **17**, 407 (2018).

21. Barchi, M., Geremia, R., Magliozzi, R. & Bianchi, E. Isolation and analyses of enriched populations of male mouse germ cells by sedimentation velocity: the centrifugal elutriation. *Methods Mol. Biol.* **558**, 299–321 (2009).

22. Gaysinskaya, V. & Bortvin, A. Flow cytometry of murine spermatocytes. *Curr. Protoc. Cytom.* **2015**, 7.44.1-7.44.24 (2015).

23. Struijk, R. B. *et al.* Simultaneous Purification of Round and Elongated Spermatids from Testis Tissue Using a FACS-Based DNA Ploidy Assay. *Cytom. Part A* **95**, 309–313 (2019).

24. Bryant, J. M., Meyer-Ficca, M. L., Dang, V. M., Berger, S. L. & Meyer, R. G. Separation of spermatogenic cell types using STA-PUT velocity sedimentation. *J. Vis. Exp.* (2013) doi:10.3791/50648.

25. Lehtiniemi, T. & Kotaja, N. Germ granule-mediated RNA regulation in male germ cells. *Reproduction* **155**, R77–R91 (2018).

26. Meikar, O. *et al.* An atlas of chromatoid body components. *RNA* **20**, 483–95 (2014).

27. Pankiv, S. & Johansen, T. FYCO1: linking autophagosomes to microtubule plus end-directing molecular motors. *Autophagy* **6**, 550–2 (2010).

28. Eberle, A. B., Lykke-Andersen, S., Muhlemann, O. & Jensen, T. H. SMG6 promotes endonucleolytic cleavage of nonsense mRNA in human cells. *Nat. Struct. Mol. Biol.* **16**, 49–55 (2009).

29. Griswold, M. D. Spermatogenesis: The Commitment to Meiosis. *Physiol. Rev.* **96**, 1 (2016).

30. Hess, R. A. & De Franca, L. R. Spermatogenesis and cycle of the seminiferous epithelium. *Adv. Exp. Med. Biol.* **636**, 1–15 (2008).

31. Yokota, S. Historical survey on chromatoid body research. *Acta Histochem. Cytochem.* **41**, 65–82 (2008).

32. Hermo, L., Pelletier, R. M., Cyr, D. G. & Smith, C. E. Surfing the wave, cycle, life history, and genes/proteins expressed by testicular germ cells. Part 1: Background to spermatogenesis, spermatogonia, and spermatocytes. *Microsc. Res. Tech.* **73**, 241–278 (2010).

33. Zhang, Y. *et al.* SpermatogenesisOnline 1.0: a resource for spermatogenesis based on manual literature curation and genome-wide data mining. *Nucleic Acids Res.* **41**, D1055 (2013).

34. Lehtiniemi, T. *et al.* SMG6 localizes to the chromatoid body and shapes the male germ cell transcriptome to drive spermatogenesis. *Nucleic Acids Res.* **50**, (2022).

35. Montoto, L. G., Arregui, L., Sánchez, N. M., Gomendio, M. & Roldan, E. R. S. Postnatal testicular development in mouse species with different levels of sperm competition. *Reproduction* **143**, 333–346 (2012).

36. Tagelenbosch, R. A. J. & de Rooij, D. G. A quantitative study of spermatogonial multiplication and stem cell renewal in the C3H/101 F1 hybrid mouse. *Mutat. Res. Mol. Mech. Mutagen.* **290**, 193–200 (1993).

37. Nagano, M. C. Homing efficiency and proliferation kinetics of male germ line stem cells following transplantation in mice. *Biol. Reprod.* **69**, 701–707 (2003).

38. Oakberg, E. F. Spermatogonial stem-cell renewal in the mouse. *Anat. Rec.* **169**, 515–531 (1971).

39. Boitani, C., Di Persio, S., Esposito, V. & Vicini, E. Spermatogonial cells: mouse, monkey and man comparison. *Semin. Cell Dev. Biol.* **59**, 79–88 (2016).

40. Handel, M. A. & Schimenti, J. C. Genetics of mammalian meiosis: regulation, dynamics and impact on fertility. *Nat. Rev. Genet.* **11**, 124–136 (2010).

41. Mäkelä, J.-A. *et al.* Transillumination-assisted dissection of specific stages of the mouse seminiferous epithelial cycle for downstream immunostaining analyses. *J. Vis. Exp.* **2020**, (2020).

42. Russell, L. D., Ettlin, R. A., Hikim, A. P. S. & Clegg, E. D. Histological and Histopathological Evaluation of the Testis. *Int. J. Androl.* **16**, 83–83 (1993).

43. Khawar, M. B., Gao, H. & Li, W. Mechanism of Acrosome Biogenesis in Mammals. *Front. Cell Dev. Biol.* **7**, 195 (2019).

44. Abou-Haila, A. & Tulsiani, D. R. P. Mammalian Sperm Acrosome: Formation, Contents, and Function. *Arch. Biochem. Biophys.* **379**, 173–182 (2000).

45. Berruti, G. Towards defining an 'origin'—The case for the mammalian acrosome. *Semin. Cell Dev. Biol.* **59**, 46–53 (2016).

46. Clermont, Y. Kinetics of spermatogenesis in mammals: seminiferous epithelium cycle and spermatogonial renewal. *Physiol. Rev.* **52**, 198–236 (1972).

47. Xiong, W., Shen, C. & Wang, Z. The molecular mechanisms underlying acrosome biogenesis elucidated by gene-manipulated mice†. *Biol. Reprod.* **105**, 789–807 (2021).

48. Khawar, M. B., Gao, H. & Li, W. Mechanism of Acrosome Biogenesis in Mammals. *Frontiers in Cell and Developmental Biology* vol. 7 (2019).

49. Koscinski, I. *et al.* DPY19L2 Deletion as a Major Cause of Globozoospermia. *Am. J. Hum. Genet.* **88**, 344–350 (2011).

50. Pierre, V. *et al.* Absence of Dpy19l2, a new inner nuclear membrane protein, causes globozoospermia in mice by preventing the anchoring of the acrosome to the nucleus. *Development* **139**, 2955–2965 (2012).

51. Castaneda, J. M. *et al.* FAM209 associates with DPY19L2, and is required for sperm acrosome biogenesis and fertility in mice. *J. Cell Sci.* **134**, (2021).

52. Morohoshi, A. *et al.* FAM71F1 binds to RAB2A and RAB2B and is essential for acrosome formation and male fertility in mice. *Development* **148**, (2021).

53. Yildiz, Y. *et al.* Mutation of beta-glucosidase 2 causes glycolipid storage disease and impaired male fertility. *J. Clin. Invest.* **116**, 2985–94 (2006).

54. Raju, D. *et al.* Accumulation of glucosylceramide in the absence of the beta-glucosidase GBA2 alters cytoskeletal dynamics. *PLoS Genet.* **11**, e1005063 (2015).

55. Yao, R. *et al.* Lack of acrosome formation in mice lacking a Golgi protein, GOPC. *Proc. Natl. Acad. Sci. U. S. A.* **99**, 11211–6 (2002).

56. Fujihara, Y. *et al.* PDCL2 is essential for sperm acrosome formation and male fertility in mice. *Andrology* (2022) doi:10.1111/ANDR.13329.

57. Xiao, N. *et al.* PICK1 deficiency causes male infertility in mice by disrupting acrosome formation. *J. Clin. Invest.* **119**, 802–12 (2009).

58. Fujihara, Y. *et al.* SPACA1-deficient male mice are infertile with abnormally shaped sperm heads reminiscent of globozoospermia. *Development* **139**, 3583–9 (2012).

59. Nozawa, K. *et al.* Knockout of serine-rich single-pass membrane protein 1 (Ssmem1) causes globozoospermia and sterility in male mice. *Biol. Reprod.* **103**, 244 (2020).

60. Lin, Y.-N., Roy, A., Yan, W., Burns, K. H. & Matzuk, M. M. Loss of zona pellucida binding proteins in the acrosomal matrix disrupts acrosome biogenesis and sperm morphogenesis. *Mol. Cell. Biol.* **27**, 6794–805 (2007).

61. Yatsenko, A. N. *et al.* Association of mutations in the zona pellucida binding protein 1 (ZPBP1) gene with abnormal sperm head morphology in infertile men. *Mol. Hum. Reprod.* **18**, 14–21 (2012).

62. Guidi, L. G. *et al.* AU040320 deficiency leads to disruption of acrosome biogenesis and infertility in homozygous mutant mice. *Sci. Reports 2018 81* **8**, 1–15 (2018).

63. Pirrello, O. *et al.* Search for mutations involved in human globozoospermia. *Hum. Reprod.* **20**, 1314–8 (2005).

64. Ghédir, H. *et al.* Identification of a new DPY19L2 mutation and a better definition of DPY19L2 deletion breakpoints leading to globozoospermia. *Mol. Hum. Reprod.* **22**, 35–45 (2016).

65. Coutton, C. *et al.* MLPA and sequence analysis of DPY19L2 reveals point mutations causing globozoospermia. *Hum. Reprod.* **27**, 2549–2558 (2012).

66. Dam, A. H. D. M. *et al.* Homozygous mutation in SPATA16 is associated with male infertility in human globozoospermia. *Am. J. Hum. Genet.* **81**, 813–20 (2007).

67. ElInati, E. *et al.* A new mutation identified in SPATA16 in two globozoospermic patients. *J. Assist. Reprod. Genet.* **33**, 815–820 (2016).

68. Yogo, K. Molecular basis of the morphogenesis of sperm head and tail in mice. *Reprod. Med. Biol.* **21**, (2022).

69. Lehti, M. S. & Sironen, A. Formation and function of the manchette and flagellum during spermatogenesis. *Reproduction* **151**, R43–R54 (2016).

70. Yamaguchi, K. *et al.* Re-evaluating the Localization of Sperm-Retained Histones Revealed the Modification-Dependent Accumulation in Specific Genome Regions. *Cell Rep.* **23**, 3920–3932 (2018).

71. Jung, Y. H. *et al.* Chromatin States in Mouse Sperm Correlate with Embryonic and Adult Regulatory Landscapes. *Cell Rep.* **18**, 1366–1382 (2017).

72. Oakberg, E. F. Duration of spermatogenesis in the mouse and timing of stages of the cycle of the seminiferous epithelium. *Am. J. Anat.* **99**, 507–516 (1956).

73. Clermont, Y. Kinetics of spermatogenesis in mammals: seminiferous epithelium cycle and spermatogonial renewal. *Physiol. Rev.* **52**, 198–236 (1972).

74. Kotaja, N. *et al.* Preparation, isolation and characterization of stage-specific spermatogenic cells for cellular and molecular analysis. *Nat. Methods* **1**, 249–254 (2004).

75. Wang, J. M., Li, Z. F., Yang, W. X. & Tan, F. Q. Follicle-stimulating hormone signaling in Sertoli cells: a licence to the early stages of spermatogenesis. *Reprod. Biol. Endocrinol. 2022 201* **20**, 1–18 (2022).

76. Witherspoon, L. & Flannigan, R. It puts the T's in fertility: testosterone and spermatogenesis. *Int. J. Impot. Res. 2022 347* **34**, 669–672 (2022).

77. Sanborn, B. M., Caston, L. A., Buzek, S. W. & Ussuf, K. K. Hormonal regulation of Sertoli cell function. *Adv. Exp. Med. Biol.* **219**, 561–88 (1987).

78. Hansson, V. *et al.* Regulation of seminiferous tubular function by FSH and androgen. *J. Reprod. Fertil.* **44**, 363–75 (1975).

79. Kanatsu-Shinohara, M. & Shinohara, T. Spermatogonial stem cell self-renewal and development. *Annu. Rev. Cell Dev. Biol.* **29**, 163–87 (2013).

80. Mateus, I. *et al.* Glucose and glutamine handling in the Sertoli cells of transgenic rats overexpressing regucalcin: plasticity towards lactate production. *Sci. Reports 2018 81* **8**, 1–13 (2018).

81. Rato, L. *et al.* Metabolic regulation is important for spermatogenesis. *Nat. Rev. Urol.* **9**, 330–8 (2012).

82. Mruk, D. D. & Cheng, C. Y. The Mammalian Blood-Testis Barrier: Its Biology and Regulation. *Endocr. Rev.* **36**, 564 (2015).

83. Cheng, C. Y. & Mruk, D. D. A local autocrine axis in the testes that regulates spermatogenesis. *Nat. Rev. Endocrinol.* **6**, 380–95 (2010).

84. Sipilä, P. & Björkgren, I. Segment-specific regulation of epididymal gene expression. *Reproduction* **152**, R91–R99 (2016).

85. Domeniconi, R. F., Souza, A. C. F., Xu, B., Washington, A. M. & Hinton, B. T. Is the Epididymis a Series of Organs Placed Side By Side? *Biol. Reprod.* **95**, 1–8 (2016).

86. Sosnicki, D. M. *et al.* Segmental differentiation of the murine epididymis: identification of segment-specific, GM1-enriched vesicles and regulation by luminal fluid factors†. *Biol. Reprod.* (2023) doi:10.1093/BIOLRE/IOAD120.

87. Sullivan, R. & Mieusset, R. The human epididymis: its function in sperm maturation. *Hum. Reprod. Update* **22**, 574–587 (2016).

88. James, E. R. *et al.* The Role of the Epididymis and the Contribution of Epididymosomes to Mammalian Reproduction. *Int. J. Mol. Sci.* **21**, 1–17 (2020).

89. Sullivan, R. Epididymosomes: a heterogeneous population of microvesicles with multiple functions in sperm maturation and storage. *Asian J. Androl.* **17**, 726–729 (2015).

90. Sullivan, R. & Saez, F. Epididymosomes, prostasomes, and liposomes: their roles in mammalian male reproductive physiology. *Reproduction* **146**, (2013).

91. Barrachina, F. *et al.* Sperm acquire epididymis-derived proteins through epididymosomes. *Hum. Reprod.* **37**, 651–668 (2022).

92. Rinaldi, V. D. *et al.* An atlas of cell types in the mouse epididymis and vas deferens. *Elife* **9**, 1–49 (2020).

93. Shi, J. *et al.* Spatio-temporal landscape of mouse epididymal cells and specific mitochondria-rich segments defined by large-scale single-cell RNA-seq. *Cell Discov. 2021 71* **7**, 1–15 (2021).

94. Björkgren, I. & Sipilä, P. The impact of epididymal proteins on sperm function. *Reproduction* **158**, R155–R167 (2019).

95. Skerget, S., Rosenow, M. A., Petritis, K. & Karr, T. L. Sperm Proteome Maturation in the Mouse Epididymis. *PLoS One* **10**, e0140650 (2015).

96. Molecular Biology of the Cell - NCBI Bookshelf. https://www.ncbi.nlm.nih.gov/books/NBK21054/.

97. Watson, J. D. *et al.* Molecular Biology of the Gene, Books a la Carte Edition (7th Edition). 912 (2013).

98. Zhao, Y. & Garcia, B. A. Comprehensive Catalog of Currently Documented Histone Modifications. *Cold Spring Harb. Perspect. Biol.* **7**, (2015).

99. Cedar, H. & Bergman, Y. Linking DNA methylation and histone modification: patterns and paradigms. *Nat. Rev. Genet. 2009 105* **10**, 295–304 (2009).

100. Bannister, A. J. & Kouzarides, T. Regulation of chromatin by histone modifications. *Cell Res. 2011 213* **21**, 381–395 (2011).

101. Zhang, F. P. *et al.* Lack of androgen receptor SUMOylation results in male infertility due to epididymal dysfunction. *Nat. Commun.* **10**, (2019).

102. Poukka, H., Karvonen, U., Jänne, O. A. & Palvimo, J. J. Covalent modification of the androgen receptor by small ubiquitin-like modifier 1 (SUMO-1). *Proc. Natl. Acad. Sci. U. S. A.* **97**, 14145 (2000).

103. Paronetto, M. P., Passacantilli, I. & Sette, C. Alternative splicing and cell survival: from tissue homeostasis to disease. *Cell Death Differ.* **23**, 1919 (2016).

104. Tian, B. & Manley, J. L. Alternative polyadenylation of mRNA precursors. *Nat. Rev. Mol. Cell Biol. 2016 181* **18**, 18–30 (2016).

105. Adesnik, M., Salditt, M., Thomas, W. & Darnell, J. E. Evidence that all messenger RNA molecules (except histone messenger RNA) contain Poly (A) sequences and that the Poly(A) has a nuclear function. *J. Mol. Biol.* **71**, 21–30 (1972).

106. Linder, P. & Jankowsky, E. From unwinding to clamping — the DEAD box RNA helicase family. *Nat. Rev. Mol. Cell Biol. 2011 128* **12**, 505–516 (2011).

107. Hentze, M. W., Castello, A., Schwarzl, T. & Preiss, T. A brave new world of RNA-binding proteins. *Nat. Rev. Mol. Cell Biol. 2018 195* **19**, 327–341 (2018).

108. Singh, G., Pratt, G., Yeo, G. W. & Moore, M. J. The Clothes Make the mRNA: Past and Present Trends in mRNP Fashion. *Annu. Rev. Biochem.* **84**, 325–354 (2015).

109. Khong, A. & Parker, R. The landscape of eukaryotic mRNPs. *RNA* **26**, 229–239 (2020).

110. Fox, A. H. & Lamond, A. I. Paraspeckles. *Cold Spring Harb. Perspect. Biol.* **2**, (2010).

111. Ivanov, P., Kedersha, N. & Anderson, P. Stress Granules and Processing Bodies in Translational Control. *Cold Spring Harb. Perspect. Biol.* **11**, (2019).

112. Emmott, E., Jovanovic, M. & Slavov, N. Ribosome stoichiometry: from form to function. *Trends Biochem. Sci.* **44**, 95 (2019).

113. Genuth, N. R. & Barna, M. The Discovery of Ribosome Heterogeneity and Its Implications for Gene Regulation and Organismal Life. *Mol. Cell* **71**, 364–374 (2018).

114. Norris, K., Hopes, T. & Aspden, J. L. Ribosome heterogeneity and specialization in development. *Wiley Interdiscip. Rev. RNA* **12**, e1644 (2021).

115. Li, H. *et al.* A male germ-cell-specific ribosome controls male fertility. *Nat. 2022 6127941* **612**, 725–731 (2022).

116. Zou, Q. *et al.* Proteostasis regulated by testis-specific ribosomal protein RPL39L maintains mouse spermatogenesis. *iScience* **24**, (2021).
117. Hinnebusch, A. G., Ivanov, I. P. & Sonenberg, N. Translational control by 5'-untranslated regions of eukaryotic mRNAs. *Science* **352**, 1413 (2016).
118. Lee, D. S. M. *et al.* Disrupting upstream translation in mRNAs is associated with human disease. *Nat. Commun. 2021 121* **12**, 1–14 (2021).
119. Renz, P. F., Valdivia Francia, F. & Sendoel, A. Some like it translated: small ORFs in the 5′UTR. *Exp. Cell Res.* **396**, 112229 (2020).
120. Leppek, K., Das, R. & Barna, M. Functional 5′ UTR mRNA structures in eukaryotic translation regulation and how to find them. *Nat. Rev. Mol. Cell Biol.* **19**, 158 (2018).
121. Mayr, C. What Are 3′ UTRs Doing? *Cold Spring Harb. Perspect. Biol.* **11**, (2019).
122. Cai, Y., Yu, X., Hu, S. & Yu, J. A brief review on the mechanisms of miRNA regulation. *Genomics. Proteomics Bioinformatics* **7**, 147–154 (2009).
123. Xie, X. *et al.* Systematic discovery of regulatory motifs in human promoters and 3′ UTRs by comparison of several mammals. *Nature* **434**, 338 (2005).
124. Farberov, L. *et al.* Multiple Copies of microRNA Binding Sites in Long 3'UTR Variants Regulate Axonal Translation. *Cells* **12**, 233 (2023).
125. Mayr, C. What Are 3' UTRs Doing? *Cold Spring Harb. Perspect. Biol.* **11**, (2019).
126. Fansler, M. M., Zhen, G. & Mayr, C. Quantification of alternative 3'UTR isoforms from single cell RNA-seq data with scUTRquant. *bioRxiv* 2021.11.22.469635 (2021) doi:10.1101/2021.11.22.469635.
127. Griesemer, D. *et al.* Genome-wide functional screen of 3'UTR variants uncovers causal variants for human disease and evolution. *Cell* **184**, 5247-5260.e19 (2021).
128. Lianoglou, S., Garg, V., Yang, J. L., Leslie, C. S. & Mayr, C. Ubiquitously transcribed genes use alternative polyadenylation to achieve tissue-specific expression. *Genes Dev.* **27**, 2380–2396 (2013).
129. Berkovits, B. D. & Mayr, C. Alternative 3′ UTRs act as scaffolds to regulate membrane protein localization. *Nat. 2015 5227556* **522**, 363–367 (2015).
130. Sandberg, R., Neilson, J. R., Sarma, A., Sharp, P. A. & Burge, C. B. Proliferating cells express mRNAs with shortened 3′ untranslated regions and fewer microRNA target sites. *Science (80-.).* **320**, 1643–1647 (2008).
131. Freimer, J. W., Krishnakumar, R., Cook, M. S. & Blelloch, R. Expression of Alternative Ago2 Isoform Associated with Loss of microRNA-Driven Translational Repression in Mouse Oocytes. *Curr. Biol.* **28**, 296-302.e3 (2018).
132. Hong, D. & Jeong, S. 3'UTR Diversity: Expanding Repertoire of RNA Alterations in Human mRNAs. *Mol. Cells* **46**, 48 (2023).
133. Gruber, A. J. & Zavolan, M. Alternative cleavage and polyadenylation in health and disease. *Nat. Rev. Genet. 2019 2010* **20**, 599–614 (2019).
134. Masamha, C. P. *et al.* CFIm25 links Alternative Polyadenylation to Glioblastoma Tumor Suppression. *Nature* **510**, 412 (2014).
135. Masamha, C. P. The emerging roles of CFIm25 (NUDT21/CPSF5) in human biology and disease. *Wiley Interdiscip. Rev. RNA* e1757 (2022) doi:10.1002/WRNA.1757.
136. Lee, S. H. *et al.* Widespread intronic polyadenylation inactivates tumor suppressorgenes in leukemia. *Nature* **561**, 127 (2018).
137. Xu, C. & Zhang, J. Alternative Polyadenylation of Mammalian Transcripts Is Generally Deleterious, Not Adaptive. *Cell Syst.* **6**, 734-742.e4 (2018).
138. Xu, C. & Zhang, J. A different perspective on alternative cleavage and polyadenylation. *Nat. Rev. Genet. 2019 211* **21**, 63–63 (2019).
139. Derti, A. *et al.* A quantitative atlas of polyadenylation in five mammals. *Genome Res.* **22**, 1173–1183 (2012).

140. Li, W. *et al.* The τCstF-64 Polyadenylation Protein Controls Genome Expression in Testis. *PLoS One* **7**, 48373 (2012).
141. Li, W. *et al.* Alternative cleavage and polyadenylation in spermatogenesis connects chromatin regulation with post-transcriptional control. *BMC Biol.* **14**, (2016).
142. Fanourgakis, G., Lesche, M., Akpinar, M., Dahl, A. & Jessberger, R. Chromatoid Body Protein TDRD6 Supports Long 3' UTR Triggered Nonsense Mediated mRNA Decay. *PLoS Genet.* **12**, e1005857 (2016).
143. Bao, J. *et al.* UPF2-Dependent Nonsense-Mediated mRNA Decay Pathway Is Essential for Spermatogenesis by Selectively Eliminating Longer 3'UTR Transcripts. *PLOS Genet.* **12**, e1005863 (2016).
144. Berry, C. W. *et al.* Developmentally regulated alternate 3' end cleavage of nascent transcripts controls dynamic changes in protein expression in an adult stem cell lineage. *bioRxiv* 2022.05.09.489277 (2022) doi:10.1101/2022.05.09.489277.
145. Hellen, C. U. T. Translation Termination and Ribosome Recycling in Eukaryotes. *Cold Spring Harb. Perspect. Biol.* **10**, (2018).
146. Carter, M. S. *et al.* A regulatory mechanism that detects premature nonsense codons in T-cell receptor transcripts in vivo is reversed by protein synthesis inhibitors in vitro. *J. Biol. Chem.* **270**, 28995–29003 (1995).
147. Lykke-Andersen, S. & Jensen, T. H. Nonsense-mediated mRNA decay: An intricate machinery that shapes transcriptomes. *Nature Reviews Molecular Cell Biology* vol. 16 665–677 (2015).
148. Nasif, S., Contu, L. & Mühlemann, O. Beyond quality control: The role of nonsense-mediated mRNA decay (NMD) in regulating gene expression. *Seminars in Cell and Developmental Biology* vol. 75 78–87 (2018).
149. Chang, Y. F., Imam, J. S. & Wilkinson, M. F. The nonsense-mediated decay RNA surveillance pathway. *Annu. Rev. Biochem.* **76**, 51–74 (2007).
150. Lee, S. R., Pratt, G. A., Martinez, F. J., Yeo, G. W. & Lykke-Andersen, J. Target Discrimination in Nonsense-Mediated mRNA Decay Requires Upf1 ATPase Activity. *Mol. Cell* **59**, 413–425 (2015).
151. Chapman, J. H. *et al.* UPF1 mutants with intact ATPase but deficient helicase activities promote efficient nonsense-mediated mRNA decay. *Nucleic Acids Res.* **50**, 11876–11894 (2022).
152. López-Perrote, A. *et al.* Human nonsense-mediated mRNA decay factor UPF2 interacts directly with eRF3 and the SURF complex. *Nucleic Acids Res.* **44**, 1909–1923 (2016).
153. Xue, G. *et al.* Modulation of RNA-binding properties of the RNA helicase UPF1 by its activator UPF2. *RNA* **29**, 178–187 (2023).
154. Shum, E. Y. *et al.* The Antagonistic Gene Paralogs Upf3a and Upf3b Govern Nonsense-Mediated RNA Decay. *Cell* **165**, 382–395 (2016).
155. Karousis, E. D. & Mühlemann, O. Nonsense-mediated mRNA decay begins where translation ends. *Cold Spring Harb. Perspect. Biol.* **11**, a032862 (2019).
156. Jonas, S., Weichenrieder, O. & Izaurralde, E. An unusual arrangement of two 14-3-3-like domains in the SMG5–SMG7 heterodimer is required for efficient nonsense-mediated mRNA decay. *Genes Dev.* **27**, 211 (2013).
157. Chakrabarti, S., Bonneau, F., Schüssler, S., Eppinger, E. & Conti, E. Phospho-dependent and phospho-independent interactions of the helicase UPF1 with the NMD factors SMG5-SMG7 and SMG6. *Nucleic Acids Res.* **42**, 9447–60 (2014).
158. Loh, B., Jonas, S. & Izaurralde, E. The SMG5–SMG7 heterodimer directly recruits the CCR4–NOT deadenylase complex to mRNAs containing nonsense codons via interaction with POP2. *Genes Dev.* **27**, 2125 (2013).
159. Chang, Y.-F., Imam, J. S. & Wilkinson, M. F. The Nonsense-Mediated Decay RNA Surveillance Pathway. *Annu. Rev. Biochem.* **76**, 51–74 (2007).

160. Colombo, M., Karousis, E. D., Bourquin, J., Bruggmann, R. & Mühlemann, O. Transcriptome-wide identification of NMD-targeted human mRNAs reveals extensive redundancy between SMG6- and SMG7-mediated degradation pathways. *RNA* **23**, 189–201 (2017).

161. Sanderlin, E. J. *et al.* CFTR mRNAs with nonsense codons are degraded by the SMG6-mediated endonucleolytic decay pathway. *Nat. Commun.* **13**, (2022).

162. Boehm, V. *et al.* SMG5-SMG7 authorize nonsense-mediated mRNA decay by enabling SMG6 endonucleolytic activity. *Nat. Commun.* **12**, (2021).

163. Chawla, R. & Azzalin, C. M. The telomeric transcriptome and SMG proteins at the crossroads. *Cytogenet. Genome Res.* **122**, 194–201 (2008).

164. Hwang, J. & Maquat, L. E. Nonsense-mediated mRNA decay (NMD) in animal embryogenesis: to die or not to die, that is the question. *Curr. Opin. Genet. Dev.* **21**, 422–430 (2011).

165. Lundblad, V. & Szostak, J. W. A mutant with a defect in telomere elongation leads to senescence in yeast. *Cell* **57**, 633–643 (1989).

166. Steiner, B. R., Hidaka, K. & Futcher, B. Association of the Est1 protein with telomerase activity in yeast. *Proc. Natl. Acad. Sci. U. S. A.* **93**, 2817–2821 (1996).

167. Evans, S. K. & Lundblad, V. The Est1 subunit of Saccharomyces cerevisiae telomerase makes multiple contributions to telomere length maintenance. *Genetics* **162**, 1101–1115 (2002).

168. Snow, B. E. *et al.* Functional conservation of the telomerase protein Est1p in humans. *Curr. Biol.* **13**, 698–704 (2003).

169. Reichenbach, P. *et al.* A human homolog of yeast Est1 associates with telomerase and uncaps chromosome ends when overexpressed. *Curr. Biol.* **13**, 568–574 (2003).

170. Azzalin, C. M., Reichenbach, P., Khoriauli, L., Giulotto, E. & Lingner, J. Telomeric repeat containing RNA and RNA surveillance factors at mammalian chromosome ends. *Science* **318**, 798–801 (2007).

171. Suzuki, K. *et al.* SMG6 regulates DNA damage and cell survival in Hippo pathway kinase LATS2-inactivated malignant mesothelioma. *Cell death Discov.* **8**, (2022).

172. Li, T. *et al.* Smg6/Est1 licenses embryonic stem cell differentiation via nonsense-mediated <scp>mRNA</scp> decay. *EMBO J.* **34**, 1630–1647 (2015).

173. Soumillon, M. *et al.* Cellular Source and Mechanisms of High Transcriptome Complexity in the Mammalian Testis. *Cell Rep.* **3**, 2179–2190 (2013).

174. Harcourt, A. H., Harveyt, P. H. & Larson, S. G. Testis weight, body weight and breeding system in primates. *Nature* **293**, (1981).

175. Yapar, E. *et al.* Convergent evolution of primate testis transcriptomes reflects mating strategy. *bioRxiv* 010553 (2021) doi:10.1101/010553.

176. Ramm, S. A., Schärer, L., Ehmcke, J. & Wistuba, J. Sperm competition and the evolution of spermatogenesis. *Mol. Hum. Reprod.* **20**, 1169–1179 (2014).

177. Bao, J. & Bedford, M. T. Epigenetic regulation of the histone-to-protamine transition during spermiogenesis. *Reproduction* vol. 151 R55–R70 (2016).

178. Kierszenbaum, A. L. & Tres, L. L. Structural and transcriptional features of the mouse spermatid genome. *J. Cell Biol.* **65**, 258–70 (1975).

179. Kleene, K. C. Connecting cis-elements and trans-factors with mechanisms of developmental regulation of mRNA translation in meiotic and haploid mammalian spermatogenic cells. *Reproduction* vol. 146 R1–R19 (2013).

180. Schmidt, E. E. Transcriptional promiscuity in testes. *Curr. Biol.* **6**, 768–769 (1996).

181. Melé, M. *et al.* Human genomics. The human transcriptome across tissues and individuals. *Science* **348**, 660–665 (2015).

182. Ramsköld, D., Wang, E. T., Burge, C. B. & Sandberg, R. An abundance of ubiquitously expressed genes revealed by tissue transcriptome sequence data. *PLoS Comput. Biol.* **5**, (2009).

183. Hammoud, S. S. *et al.* Chromatin and transcription transitions of mammalian adult germline stem cells and spermatogenesis. *Cell Stem Cell* **15**, 239–253 (2014).

184. Hammoud, S. S. *et al.* Transcription and imprinting dynamics in developing postnatal male germline stem cells. *Genes Dev.* **29**, 2312–2324 (2015).

185. Green, C. D. *et al.* A comprehensive roadmap of murine spermatogenesis defined by single-cell RNA-seq. *Dev. Cell* **46**, 651 (2018).

186. Guo, J. *et al.* The adult human testis transcriptional cell atlas. *Cell Res. 2018 2812* **28**, 1141–1157 (2018).

187. Xia, B. *et al.* Widespread Transcriptional Scanning in the Testis Modulates Gene Evolution Rates. *Cell* **180**, 248-262.e21 (2020).

188. D, D. *et al.* The human testis-specific proteome defined by transcriptomics and antibody-based profiling. *Mol. Hum. Reprod.* **20**, 476–488 (2014).

189. Schultz, N., Hamra, F. K. & Garbers, D. L. A multitude of genes expressed solely in meiotic or postmeiotic spermatogenic cells offers a myriad of contraceptive targets. *Proc. Natl. Acad. Sci. U. S. A.* **100**, 12201–12206 (2003).

190. Kleene, K. C. & Kleene, K. C. Patterns, mechanisms, and functions of translation regulation in mammalian spermatogenic cells. *Cytogenet Genome Res* **103**, 217–224 (2003).

191. Wang, D. *et al.* A deep proteome and transcriptome abundance atlas of 29 healthy human tissues. *Mol. Syst. Biol.* **15**, (2019).

192. Rathke, C., Baarends, W. M., Awe, S. & Renkawitz-Pohl, R. Chromatin dynamics during spermiogenesis. *Biochim. Biophys. Acta* **1839**, 155–68 (2014).

193. Necsulea, A. & Kaessmann, H. Evolutionary dynamics of coding and non-coding transcriptomes. *Nat. Rev. Genet.* **15**, 734–748 (2014).

194. Maezawa, S., Yukawa, M., Alavattam, K. G., Barski, A. & Namekawa, S. H. Dynamic reorganization of open chromatin underlies diverse transcriptomes during spermatogenesis. *Nucleic Acids Res.* **46**, 593 (2018).

195. Jinks-Robertson, S. & Bhagwat, A. S. Transcription-Associated Mutagenesis. *https://doi.org/10.1146/annurev-genet-120213-092015* **48**, 341–359 (2014).

196. Bhutani, K. *et al.* Widespread haploid-biased gene expression enables sperm-level natural selection. *Science (80-.).* eabb1723 (2021) doi:10.1126/science.abb1723.

197. Schmid, R. *et al.* The splicing landscape is globally reprogrammed during male meiosis. *Nucleic Acids Res.* **41**, 10170–84 (2013).

198. Margolin, G., Khil, P. P., Kim, J., Bellani, M. A. & Camerini-Otero, R. D. Integrated transcriptome analysis of mouse spermatogenesis. *BMC Genomics* **15**, 39 (2014).

199. Song, H., Wang, L., Chen, D. & Li, F. The function of pre-mRNA alternative splicing in mammal spermatogenesis. *International Journal of Biological Sciences* vol. 16 38–48 (2020).

200. Naro, C. *et al.* An Orchestrated Intron Retention Program in Meiosis Controls Timely Usage of Transcripts during Germ Cell Differentiation. *Dev. Cell* **41**, 82-93.e4 (2017).

201. Rolland, A. D. *et al.* RNA profiling of human testicular cells identifies syntenic lncRNAs associated with spermatogenesis. *Hum. Reprod.* **34**, 1278–1290 (2019).

202. Chalmel, F. *et al.* High-resolution profiling of novel transcribed regions during rat spermatogenesis. *Biol. Reprod.* **91**, (2014).

203. Gamble, J. *et al.* An expanded mouse testis transcriptome and mass spectrometry defines novel proteins. *Reproduction* **159**, 15 (2020).

204. Baralle, F. E. & Giudice, J. Alternative splicing as a regulator of development and tissue identity. *Nat. Rev. Mol. Cell Biol. 2017 187* **18**, 437–451 (2017).

205. Fu, X.-D. & Manuel Ares, J. Context-dependent control of alternative splicing by RNA-binding proteins. *Nat. Rev. Genet.* **15**, 689 (2014).

206. Pan, Q. *et al.* Revealing global regulatory features of mammalian alternative splicing using a quantitative microarray platform. *Mol. Cell* **16**, 929–941 (2004).

207. Clark, T. A. *et al.* Discovery of tissue-specific exons using comprehensive human exon microarrays. *Genome Biol.* **8**, R64 (2007).

208. Grosso, A. R. *et al.* Tissue-specific splicing factor gene expression signatures. *Nucleic Acids Res.* **36**, 4823 (2008).

209. Mazin, P. V., Khaitovich, P., Cardoso-Moreira, M. & Kaessmann, H. Alternative splicing during mammalian organ development. *Nat. Genet. 2021 536* **53**, 925–934 (2021).

210. Tautz, D. & Domazet-Lošo, T. The evolutionary origin of orphan genes. *Nat. Rev. Genet. 2011 1210* **12**, 692–702 (2011).

211. Siepel, A. Darwinian alchemy: Human genes from noncoding DNA. *Genome Res.* **19**, 1693–1695 (2009).

212. Ruiz-Orera, J. *et al.* Origins of De Novo Genes in Human and Chimpanzee. *PLOS Genet.* **11**, e1005721 (2015).

213. Luis, J. *et al.* New Genes and Functional Innovation in Mammals. doi:10.6084/m9.fig.

214. Zhang, J. Y. & Zhou, Q. On the Regulatory Evolution of New Genes Throughout Their Life History. *Mol. Biol. Evol.* **36**, 15–27 (2019).

215. Schultz, N., Hamra, F. K. & Garbers, D. L. A multitude of genes expressed solely in meiotic or postmeiotic spermatogenic cells offers a myriad of contraceptive targets. *Proc. Natl. Acad. Sci. U. S. A.* **100**, 12201–12206 (2003).

216. Miyata, H. *et al.* Genome engineering uncovers 54 evolutionarily conserved and testis-enriched genes that are not required for male fertility in mice. *Proc. Natl. Acad. Sci. U. S. A.* **113**, 7704–7710 (2016).

217. Zhang, R. *et al.* Testis-enriched Asb12 is not required for spermatogenesis and fertility in mice. *Transl. Androl. Urol.* **11**, 168–178 (2022).

218. Xu, H., Ding, H. & Zheng, H. Murine fertility and spermatogenesis are independent of the testis-specific Spdye4a gene. *Gen. Comp. Endocrinol.* **330**, (2023).

219. Xia, M. *et al.* Testis-expressed protein 33 is not essential for spermiogenesis and fertility in mice. *Mol. Med. Rep.* **23**, (2021).

220. Ahn, J. *et al.* A novel testis-enriched gene, Samd4a, regulates spermatogenesis as a spermatid-specific factor. *Front. cell Dev. Biol.* **10**, (2022).

221. Noda, T. *et al.* Sperm proteins SOF1, TMEM95, and SPACA6 are required for sperm-oocyte fusion in mice. *Proc. Natl. Acad. Sci. U. S. A.* **117**, (2020).

222. Oyama, Y. *et al.* CRISPR/Cas9-mediated genome editing reveals 12 testis-enriched genes dispensable for male fertility in mice. *Asian J. Androl.* **24**, 266 (2022).

223. Friedman, J. R. & Nunnari, J. Mitochondrial form and function. *Nature* **505**, 335–343 (2014).

224. Lewis, V. *et al.* Glycoproteins of the lysosomal membrane. *J. Cell Biol.* **100**, 1839–1847 (1985).

225. Eddy, E. M. Cytochemical observations on the chromatoid body of the male germ cells. *Biol. Reprod.* **2**, 114–28 (1970).

226. Parvinen, M. The chromatoid body in spermatogenesis. *Int. J. Androl.* **28**, 189–201 (2005).

227. Chuma, S., Hosokawa, M., Tanaka, T. & Nakatsuji, N. Ultrastructural characterization of spermatogenesis and its evolutionary conservation in the germline: germinal granules in mammals. *Mol. Cell. Endocrinol.* **306**, 17–23 (2009).

228. Leatherman, J. L. & Jongens, T. A. Transcriptional silencing and translational control: key features of early germline development. *BioEssays* **25**, 326–335 (2003).

229. Jamieson-Lucy, A. & Mullins, M. C. The vertebrate Balbiani body, germ plasm, and oocyte polarity. *Curr. Top. Dev. Biol.* **135**, 1–34 (2019).

230. Banani, S. F., Lee, H. O., Hyman, A. A. & Rosen, M. K. Biomolecular condensates: organizers of cellular biochemistry. *Nat. Rev. Mol. Cell Biol. 2017 185* **18**, 285–298 (2017).

231. Woodruff, J. B., Hyman, A. A. & Boke, E. Organization and Function of Non-dynamic Biomolecular Condensates. *Trends Biochem. Sci.* **43**, 81–94 (2018).

232. Wu, H. & Fuxreiter, M. The Structure and Dynamics of Higher-Order Assemblies: Amyloids, Signalosomes, and Granules. *Cell* **165**, 1055–1066 (2016).

233. Dodson, A. E. & Kennedy, S. Phase Separation in Germ Cells and Development. (2020) doi:10.1016/j.devcel.2020.09.004.

234. Hyman, A. A., Weber, C. A. & Jülicher, F. Liquid-Liquid Phase Separation in Biology. *https://doi.org/10.1146/annurev-cellbio-100913-013325* **30**, 39–58 (2014).

235. Brangwynne, C. P. *et al.* Germline P granules are liquid droplets that localize by controlled dissolution/condensation. *Science (80-.).* **324**, 1729–1732 (2009).

236. Lehtiniemi, T. & Kotaja, N. Germ granule-mediated RNA regulation in male germ cells. *Reproduction* vol. 155 R77–R91 (2018).

237. Fawcett, D. W., Eddy, E. M. & Phillips, D. M. Observations on the fine structure and relationships of the chromatoid body in mammalian spermatogenesis. *Biol. Reprod.* **2**, 129–53 (1970).

238. Yokota, S. Nuage proteins: their localization in subcellular structures of spermatogenic cells as revealed by immunoelectron microscopy. *Histochem. Cell Biol.* **138**, 1–11 (2012).

239. Russell, L. & Frank, B. Ultrastructural characterization of nuage in spermatocytes of the rat testis. *Anat. Rec.* **190**, 79–97 (1978).

240. Meikar, O., Da Ros, M., Korhonen, H. & Kotaja, N. Chromatoid body and small RNAs in male germ cells. *Reproduction* **142**, 195–209 (2011).

241. Lehti, M. S., Kotaja, N. & Sironen, A. KIF1-binding protein interacts with KIF3A in haploid male germ cells. *Reproduction* **150**, 209–216 (2015).

242. Susi, F. R. & Clermont, Y. Fine structural modifications of the rat chromatoid body during spermiogenesis. *Am. J. Anat.* **129**, 177–191 (1970).

243. Shang, P. *et al.* Functional transformation of the chromatoid body in mouse spermatids requires testis-specific serine/threonine kinases. *J. Cell Sci.* **123**, 331–9 (2010).

244. Parvinen, L. M., Jokelainen, P. & Parvinen, M. Chromatoid body and haploid gene activity: actinomycin D induced morphological alterations. *Hereditas* **88**, 75–80 (1978).

245. Parvinen, M. The chromatoid body in spermatogenesis. *Int. J. Androl.* **28**, 189–201 (2005).

246. Parvinen, M. *et al.* Computer analysis of living cells: movements of the chromatoid body in early spermatids compared with its ultrastructure in snap-frozen preparations. *Histochem. Cell Biol.* **108**, 77–81 (1997).

247. Ventelä, S., Toppari, J. & Parvinen, M. Intercellular organelle traffic through cytoplasmic bridges in early spermatids of the rat: mechanisms of haploid gene product sharing. *Mol. Biol. Cell* **14**, 2768–80 (2003).

248. Söderström, K. O. & Parvinen, M. Transport of material between the nucleus, the chromatoid body and the Golgi complex in the early spermatids of the rat. *Cell Tissue Res.* **168**, 335–42 (1976).

249. Parvinen, M. & Parvinen, L. M. Active movements of the chromatoid body. A possible transport mechanism for haploid gene products. *J. Cell Biol.* **80**, 621–8 (1979).

250. Wang, X., Lv, C., Guo, Y. & Yuan, S. Mitochondria Associated Germinal Structures in Spermatogenesis: piRNA Pathway Regulation and Beyond. *Cells* **9**, (2020).

251. Da Ros, M., Hirvonen, N., Olotu, O., Toppari, J. & Kotaja, N. Retromer vesicles interact with RNA granules in haploid male germ cells. *Mol. Cell. Endocrinol.* **401**, 73–83 (2015).

252. Fujii, Y., Onohara, Y., Fujita, H. & Yokota, S. Argonaute2 Protein in Rat Spermatogenic Cells Is Localized to Nuage Structures and LAMP2-Positive Vesicles Surrounding Chromatoid Bodies. *J. Histochem. Cytochem.* **64**, 268–79 (2016).

253. Haraguchi, C. M. *et al.* Chromatoid bodies: Aggresome-like characteristics and degradation sites for organelles of spermiogenic cells. *J. Histochem. Cytochem.* **53**, 455–465 (2005).

254. Bourdenx, M., Gavathiotis, E. & Cuervo, A. M. Chaperone-mediated autophagy: a gatekeeper of neuronal proteostasis. *Autophagy* **17**, 2040–2042 (2021).

255. Tekirdag, K. & Cuervo, A. M. Chaperone-mediated autophagy and endosomal microautophagy: Joint by a chaperone. *J. Biol. Chem.* **293**, 5414–5424 (2018).

256. Saxton, R. A. & Sabatini, D. M. mTOR Signaling in Growth, Metabolism, and Disease. *Cell* **168**, 960–976 (2017).

257. Foster, K. G. & Fingar, D. C. Mammalian target of rapamycin (mTOR): conducting the cellular signaling symphony. *J. Biol. Chem.* **285**, 14071–7 (2010).

258. Takahashi, Y. *et al.* An autophagy assay reveals the ESCRT-III component CHMP2A as a regulator of phagophore closure. *Nat. Commun.* **9**, (2018).

259. Yu, L., Chen, Y. & Tooze, S. A. Autophagy pathway: Cellular and molecular mechanisms. (2018) doi:10.1080/15548627.2017.1378838.

260. Eskelinen, E. L., Reggiori, F., Baba, M., Kovács, A. L. & Seglen, P. O. Seeing is believing: The impact of electron microscopy on autophagy research. *https://doi.org/10.4161/auto.7.9.15760* **7**, 935–956 (2011).

261. Cebollero, E., Reggiori, F. & Kraft, C. Reticulophagy and ribophagy: regulated degradation of protein production factories. *Int. J. Cell Biol.* **2012**, 182834 (2012).

262. Wyant, G. A. *et al.* NUFIP1 is a ribosome receptor for starvation-induced ribophagy. *Science* **360**, 751 (2018).

263. Ashrafi, G. & Schwarz, T. L. The pathways of mitophagy for quality control and clearance of mitochondria. *Cell Death Differ.* **20**, 31–42 (2013).

264. Stolz, A. & Grumati, P. The various shades of ER-phagy. *FEBS J.* **286**, 4642–4649 (2019).

265. Papadopoulos, C., Kravic, B. & Meyer, H. Repair or Lysophagy: Dealing with Damaged Lysosomes. *J. Mol. Biol.* **432**, 231–239 (2020).

266. Hasegawa, J., Maejima, I., Iwamoto, R. & Yoshimori, T. Selective autophagy: Lysophagy. *Methods* (2014) doi:10.1016/j.ymeth.2014.12.014.

267. Gallagher, E. R. & Holzbaur, E. L. F. The selective autophagy adaptor p62/SQSTM1 forms phase condensates regulated by HSP27 that facilitate the clearance of damaged lysosomes via lysophagy. *Cell Rep.* **42**, (2023).

268. Hyttinen, J. M. T. *et al.* Clearance of misfolded and aggregated proteins by aggrephagy and implications for aggregation diseases. *Ageing Res. Rev.* **18C**, 16–28 (2014).

269. Johansen, T. & Lamark, T. Selective autophagy mediated by autophagic adapter proteins. *http://dx.doi.org/10.4161/auto.7.3.14487* **7**, 279–296 (2011).

270. Pankiv, S. *et al.* Nucleocytoplasmic Shuttling of p62/SQSTM1 and Its Role in Recruitment of Nuclear Polyubiquitinated Proteins to Promyelocytic Leukemia Bodies. *J. Biol. Chem.* **285**, 5941 (2010).

271. Bjørkøy, G. *et al.* p62/SQSTM1 forms protein aggregates degraded by autophagy and has a protective effect on huntingtin-induced cell death. *J. Cell Biol.* **171**, 603 (2005).

272. J E Darnell, J. Ribonucleic acids from animal cells. *Bacteriol. Rev.* **32**, 262 (1968).

273. Weinberg, D. E. *et al.* Improved ribosome-footprint and mRNA measurements provide insights into dynamics and regulation of yeast translation. *Cell Rep.* **14**, 1787 (2016).

274. Fujiwara, Y. *et al.* Discovery of a novel type of autophagy targeting RNA. *Autophagy* **9**, 403 (2013).

275. Fujiwara, Y., Hase, K., Wada, K. & Kabuta, T. An RNautophagy/DNautophagy receptor, LAMP2C, possesses an arginine-rich motif that mediates RNA/DNA-binding. *Biochem. Biophys. Res. Commun.* **460**, 281–286 (2015).

276. Aizawa, S. *et al.* Lysosomal putative RNA transporter SIDT2 mediates direct uptake of RNA by lysosomes. *Autophagy* **12**, 565–578 (2016).

277. Klionsky, D. J. *et al.* Autophagy in major human diseases. *EMBO J.* **40**, 108863 (2021).

278. Onorati, A. V., Dyczynski, M., Ojha, R. & Amaravadi, R. K. Targeting autophagy in cancer. *Cancer* **124**, 3307–3318 (2018).

279. Tang, C., Livingston, M. J., Liu, Z. & Dong, Z. Autophagy in kidney homeostasis and disease. *Nat. Rev. Nephrol.* **16**, 489–508 (2020).

280. Liao, S. X. *et al.* Autophagy and pulmonary disease. *Ther. Adv. Respir. Dis.* **13**, (2019).

281. Miyamoto, S. Autophagy and cardiac aging. *Cell Death Differ.* **26**, 653–664 (2019).

282. Houghton, O. H., Mizielinska, S. & Gomez-Suaga, P. The Interplay Between Autophagy and RNA Homeostasis: Implications for Amyotrophic Lateral Sclerosis and Frontotemporal Dementia. *Front. Cell Dev. Biol.* **10**, (2022).

283. Lizama, B. N. & Chu, C. T. Neuronal autophagy and mitophagy in Parkinson's disease. *Mol. Aspects Med.* **82**, (2021).

284. Shang, Y. *et al.* Autophagy regulates spermatid differentiation via degradation of PDLIM1. *Autophagy* **12**, 1575–1592 (2016).

285. Liu, C. *et al.* Autophagy is required for ectoplasmic specialization assembly in sertoli cells. *Autophagy* **12**, 814–832 (2016).

286. Huang, J. *et al.* Autophagy facilitates age-related cell apoptosis—a new insight from senile cataract. *Cell Death Dis. 2021 131* **13**, 1–15 (2022).

287. Lapierre, L. R., Kumsta, C., Sandri, M., Ballabio, A. & Hansen, M. Transcriptional and epigenetic regulation of autophagy in aging. *Autophagy* **11**, 867–880 (2015).

288. Xu, C. *et al.* SIRT1 is downregulated by autophagy in senescence and ageing. *Nat. Cell Biol.* **22**, 1170–1179 (2020).

289. Ganassi, M. *et al.* A Surveillance Function of the HSPB8-BAG3-HSP70 Chaperone Complex Ensures Stress Granule Integrity and Dynamism. *Mol. Cell* **63**, 796–810 (2016).

290. Turakhiya, A. *et al.* ZFAND1 Recruits p97 and the 26S Proteasome to Promote the Clearance of Arsenite-Induced Stress Granules. *Mol. Cell* **70**, 906-919.e7 (2018).

291. Alberti, S. & Carra, S. Quality Control of Membraneless Organelles. *J. Mol. Biol.* **430**, 4711–4729 (2018).

292. Sato, K. Multiple roles of endocytosis and autophagy in intracellular remodeling during oocyte-to-embryo transition. *Proc. Jpn. Acad. Ser. B. Phys. Biol. Sci.* **98**, 207 (2022).

293. Zhang, Y. *et al.* SEPA-1 mediates the specific recognition and degradation of P granule components by autophagy in C. elegans. *Cell* **136**, 308–321 (2009).

294. Pankiv, S. *et al.* FYCO1 is a Rab7 effector that binds to LC3 and PI3P to mediate microtubule plus end-directed vesicle transport. *J. Cell Biol.* **188**, 253–69 (2010).

295. Raiborg, C. *et al.* Repeated ER–endosome contacts promote endosome translocation and neurite outgrowth. *Nature* **520**, 234–238 (2015).

296. Cheng, X. *et al.* Structural basis of FYCO1 and MAP1LC3A interaction reveals a novel binding mode for Atg8-family proteins. *Autophagy* **12**, 1330–1339 (2016).

297. Ma, J., Becker, C., Reyes, C. & Underhill, D. M. Cutting edge: FYCO1 recruitment to dectin-1 phagosomes is accelerated by light chain 3 protein and regulates phagosome maturation and reactive oxygen production. *J. Immunol.* **192**, 1356–60 (2014).

298. Olsvik, H. L. *et al.* FYCO1 Contains a C-terminally Extended, LC3A/B-preferring LC3-interacting Region (LIR) Motif Required for Efficient Maturation of Autophagosomes during Basal Autophagy. *J. Biol. Chem.* **290**, 29361–74 (2015).

299. Mei, S., Lin, J., Liu, Z. & Li, C. A Novel Mutation in the FYCO1 Gene Causing Congenital Cataract: Case Study of a Chinese Family. *Dis. Markers* **2022**, (2022).

300. Frost, L. S., Mitchell, C. H. & Boesze-Battaglia, K. Autophagy in the eye: implications for ocular cell health. *Exp. Eye Res.* **124**, 56–66 (2014).

301. Chen, J. *et al.* Mutations in FYCO1 cause autosomal-recessive congenital cataracts. *Am. J. Hum. Genet.* **88**, 827–38 (2011).

302. Saleem, R. S. *et al.* Targeted gene sequencing of FYCO1 identified a novel mutation in a Pakistani family for autosomal recessive congenital cataract. *Mol. Genet. genomic Med.* **10**, (2022).

303. Tanaka, S. S. *et al.* The mouse homolog of Drosophila Vasa is required for the development of male germ cells. *Genes Dev.* **14**, 841–53 (2000).

304. Tanaka, T. *et al.* Tudor domain containing 7 (Tdrd7) is essential for dynamic ribonucleoprotein (RNP) remodeling of chromatoid bodies during spermatogenesis. *Proc. Natl. Acad. Sci. U. S. A.* **108**, 10579–84 (2011).

305. Deng, W. & Lin, H. miwi, a murine homolog of piwi, encodes a cytoplasmic protein essential for spermatogenesis. *Dev. Cell* **2**, 819–30 (2002).

306. Kuramochi-Miyagawa, S. *et al.* Mili, a mammalian member of piwi family gene, is essential for spermatogenesis. *Development* **131**, 839–49 (2004).

307. Tsai-Morris, C.-H., Sheng, Y., Lee, E., Lei, K.-J. & Dufau, M. L. Gonadotropin-regulated testicular RNA helicase (GRTH/Ddx25) is essential for spermatid development and completion of spermatogenesis. *Proc. Natl. Acad. Sci. U. S. A.* **101**, 6373–8 (2004).

308. Chuma, S. *et al.* Tdrd1/Mtr-1, a tudor-related gene, is essential for male germ-cell differentiation and nuage/germinal granule formation in mice. *Proc. Natl. Acad. Sci.* **103**, 15894–15899 (2006).

309. Vasileva, A., Tiedau, D., Firooznia, A., Müller-Reichert, T. & Jessberger, R. Tdrd6 is required for spermiogenesis, chromatoid body architecture, and regulation of miRNA expression. *Curr. Biol.* **19**, 630–9 (2009).

310. Patil, V. S., Anand, A., Chakrabarti, A. & Kai, T. The Tudor domain protein Tapas, a homolog of the vertebrate Tdrd7, functions in the piRNA pathway to regulate retrotransposons in germline of Drosophila melanogaster. *BMC Biol.* **12**, 61 (2014).

311. Yabuta, Y. *et al.* TDRD5 is required for retrotransposon silencing, chromatoid body assembly, and spermiogenesis in mice. *J. Cell Biol.* **192**, 781–795 (2011).

312. Pan, J. *et al.* RNF17, a component of the mammalian germ cell nuage, is essential for spermiogenesis. *Development* **132**, 4029–4039 (2005).

313. Wasik, K. A. *et al.* RNF17 blocks promiscuous activity of PIWI proteins in mouse testes. *Genes Dev.* **29**, 1403–15 (2015).

314. Ozata, D. M., Gainetdinov, I., Zoch, A., O'Carroll, D. & Zamore, P. D. PIWI-interacting RNAs: small RNAs with big functions. *Nature Reviews Genetics* vol. 20 89–108 (2019).

315. Siomi, M. C. M. C., Sato, K., Pezic, D. & Aravin, A. A. A. PIWI-interacting small RNAs: the vanguard of genome defence. *Nat. Rev. cell Biol.* **12**, 246–258 (2011).

316. Aravin, A. A. *et al.* A piRNA pathway primed by individual transposons is linked to de novo DNA methylation in mice. *Mol. Cell* **31**, 785 (2008).

317. Kuramochi-Miyagawa, S. *et al.* DNA methylation of retrotransposon genes is regulated by Piwi family members MILI and MIWI2 in murine fetal testes. *Genes Dev.* **22**, 908–917 (2008).

318. Pezic, D., Manakov, S. A., Sachidanandam, R. & Aravin, A. A. piRNA pathway targets active LINE1 elements to establish the repressive H3K9me3 mark in germ cells. *Genes Dev.* **28**, 1410–28 (2014).

319. Reuter, M. *et al.* Miwi catalysis is required for piRNA amplification-independent LINE1 transposon silencing. *Nature* **480**, 264–7 (2011).

320. Gou, L.-T. *et al.* Pachytene piRNAs instruct massive mRNA elimination during late spermiogenesis. *Cell Res.* **24**, 680–700 (2014).

321. Goh, W. S. S. W. S. S. *et al.* piRNA-directed cleavage of meiotic transcripts regulates spermatogenesis. *Genes Dev.* **29**, 1032–1044 (2015).

322. Vagin, V. V *et al.* Proteomic analysis of murine Piwi proteins reveals a role for arginine methylation in specifying interaction with Tudor family members. *Genes Dev.* **23**, 1749–62 (2009).

323. Grivna, S. T., Beyret, E., Wang, Z. & Lin, H. A novel class of small RNAs in mouse spermatogenic cells. *Genes Dev.* **20**, 1709–14 (2006).

324. Watanabe, T. *et al.* Identification and characterization of two novel classes of small RNAs in the mouse germline: retrotransposon-derived siRNAs in oocytes and germline small RNAs in testes. *Genes Dev.* **20**, 1732–43 (2006).

325. O'Donnell, K. A. & Boeke, J. D. Mighty Piwis defend the germline against genome intruders. *Cell* **129**, 37–44 (2007).

326. Ozata, D. M., Gainetdinov, I., Zoch, A., O'Carroll, D. & Zamore, P. D. PIWI-interacting RNAs: small RNAs with big functions. *Nat. Rev. Genet. 2018 202* **20**, 89–108 (2018).

327. Guo, M. & Wu, Y. Fighting an old war with a new weapon--silencing transposons by Piwi-interacting RNA. *IUBMB Life* **65**, 739–47 (2013).

328. Li, X. Z. *et al.* An ancient transcription factor initiates the burst of piRNA production during early meiosis in mouse testes. *Mol. Cell* **50**, 67–81 (2013).

329. Li, X. Z. *et al.* An ancient transcription factor initiates the burst of piRNA production during early meiosis in mouse testes. *Mol. Cell* **50**, 67–81 (2013).

330. Özata, D. M. *et al.* Evolutionarily conserved pachytene piRNA loci are highly divergent among modern humans. *Nat. Ecol. Evol.* **4**, 156–168 (2020).

331. Gainetdinov, I., Colpan, C., Arif, A., Cecchini, K. & Zamore, P. D. A Single Mechanism of Biogenesis, Initiated and Directed by PIWI Proteins, Explains piRNA Production in Most Animals. *Mol. Cell* **71**, 775 (2018).

332. Dai, P. *et al.* A Translation-Activating Function of MIWI/piRNA during Mouse Spermiogenesis. *Cell* **179**, 1566-1581.e16 (2019).

333. Zhang, P. *et al.* MIWI and piRNA-mediated cleavage of messenger RNAs in mouse testes. *Cell Res.* **25**, 193–207 (2015).

334. Lim, S. L. *et al.* HENMT1 and piRNA Stability Are Required for Adult Male Germ Cell Transposon Repression and to Define the Spermatogenic Program in the Mouse. *PLoS Genet.* **11**, e1005620 (2015).

335. Gainetdinov, I. *et al.* Terminal modification, sequence, length, and PIWI-protein identity determine piRNA stability. *Mol. Cell* **81**, 4826-4842.e8 (2021).

336. Girard, A., Sachidanandam, R., Hannon, G. J. & Carmell, M. A. A germline-specific class of small RNAs binds mammalian Piwi proteins. *Nature* **442**, 199–202 (2006).

337. Olotu, O. *et al.* Intermitochondrial cement (IMC) harbors piRNA biogenesis machinery and exonuclease domain-containing proteins EXD1 and EXD2 in mouse spermatocytes. *Andrology* **11**, 710–723 (2023).

338. Vourekas, A., Alexiou, P., Vrettos, N., Maragkakis, M. & Mourelatos, Z. Sequence-dependent but not sequence-specific piRNA adhesion traps mRNAs to the germ plasm. *Nature* **531**, 390–394 (2016).

339. Wu, P. H. *et al.* The evolutionarily conserved piRNA-producing locus pi6 is required for male mouse fertility. *Nat. Genet.* **52**, 728–739 (2020).

340. Korhonen, H. M. H. M. *et al.* Dicer is required for haploid male germ cell differentiation in mice. *PLoS One* **6**, e24821 (2011).

341. Lehti, M. S. S., Kotaja, N. & Sironen, A. KIF3A is essential for sperm tail formation and manchette function. *Mol. Cell. Endocrinol.* **377**, 44–55 (2013).

342. Kotaja, N. *et al.* Preparation, isolation and characterization of stage-specific spermatogenic cells for cellular and molecular analysis. *Nat. Methods 2004 13* **1**, 249–254 (2004).

343. Belevich, I., Joensuu, M., Kumar, D., Vihinen, H. & Jokitalo, E. Microscopy Image Browser: A Platform for Segmentation and Analysis of Multidimensional Datasets. *PLoS Biol.* **14**, (2016).

344. Meikar, O. & Kotaja, N. Isolation of chromatoid bodies from mouse testis as a rich source of short RNAs. *Methods Mol. Biol.* **1173**, 11–25 (2014).

345. Da Ros, M., Lehtiniemi, T., Olotu, O., Meikar, O. & Kotaja, N. Enrichment of pachytene spermatocytes and spermatids from mouse testes using standard laboratory equipment. *J. Vis. Exp.* **2019**, (2019).

346. Robinson, M. D., McCarthy, D. J. & Smyth, G. K. edgeR: a Bioconductor package for differential expression analysis of digital gene expression data. *Bioinformatics* **26**, 139–140 (2010).

347. Meikar, O., Da Ros, M., Liljenbäck, H., Toppari, J. & Kotaja, N. Accumulation of piRNAs in the chromatoid bodies purified by a novel isolation protocol. *Exp. Cell Res.* **316**, 1567–75 (2010).

348. Han, B. W., Wang, W., Zamore, P. D. & Weng, Z. piPipes: a set of pipelines for piRNA and transposon analysis via small RNA-seq, RNA-seq, degradome- and CAGE-seq, ChIP-seq and genomic DNA sequencing. *Bioinformatics* **31**, 593–595 (2015).

349. Trapnell, C. *et al.* nature biotechnology Differential analysis of gene regulation at transcript resolution with rNA-seq. *Nat. Biotechnol.* **31**, (2012).

350. Jin, Y. & Hammell, M. Analysis of RNA-seq data using tetranscripts. in *Methods in Molecular Biology* vol. 1751 153–167 (Humana Press Inc., 2018).

351. Tan, K. *et al.* The role of the nmd factor upf3b in olfactory sensory neurons. *Elife* **9**, 1–29 (2020).

352. Alkallas, R., Fish, L., Goodarzi, H. & Najafabadi, H. S. Inference of RNA decay rate from transcriptional profiling highlights the regulatory programs of Alzheimer's disease. *Nat. Commun. 2017 81* **8**, 1–11 (2017).

353. Shi, J., Ko, E.-A., Sanders, K. M., Chen, Q. & Zhou, T. SPORTS1.0: A Tool for Annotating and Profiling Non-coding RNAs Optimized for rRNA- and tRNA-derived Small RNAs. *Genomics. Proteomics Bioinformatics* **16**, 144–151 (2018).

354. Korhonen, H. M. *et al.* DICER regulates the formation and maintenance of cell-Cell junctions in the mouse seminiferous epithelium. *Biol. Reprod.* **93**, (2015).

355. Da Ros, M. *et al.* FYCO1 and autophagy control the integrity of the haploid male germ cell-specific RNP granules. *Autophagy* **13**, (2017).

356. Ma, Q. *et al.* AXDND1, a novel testis-enriched gene, is required for spermiogenesis and male fertility. *Cell Death Discov. 2021 71* **7**, 1–9 (2021).

357. Liu, M. *et al.* The polycomb group protein PCGF6 mediates germline gene silencing by recruiting histone-modifying proteins to target gene promoters. *J. Biol. Chem.* **295**, 9712 (2020).

358. Li, Z. *et al.* H3K36me2 methyltransferase NSD2 orchestrates epigenetic reprogramming during spermatogenesis. *Nucleic Acids Res.* **50**, 6786 (2022).

359. Romrell, L. J., Bellvé, A. R. & Fawcett, D. W. Separation of mouse spermatogenic cells by sedimentation velocity. A morphological characterization. *Dev. Biol.* **49**, 119–131 (1976).

360. Da Ros, M., Lehtiniemi, T., Olotu, O., Meikar, O. & Kotaja, N. Enrichment of pachytene spermatocytes and spermatids from mouse testes using standard laboratory equipment. *J. Vis. Exp.* **2019**, 60271 (2019).

361. Bryant, J. M., Meyer-Ficca, M. L., Dang, V. M., Berger, S. L. & Meyer, R. G. Separation of Spermatogenic cell types using STA-PUT velocity sedimentation. *J. Vis. Exp.* (2013) doi:10.3791/50648.

362. Chang, J. H. *et al.* LCRMP-1 is required for spermatogenesis and stabilises spermatid F-actin organization via the PI3K-Akt pathway. *Commun. Biol. 2023 61* **6**, 1–15 (2023).

363. Parvinen, M. The chromatoid body in spermatogenesis. *Int. J. Androl.* **28**, 189–201 (2005).

364. Da Ros, M., Hirvonen, N., Olotu, O., Toppari, J. & Kotaja, N. Retromer vesicles interact with RNA granules in haploid male germ cells. *Mol. Cell. Endocrinol.* (2014) doi:10.1016/j.mce.2014.11.026.

365. Satoh, K., Takemura, Y., Satoh, M., Ozaki, K. & Kubota, S. Loss of FYCO1 leads to cataract formation. *Sci. Reports 2021 111* **11**, 1–12 (2021).

366. Wymann, M. P. *et al.* Wortmannin inactivates phosphoinositide 3-kinase by covalent modification of Lys-802, a residue involved in the phosphate transfer reaction. *Mol. Cell. Biol.* **16**, 1722–1733 (1996).

367. Mauthe, M. *et al.* Chloroquine inhibits autophagic flux by decreasing autophagosome-lysosome fusion. *Autophagy* **14**, 1435–1455 (2018).

368. Kuhn, C. *et al.* FYCO1 Regulates Cardiomyocyte Autophagy and Prevents Heart Failure Due to Pressure Overload In Vivo. *JACC Basic to Transl. Sci.* **6**, 365 (2021).

369. Brennan, L. A. *et al.* Spatial expression patterns of autophagy genes in the eye lens and induction of autophagy in lens cells. *Mol. Vis.* **18**, 1773–86 (2012).

370. Aprahamian, R. *et al.* Identification of a novel nonsense variant in FYCO1 gene associated with infantile cataract and cortical atrophy. *Ophthalmic Genet.* **42**, 744–746 (2021).

371. Shirzadeh, E., Piryaei, F., Naddaf, H. & Barabadi, Z. Two New Variants in FYCO1 Are Responsible for AutosomalRecessive Congenital Cataract in Iranian Population. *Cell J.* **24**, 546 (2022).

372. Yuan, W., Yang, M. & Zhu, Y. Development and validation of a gene signature predicting the risk of postmenopausal osteoporosis. *Bone Joint Res.* **11**, 548–560 (2022).

373. Ashley, T., Gaeth, A. P., Creemers, L. B., Hack, A. M. & de Rooij, D. G. Correlation of meiotic events in testis sections and microspreads of mouse spermatocytes relative to the mid-pachytene checkpoint. *Chromosoma* **113**, 126–136 (2004).

374. Tan, K. *et al.* The role of the nmd factor upf3b in olfactory sensory neurons. *Elife* **9**, 1–29 (2020).

375. Shum, E. Y. *et al.* The Antagonistic Gene Paralogs Upf3a and Upf3b Govern Nonsense-Mediated RNA Decay. *Cell* **165**, 382–95 (2016).

376. Wittkopp, N. *et al.* Nonsense-mediated mRNA decay effectors are essential for zebrafish embryonic development and survival. *Mol. Cell. Biol.* **29**, 3517–3528 (2009).

377. Foulkes, N. S., Mellström, B., Benusiglio, E. & Sassone-Corsi, P. Developmental switch of CREM function during spermatogenesis: from antagonist to activator. *Nature* **355**, 80–4 (1992).

378. Blendy, J. A., Kaestner, K. H., Weinbauer, G. F., Nieschlag, E. & Schütz, G. Severe impairment of spermatogenesis in mice lacking the CREM gene. *Nature* **380**, 162–5 (1996).

379. White-Cooper, H. & Davidson, I. Unique aspects of transcription regulation in male germ cells. *Cold Spring Harb. Perspect. Biol.* **3**, (2011).

380. Tsai-Morris, C. H., Sheng, Y., Lee, E., Lei, K. J. & Dufau, M. L. Gonadotropin-regulated testicular RNA helicase (GRTH/Ddx25) is essential for spermatid development and completion of spermatogenesis. *Proc. Natl. Acad. Sci. U. S. A.* **101**, 6373 (2004).

381. Martianov, I. *et al.* Late arrest of spermiogenesis and germ cell apoptosis in mice lacking the TBP-like TLF/TRF2 gene. *Mol. Cell* **7**, 509–515 (2001).

382. Kashiwabara, S. I. *et al.* PAPOLB/TPAP regulates spermiogenesis independently of chromatoid body-associated factors. *J. Reprod. Dev.* **64**, 25 (2018).

383. Kashiwabara, S. I., Tsuruta, S., Okada, K., Yamaoka, Y. & Baba, T. Adenylation by testis-specific cytoplasmic poly(A) polymerase, PAPOLB/TPAP, is essential for spermatogenesis. *J. Reprod. Dev.* **62**, 607–614 (2016).

384. Zhuang, T., Kashiwabara, S. I., Noguchi, J. & Baba, T. Transgenic expression of testis-specific poly(A) polymerase TPAP in wild-type and TPAP-deficient mice. *J. Reprod. Dev.* **50**, 207–213 (2004).

385. Chen, Y. *et al.* Regulation of Miwi-mediated mRNA stabilization by Ck137956/Tssa is essential for male fertility. *BMC Biol.* **21**, 89 (2023).

386. Kotaja, N. *et al.* Abnormal sperm in mice with targeted deletion of the act (activator of cAMP-responsive element modulator in testis) gene. *Proc. Natl. Acad. Sci. U. S. A.* **101**, 10620–10625 (2004).

387. He, X.-J. *et al.* CREM variants rs4934540 and rs2295415 conferred susceptibility to nonobstructive azoospermia risk in the Chinese population. *Biol. Reprod.* **91**, 52 (2014).

388. Katsioudi, G. *et al.* A conditional Smg6 mutant mouse model reveals circadian clock regulation through the nonsense-mediated mRNA decay pathway. *Sci. Adv.* **9**, (2023).

389. Kleene, K. C. Patterns, mechanisms, and functions of translation regulation in mammalian spermatogenic cells. *Cytogenet. Genome Res.* **103**, 217–24 (2003).

390. Fajardo, M. A., Haugen, H. S., Clegg, C. H. & Braun, R. E. Separate elements in the 3' untranslated region of the mouse protamine 1 mRNA regulate translational repression and activation during murine spermatogenesis. *Dev. Biol.* **191**, 42–52 (1997).

391. Kleene, K. C. Poly(A) shortening accompanies the activation of translation of five mRNAs during spermiogenesis in the mouse. *Development* **106**, (1989).

392. Lachke, S. A. *et al.* Mutations in the RNA granule component TDRD7 cause cataract and glaucoma. *Science* **331**, 1571–6 (2011).

393. Aravin, A. A. *et al.* Cytoplasmic compartmentalization of the fetal piRNA pathway in mice. *PLoS Genet.* **5**, e1000764 (2009).

394. Kirino, Y. *et al.* Arginine methylation of Aubergine mediates Tudor binding and germ plasm localization. *RNA* **16**, 70–8 (2010).

395. Nicholson, P., Josi, C., Kurosawa, H., Yamashita, A. & Mühlemann, O. A novel phosphorylation-independent interaction between SMG6 and UPF1 is essential for human NMD. *Nucleic Acids Res.* **42**, 9217–9235 (2014).

396. Watanabe, T. *et al.* MITOPLD is a mitochondrial protein essential for nuage formation and piRNA biogenesis in the mouse germline. *Dev. Cell* **20**, 364–75 (2011).

397. Vourekas, A. & Mourelatos, Z. Set Phasers to Cleave: PIWI Cleavage Directs All piRNA Biogenesis. *Mol. Cell* **71**, 651–652 (2018).

398. Hosokawa, M. *et al.* Tudor-related proteins TDRD1/MTR-1, TDRD6 and TDRD7/TRAP: domain composition, intracellular localization, and function in male germ cells in mice. *Dev. Biol.* **301**, 38–52 (2007).

399. Boswell, R. E. & Mahowald, A. P. tudor, a gene required for assembly of the germ plasm in Drosophila melanogaster. *Cell* **43**, 97–104 (1985).

400. Raz, E. The function and regulation of vasa-like genes in germ-cell development. *Genome Biol.* **1**, REVIEWS1017 (2000).

401. Wang, J., Saxe, J. P., Tanaka, T., Chuma, S. & Lin, H. Mili interacts with tudor domain-containing protein 1 in regulating spermatogenesis. *Curr. Biol.* **19**, 640–4 (2009).

402. Pek, J. W., Anand, A. & Kai, T. Tudor domain proteins in development. *Development* **139**, 2255–2266 (2012).

403. Vourekas, A., Alexiou, P., Vrettos, N., Maragkakis, M. & Mourelatos, Z. Sequence-dependent but not sequence-specific piRNA adhesion traps mRNAs to the germ plasm. *Nature* **531**, 390–4 (2016).

404. M, S. *et al.* Cellular source and mechanisms of high transcriptome complexity in the mammalian testis. *Cell Rep.* **3**, 2179–2190 (2013).

405. Kuramochi-Miyagawa, S. *et al.* Mili, a mammalian member of piwi family gene, is essential for spermatogenesis. *Development* **131**, 839–49 (2004).

406. Messina, V. *et al.* The RNA binding protein SAM68 transiently localizes in the chromatoid body of male germ cells and influences expression of select microRNAs. *PLoS One* **7**, (2012).

407. Lee, C. Y. S. *et al.* Recruitment of mRNAs to P granules by condensation with intrinsically-disordered proteins. *Elife* **9**, (2020).

408. Dai, P. *et al.* A Translation-Activating Function of MIWI/piRNA during MouseSpermiogenesis. *Cell* **179**, 1566 (2019).

409. Ramat, A. *et al.* The PIWI protein Aubergine recruits eIF3 to activate translation in the germ plasm. *Cell Res. 2020 305* **30**, 421–435 (2020).